УДК 512.6, 517.9, 519.6

UNMANNED AERIAL ROBOTIC VEHICLES. PT. 2: UNCONVENTIONAL MODELS OF UNMANNED AERIAL SYSTEMS AND AERIAL EMBEDING MANIPULATORS

Tyatyushkina Olga Yu.[1], Ulyanov Sergey V.[2]

[1]PhD in Engineering sciences, associate professor;
Dubna State University,
19 Universitetskaya Str., Dubna, Moscow region, 141980, Russia;
e-mail: tyatyushkina @mail.ru.

[2]Grand PhD in Physical and Mathematical Sciences, professor;
Dubna State University,
19 Universitetskaya Str., Dubna, Moscow region, 141980, Russia;
e-mail: ulyanovsv@mail.ru.

This paper describes the state-of-the art in the area of unmanned aerial systems and aerial manipulators, of underwater robot manipulator systems. A brief introduction is given on the use of manipulators in various offshore industries for different subsea intervention applications. It provides a comprehensive summary of existing commercial and prototype underwater manipulators, covering relevant aspects such as design features, their capabilities and merits, and provides a detailed comparison. This is followed by a thorough analysis of advantages and disadvantages of both electrically and hydraulically actuated manipulators. Furthermore, a detailed description of commercially available underwater manipulator control systems is presented in order to provide a realistic picture of the existing technology and its limitation. In addition, an extensive bibliography covering research results in the field of control algorithms is presented, including low level motion control, high level kinematic control and motion planning schemes along with the implementation issues.

Keywords: unmanned aerial vehicle, aerial manipulators, underwater robot manipulator, control systems.

For citation:
Tyatyushkina O. Yu., Ulyanov S. V. Unmanned Aerial Robotic Vehicles. Pt. 2: Unconventional models of unmanned aerial systems and aerial embeding manipulators. *System analysis in science and education*, 2022;(3):53-109. Available from: http: //sanse.ru/download/474.

БЕСПИЛОТНЫЕ РОБОТОТЕХНИЧЕСКИЕ НЕТРАДИЦИОННЫЕ ЛЕТАТЕЛЬНЫЕ АППАРАТЫ. Ч. 2: МОДЕЛИ БЕСПИЛОТНЫХ АВИАКОМПЛЕКСОВ СО ВСТРОЕННЫМИ МАНИПУЛЯТОРАМИ

Тятюшкина Ольга Юрьевна[1], Ульянов Сергей Викторович [2]

[1]Кандидат технических наук, доцент;
Государственный университет «Дубна»;
141980, Московская обл., г. Дубна, ул. Университетская, 19;
e-mail: tyatyushkina@mail.ru.

[2]Доктор физико-математических наук, профессор;
Государственный университет «Дубна»;
141980, Московская обл., г. Дубна, ул. Университетская, 19;
e-mail: ulyanovsv@mail.ru.

В статье описано современное состояние в области беспилотных авиационных комплексов и воздушных манипуляторов, систем подводных роботов-манипуляторов. Дано краткое введение в использование манипуляторов в различных отраслях для различных приложений воздушного и подводного пространства. Представлен исчерпывающий обзор существующих коммерческих и экспериментальных прототипов подводных манипуляторов, охватывающий соответствующие аспекты, такие как конструктивные особенности, их возможности и достоинства, а также подробное сравнение. Проведен анализ преимуществ и недостатков как электрических, так и гидравлических манипуляторов. Кроме того, представлено подробное описание коммерчески доступных систем

управления подводными манипуляторами, чтобы дать реалистичную картину существующей технологии и ее ограничений. Кроме того, представлена обширная библиография, охватывающая результаты исследований в области алгоритмов управления, включая низкоуровневое управление движением, высокоуровневое кинематическое управление и схемы планирования движения, а также вопросы реализации.

Ключевые слова: беспилотный летательный аппарат, воздушные манипуляторы, подводный робот-манипулятор, системы управления.

Для цитирования:

Тятюшкина О. Ю., Ульянов С. В. Беспилотные летательные аппараты. Ч. 2: Модели беспилотных авиакомплексов со встроенными манипуляторами // Системный анализ в науке и образовании: сетевое научное издание. 2022. № 3. С.53-109. На англ. языке. URL:http://sanse.ru/download/474.

1. Introduction

In the past few decades, the increasing interest towards Unmanned Aerial Vehicles (UAVs) has sprouted a number of industrial and civil applications in which these platforms are being used. Thanks to their unbounded workspace and inherent versatility, UAVs are deployed for a number of contact-less operations which exploit advanced on-board sensing, e.g. cameras, pressure sensors, flow sensors, LIDAR. Some example applications in which aerial vehicles are currently being used are civilian security, border security, fire and rescue, mountain rescue, distribution network monitoring, environmental monitoring, aerial photography, mapping and surveying. Despite proving very useful and successful, these applications are mostly limited to passive observation. However, huge potential lies in tasks that do require manipulation and physical interaction with the environment.

In the past decade a new research area has risen, aerial manipulation, which con-siders endowing multicopters with mechanical devices to enable airborne manipulation tasks. Multicopters, e.g. quadcopters, hexacopters, octocopters, are Vertical Take-off and Landing (VTOL) aircraft that can hover, take off, and land vertically. This feature, together with the ability to fly stably at low speeds, higher manoeuvrability with respect to fixed-wing UAVs, and greater payload capacity has made them particularly attractive for these types of applications. Unmanned Aerial Manipulators (UAMs) could be deployed to carry out inspection and maintenance operations in remote areas and hard-to-reach locations, performing tasks that are too risky for human operators and that require costly equipment. Example scenarios where UAMs could be exploited can include cracks repair on wind turbine blades, cleaning of clogged-up thermocouples on industrial chimneys, contact-based inspection of bridges and dams, installation and retrieval of smart sensors in wide spread areas for monitoring purposes.

Figure 1 shows some possible scenarios [1] for the deployment of UAMs.

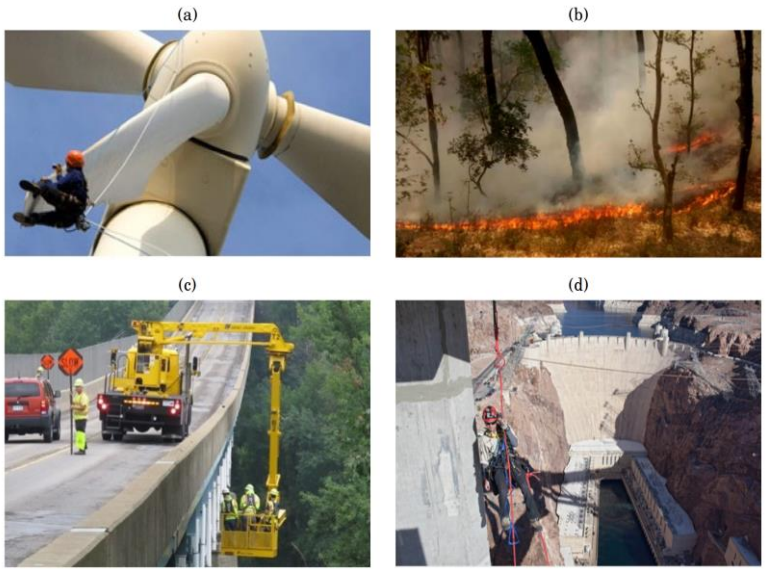

Fig. 1. Example application scenarios for the deployment of unmanned aerial manipulators in the environment to (a) perform continuity checks on top of wind turbine blades; (b) install smoke detectors in forests for fire prevention; (c) monitor the induced traffic vibrations on bridges; (d) check the slope stability on dams

All these tasks are nowadays conducted by human operators and often require supporting structures such as scaffolding around the area or other special equipment to allow the operator to reach the site and safely conduct inspection and maintenance tasks. For these reasons, such example scenarios have been the case study of several investigations as part of multiple European funded projects in the past years, starting from AI Robots in 2010 until more recent project such as ARCAS, Aeroarms, Aerobi, AEROWORKS, etc.

Based on robotics, the systems may be divided into three categories: autonomous, shared autonomous, and teleoperation systems. An autonomous system is a system with some level of automation to assist or replace human control. Based on the Society of Automotive Engineers (SAE), automated functionality ranges from no automated features (level 0) to full automation (level 5). While the shared autonomous system is the integration of human interaction using a feedback loop with system autonomy to generate a bilateral shared control system. It is a user-system interaction to achieve shared goals. Meanwhile, teleoperation is the full operation of the system by the user but performed remotely.

Regarding unmanned aerial systems (UASs), a block diagram architecture of the different systems [2,3] is demonstrated in Fig. 2.

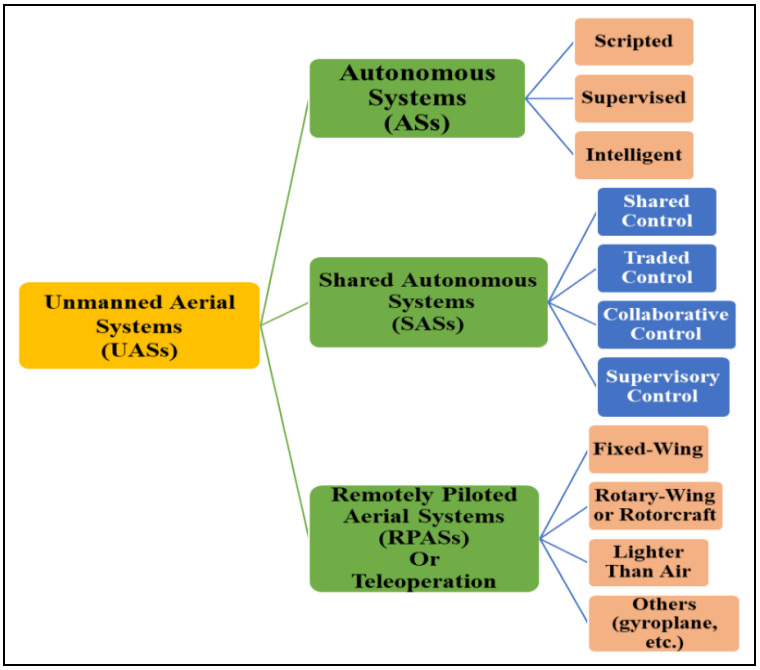

Fig. 2. The different unmanned aerial systems

While the different types of autonomous and shared autonomous systems with their advantages and disadvantages as well as real-time applications [2] are shown in Table 1.

Based on the classification of aerodynamic configuration, UAVs are usually classified into three categories [3] as shown in Fig. 3.

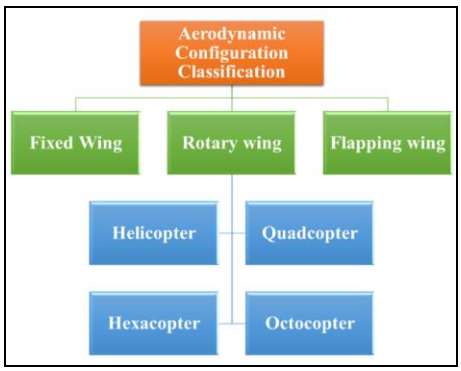

Fig. 3. UAVs classification based on aerodynamic configuration

Table 1. Types of autonomous and shared autonomous systems with their advantages, disadvantages, and real-time applications

	Autonomous Systems	Shared Autonomous Systems
Types	**Scripted** • Systems that are basically autopilots • Perform preplanned scripts of actions based on foreseen events to accomplish the mission objective **Supervised** • Allow the evolution of mission sequence **Intelligent** • Allow the evolution of mission objective • Aims to implement the human directives • Adapt to unforeseen events	**Shared/Guided Control** • Focus on the control generating from the user towards the system which has its own control loop and is autonomously reacting to the environment and executes the specified action. **Traded Control** • The user and system take turns. **Collaborative Control / Mixed-Initiative Control** • The user and system share a task and work as a group collaboratively in the same space and at the same time **Supervisory Control** • The user only monitors the execution of the autonomously working system.
Advantages	• Time-saving • Much safer • Extra navigation systems and maps	• Exploit the benefits of human control and machine control. • Safe navigation, control, and stable interaction. • Extend human operators sensing and manipulation capability.
Disadvantages	• High cost for implementing the technology • Complex communication networks • Hacking and security aspects • Lacks adaptation in difficult and complex tasks	• Safety concerns • Policy and operational framework • Large time delay • Limited bandwidth and insufficient visibility of visual feedback signal-based design
Real-time applications	• UAVs • Flying in hazardous or radiation areas	• Search and rescue mission • Monitoring and inspection tasks

Another promising trend is the hybrid UAVs, which can combine the advantages of both fixed-wing and VTOL systems.

Rotorcraft or rotary-wing systems, among other types of UAVs, are distinguished by their ability to take-off and land vertically, hover in one spot or limited zones, perform swift maneuvers, and fly backward or sideways. The different types of fixed and multirotor with their advantages and disadvantages as well as real-time applications are shown in Table 2.

Table 2. The different types of fixed and multirotor

	Fixed	Multirotor
Types	**Straight Wing:** • Rectangular Straight Wing • Tapered Straight Wing • Rounded or elliptical straight wing **Swept Wing:** • Slightly swept wing • Moderately swept wing • Highly swept wing **Delta Wing:** • Simple delta wing • Complex delta wing	**Helicopter** UAV with dual rotors **Quadcopter** UAV with four rotors **Hexacopter** UAV with six rotors **Octocopter** UAV with eight rotors **Decacopter** UAV with twelve rotors
Advantages	• Higher flight safety • More energy-efficient • Longer range and endurance • Excellent stability	• Ability to take-off and land vertically • Landing/take-off substantial area is not required • Ability to hover in one spot • Ability to perform agile maneuvering
Disadvantages	• Lacks hovering capability • Need more space for take-off and landing	• Lower speeds and shorter flight ranges • Small payload capacity
Real-time applications	• Surveillance • Aerial mapping • Military tasks	• Aerial photography and video recording • Aerial inspection

There are various types of rotorcraft systems, such as the helicopter, quadcopter, hexacopter, octocopter, decacopter, etc. Among these models, helicopter and quadcopter can be considered the most widespread flying machines nowadays and have attracted many researchers over the past few years due to their many benefits and uses. However, for heavy pay-loads and shorter flight durations, hexacopter and octocopter are the best options however are relatively expensive and heavy with higher energy consumption. Thus, many researchers concentrate on the twin-rotor helicopter and quadcopter and the derivation of their mathematical models, as case studies while various control strategies for all rotorcraft UAVs were discussed.

2. Simplified description of quadrocopter movements

The helicopter is a multivariable, nonlinear, and strongly coupled system. A two degrees of freedom (2-DOF's) helicopter model is a dual-rotor laboratory experimental rig that is commonly used as a test platform, to verify the effectiveness of control strategies designed for a real helicopter system. It consists of two pro-

pellers at both ends of a beam pivoted on its fixed base allowing to rotate freely in both the vertical and horizontal planes. The front rotor, which is horizontal to the ground, is the main rotor and causes a pitching moment around the pitch axis while the back or tail rotor generates a yawing moment around the yaw axis. Both the front and back rotors generate a torque on each other resulting in the coupling effect. The beam is driven by two perpendicular propellers that are actuated by two DC motors. A number of researches have been conducted to develop control techniques for the twin-rotor helicopter over the past decades to provide appropriate robust solutions in demanding environments. On the other hand, the quadcopter is a multirotor UAV that is lifted by four rotors and consists of a rigid body connected by four propellers with fixed-pitch blades as their airflows point downward to generate a lifting upward force. The propellers' axes of rotation are fixed and parallel to each other. Also, the quadcopter has two pairs of identical propellers, two rotate clockwise (CW) while the other two counter-clockwise (CCW), allowing the quadcopter to be controlled by varying the speed of rotors. The arrangements of rotors with respect to the quadcopter body coordinate system usually lead to three quadcopter configurations: the `*X*', `*C*', and `*H*' types. Each configuration has its advantages as the first type is the most stable design among them while the second configuration is more used for acrobatic fight and the last one is utilized for races.

The quadcopter has six DoFs, namely, *x*, *y*, and *z* which are translational motions, and ϕ, θ and ψ which are rotational motions, and only four propellers (inputs); throttle, roll, pitch, and yaw motions. If one of the pairs rotates CW and the other CCW (equal in magnitude), then this is considered having a yaw motion tendency causing the quadcopter to bend either right or left around the vertical axis. For the upward and downward movements (+ Throttle and – Throttle), all four rotors should be accelerated up or down at the same speed. To move forward/backward (pitching) or right/left (rolling), a difference in the angular velocities must occur between the pairs, as shown in Fig. 4

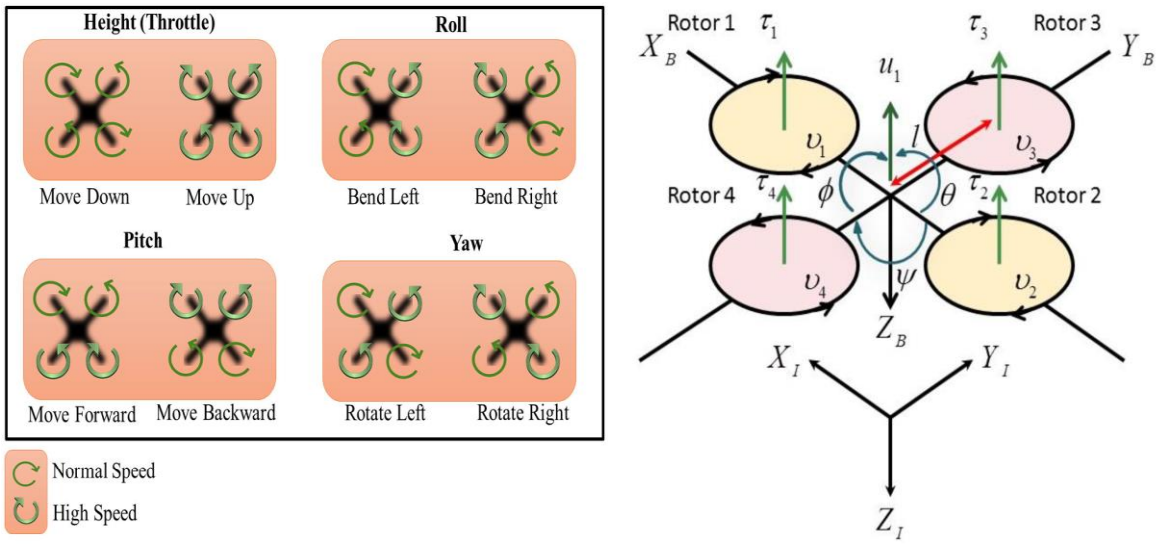

Fig. 4. Quadcopter movements

Therefore, the quadcopter model is an underactuated mechanical system with two degrees of under actuation.

A coaxial quadrotor robot contains eight rotors which properly control to preserve the attitude control and the flight stability. The safe and the better flying experience can be concluded by a stable flight and therefore, a successful task is achieved. Moreover, Octorotor can be defined as an eight-rotorcraft using four arms, eight motors. Since all the propellers axes of rotation are fixed and parallel so, these eight motors of Octorotor are coaxially installed.

Indeed, by increasing the motors number in a rotorcraft, the resultant thrust force is usually increased. In addition, since the coaxial configuration cancel the resulted torque so, more flight stability is attained by increasing the number of rotating propeller. As like as the Quadrotor, the Octorotor has only four independent inputs (rotor speeds). So, this flying robot can be considered as an under-actuated system with six Degrees of Freedom (DoFs) for translational and rotational movement. Moreover, this results in the highly states coupling. To this end, the Octorotor has the nonlinear dynamics. Therefore, many controllers have been studied to control its position and attitude [4], Fig. 5 shows the stated Octorotor

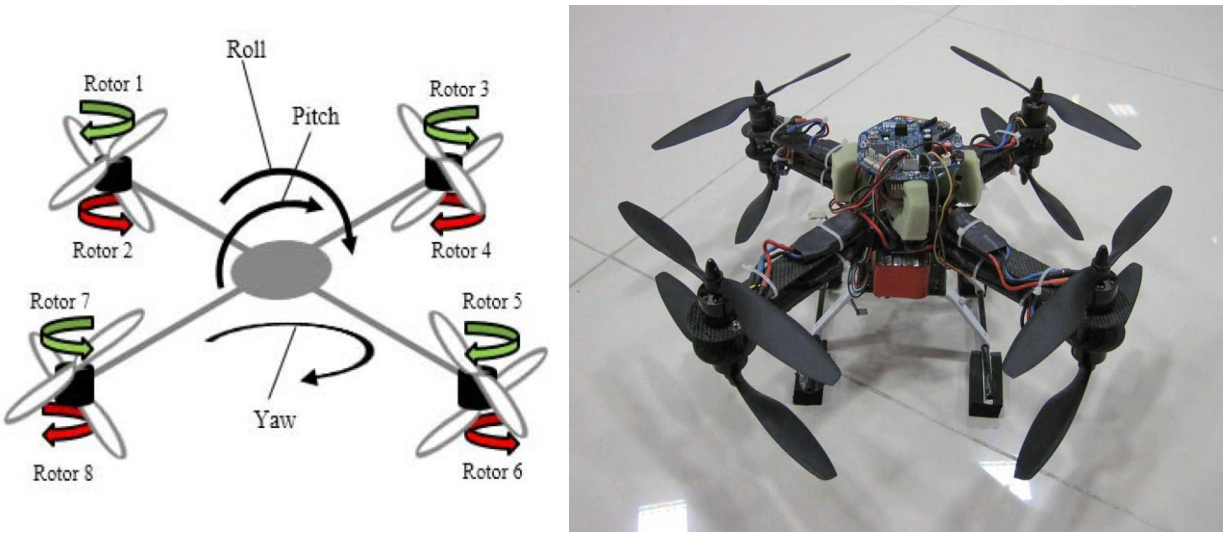

(a) (b)

Fig. 5. (a) Flight Concept of Octorotor; (b) Cbonsidered Octorotor frame

The Octorotor flying robot has the same concept with the Quadrotor. It should be noted that since there is not any gear set, all of the eight propellers are directly installed on the motors. Moreover, the rotation axes of propeller are distinctly fixed. Also, the flight concept of this flying robot is shown in Fig. 5,a.

Rotorcraft UAVs encounter several challenges during the flight-related to instability, moving and fixed obstacles, motors failure, trajectory tracking, external disturbances, model uncertainties, etc. Before discussing the different control strategies that have been proposed to solve some of these impediments, it is deemed necessary to describe adequately the mathematical model as it plays a vital role in understanding the behavior of the dynamic system. In this study, the mathematical models for both the 2-DOF helicopter and quadcopter systems were fully derived in the following section as case studies.

Actually, as same as Quadrotor, Octorotor is a 6 DoFs rigid body whereas its throttle is supplied using eight brushless DC motors. In the same way, the Octorotor flying robot is a four-input control system. Also, the gravitational vector and movement state vector of the Octorotor can be calculated by considering the gyroscope effect. So, the dynamic equations of the Octorotor flying robot can be extracted. Indeed, dynamic equations of Octorotor can be calculated as the same with dynamic equations of Quadrotor by considering the flight concepts of Quadrotor.

Quadrotors can perform basic flight movements on different axes by turning four motors at different speeds. Quadrotor has four basic movements, such as altitude, roll, yaw, and pitch. The altitude movement is used for the up and down movements of the quadrotor on the vertical axis.

Roll movement is used to move left and right along the x-axis of the quadrotor. Pitch movement is used to move forward and backward on the y-axis of the quadrotor. Yaw movement is used to rotate around the z-axis of the quad-rotor. Figure 6(i) shows the quadrotor's movements.

Figure 6 shows in details the axis movements made on the quadrotor depending on the motor movements.

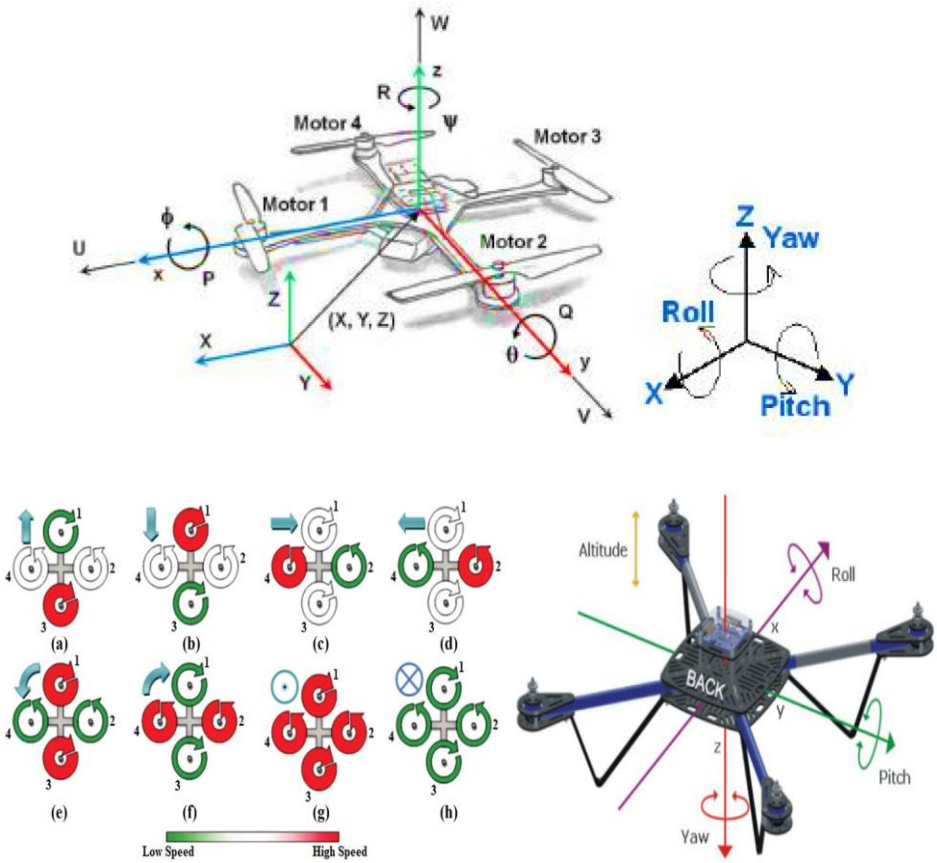

Fig. 6. (a–h) Quadrotor axis movements; (i) Quadrotor's movements

This figure shows the axis movement according to the speed values of the motors. For example, Figure 6 (a) shows changes in the pitch angle due to the speed difference between the first and third motors; Figure 6(c) shows changes in the roll angle due to the speed difference between the second and fourth motors. The figure shows forward, backward, right, left, turn left, turn right, takeoff, and landing movements, respectively.

2.1. Quadcopter Flight Dynamics

A quadcopter is an aircraft with six degrees of freedom (DOF), three rotational and three translational. With four control inputs (one to each motor) this results in an underactuated system that requires an onboard computer to compute motor signals to provide stable flight (Fig. 7).

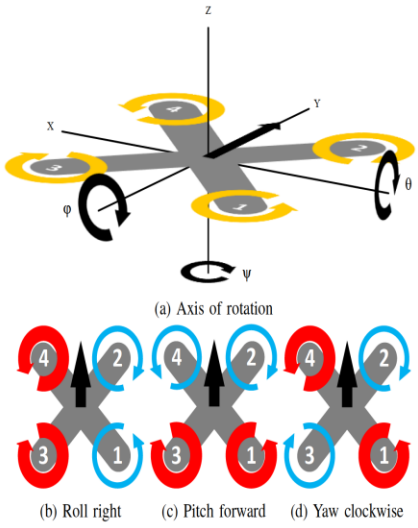

Fig. 7. A quadcopter model

We indicate with $\omega_i,\ i \in 1,\ldots,M$ the rotation speed of each rotor where $M = 4$ is the total number of motors for a quadcopter. These have a direct impact on the resulting Euler angles ϕ,θ,ψ, i.e. roll, pitch, yaw respectively which provide rotation in D = 3 dimensions. Moreover, they produce a certain amount of upward thrust, indicated with *f*. The aerodynamic effect that each ω_i produces depends upon the configuration of the motors. The most popular configuration is an "X" configuration, depicted in Fig. 7a which has the motors mounted in an "X" formation relative to what is considered the front of the aircraft. This configuration provides more stability compared to a "+" configuration which in contrast has its motor configuration rotated an additional 450 along the *z*-axis. This is due to the differences in torque generated along each axis of rotation in respect to the distance of the motor from the axis. The aerodynamic affect u that each rotor speed ω_i has on thrust and Euler angles, is given by:

$u_f = b\left(\omega_1^2 + \omega_2^2 + \omega_3^2 + \omega_4^2\right)$	$u_\theta = b\left(\omega_1^2 - \omega_2^2 + \omega_3^2 - \omega_4^2\right)$
$u_\phi = b\left(\omega_1^2 + \omega_2^2 - \omega_3^2 - \omega_4^2\right)$	$u_\psi = b\left(\omega_1^2 - \omega_2^2 - \omega_3^2 + \omega_4^2\right)$

where $u_f, u_\phi, u_\theta, u_\psi$ is the thrust, roll, pitch, and yaw effect respectively, while *b* is a thrust factor that captures propeller geometry and frame characteristics. To perform a rotational movement the velocity of each rotor is manipulated according to the relationship expressed, for example, in equation for u_ψ and as illustrated in Figs 7b, 7c, 7d. For example, to roll right (Fig. 7b) more thrust is delivered to motors 3 and 4. Yaw (Fig. 7d) is not achieved directly through difference in thrust generated by the rotor as roll and pitch are, but instead through a difference in torque in the rotation speed of rotors spinning in opposite directions. For example, as shown in Fig. 7d, higher rotation speed for rotors 1 and 4 allow the aircraft to yaw clockwise. Because a net positive torque counter-clockwise causes the aircraft to rotate clockwise due to Newton's second law of motion.

Attitude, in respect to orientation of a quadcopter, can be expressed by its angular velocities of each axis $\Omega = \left[\Omega_\phi, \Omega_\theta, \Omega_\psi\right]$. The objective of attitude control is to compute the required motor signals to achieve some desired attitude Ω^*.

2.2. A vehicle type Quadrotor helicopter

This work presents a study of the dynamics for a vehicle type Quadrotor helicopter. This one consists of a central body and four beams joined it. Each beam has a motor with two rotating wings at the far extreme. The body is formed by a box with batteries and on-board computers for control and avionic functions. The wings give sustentation to the vehicle and the possibility of controlling the orientation and translation of the system. The dynamic model of the vehicle takes into account the dynamics of the rotating wings and results in a non-linear system. It is made a simplification by linearization of the nonlinear and unstable model for the Quadrotor attitude and it is designed a LQR (Linear Quadratic Regulator) control with integral effect to track reference paths for the roll, pitch and yaw angles.

Model description. Figure 8 shows the Quadrotor and its reference frame which is represented with the rotational transformation of the Roll-Pitch-Yaw Euler angles.

Euler angles - Roll (ϕ), Pitch (θ) and Yaw (ψ) - are defined as reference frame *x, y, z* rotations around *Z*, y' and x'' in the amounts ψ, θ and ϕ respectively, as can be seen in Fig. 8.

The translational and rotational accelerations for the Quadrotor aerial vehicle can be written as according with Newton-Euler equation.

A quadrotor is agile to attain the full range of motion propelled by four rotors symmetrically across its center with smaller dimension and simple fabrication, unlike a conventional helicopter with complicated mechanism. Generally, it should be classified as a rotary-wing aircraft according to its capability of hover, horizontal flight, and vertical take-off and landing (VTOL). A quadrotor helicopter is a highly nonlinear, multi-variable, strongly coupled, underactuated, and basically an unstable system (6 DOF with only 4 actuators), which acts as preliminary foundation for design of control strategy. Many controllers have been presented to overcome the complexity of the control resulting from the variable nature of the aerodynamic

forces in different conditions of flight. The treatments to the vehicle dynamics, based on some simplistic assumptions, have often ignored known aerodynamic effects of rotorcraft vehicles. In the case of hovering and forward flight with slow velocity, those assumptions are approximately reasonable.

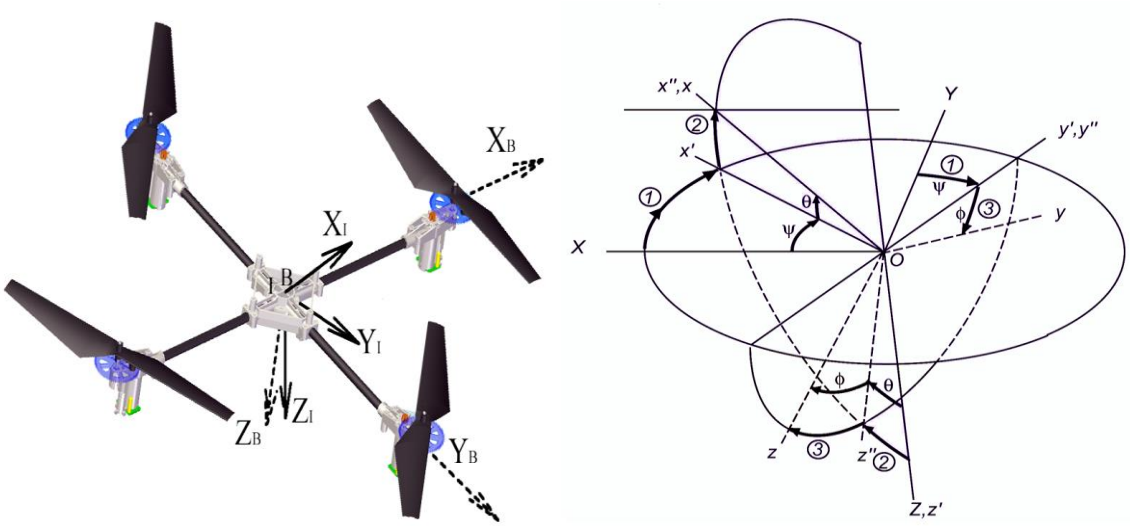

(a) (b)

Fig. 8. (a) Reference frame in Quadrotor; (b) Definition of Roll, Pitch and Yaw angles

When aggressive maneuvers such as fast forward and heave flight actions, VTOL, and the ground effect appear, the dynamics of quadrotors could be influenced significantly under these aerodynamic force and moment. It is shown that existing techniques of modeling and control are inadequate for accurate trajectory tracking at higher speed and in uncertain environments if aerodynamic influence is ignored. The model incorporated with a full spectrum of aerodynamic effects that impact on the quadrotor in faster climb, heave, and forward flight has become an area of active research with considerable effort focusing on strategies for generating sequences of controllers to stabilize the robot to a desired state.

2.3. Characteristics of Quadrotor

Typically, the structure of a quadrotor is simple enough, which comprises four rotors attached at the ends of arms under a symmetric frame. The dominating forces and moments acting on the quadrotor are given by rotors driven with motors, especially BLDC motors. According to the orientation of the blades, relative to the body coordinate system, there are two basic types of quadrotor configurations: plus, and cross-configurations shown in Fig. 9.

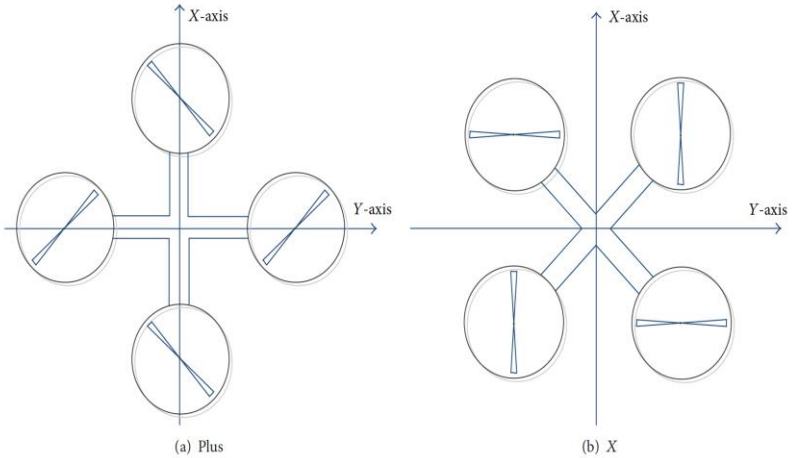

Fig. 9. Plus and X - quadrotor configurations

In the plus configuration selected by most of the quadrotors, a pair of blades, spinning in the same clockwise or counter-clockwise direction, are fabricated on x and y coordinates of the body frame coordinate system, such as the assemble of the Draganflyer XPro. On the contrary, a different cross-configuration is adopted by some other quadrotors, such as the Converta-wings model A, the Piasecki PA-39, or the Curtiss-Wright VZ-7AP, in which there is no rotor at the front or the rear but instead two rotors are on the right side and two on the left. In contrast with the plus configuration, for the same desired motion, the cross-style provides higher momentum which can increase the maneuverability performance as each move requires all four blades to vary their rotation speed. However, the attitude control is basically analogous.

It is the configuration of a quadrotor that shows the inherent characteristics. Basic control sequences of cross-configuration are shown in Fig. 10.

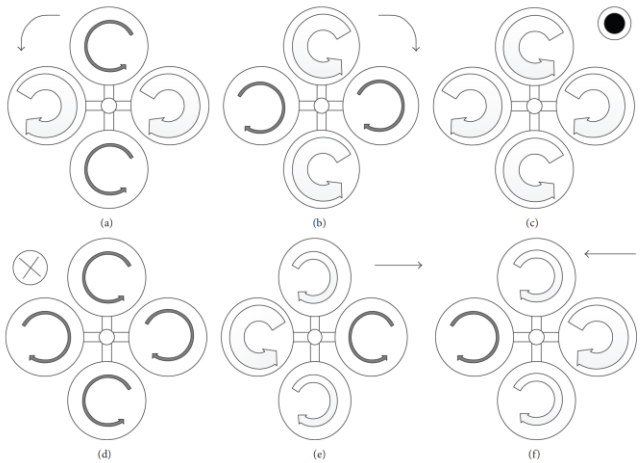

Fig. 10. Quadrotor dynamics: (a) and (b) difference in torque to manipulate the yaw angle (Ψ); (c) and (d) hovering motion and vertical propulsion due to balanced torques; (e) and (f) difference in thrust to manipulate the pitch angle (θ) and the roll angle (ϕ)

The quadrotor's translational motion depends on the tilting of rotorcraft platform towards the desired orientation. Hence, it should be noted that the translational and rotational motion are tightly coupled because the change of rotating speed of one rotor causes a motion in three degrees of freedom. This is the reason that allows the quadrotor with six degrees of freedom (DOF) to be controlled by four inputs; therefore, the quadrotor is an underactuated system.

In principle, a quadrotor is dynamically unstable and therefore proper control is necessary to make it stable. Despite of unstable dynamics, it is good for agility. The instability comes from the changing rotorcraft parameters and the environmental disturbances such as wind. In addition, the lack of damping and the cross-coupling between degrees of freedom make it very sensitive to disturbances.

3. 6-DOF Airframe Dynamics

Dominating methods as Euler-Lagrange formalism and Newton-Euler formalism are applied to model the dynamics for an aircraft. It has been noted that the Newton-Euler method is easy to be understood and accepted physically despite of the compact formulation and generalization shown by Euler-Lagrange formalism. Nevertheless, two methods are consistent for the description of dynamics. That is to say, it is indicated that after a speed transform matrix the Lagrange equation is an expression form of the second Newton Law.

3.1. Euler-Lagrange Formalism

The generalized coordinates of the rotorcraft are given as: $\mathrm{q} = (x, y, z, \psi, \theta, \phi) \in \mathbb{R}^6$, where $(x, y, z) = \xi \in \mathbb{R}^3$ denotes the position of the mass center of the quadrotor relative to the inertial frame and $(\psi, \theta, \phi) = \eta \in \mathbb{R}^3$ are the three Euler angles (resp., yaw, pitch, and roll), under the conditions

$(-\pi \le \psi \le \pi)$ for yaw, $(-\pi/2 \le \theta \le \pi/2)$ for pitch, and $(-\pi/2 \le \phi \le \pi/2)$ for roll, which represent the orientation of the rotorcraft (see Fig. 11).

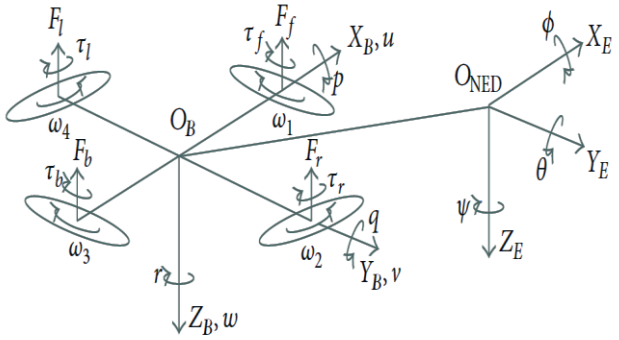

$$L(\mathrm{q},\dot{\mathrm{q}}) = T_{\text{trans}} + T_{\text{rot}} - U, \qquad \dot{\xi}^T \dot{\xi} + \frac{1}{2}\dot{\eta}^T J \dot{\eta} - mgz_E = \frac{m}{2}$$

Fig. 11. Quadrotor's body-fixed and inertial coordinate systems

Naturally, translational and rotational coordinates are obtained from the model
$\xi = (x, y, z) \in \mathbb{R}^3, \quad \eta = (\psi, \theta, \phi) \in \mathbb{R}^3.$

The translational and the rotational kinetic energy of the rotorcraft are $T_{\text{trans}} = \frac{m}{2}\dot{\xi}^T\dot{\xi}$, $T_{rot} = \frac{1}{2}\dot{\eta}^T J \dot{\eta}$, where *m* denotes the mass of the quadrotor. $J = \mathbf{W}^{\mathrm{T}}\mathrm{I}\mathbf{W}$ is the moment of inertia matrix in the inertial coordinate system after being transformed from the body frame, by matrix **W:**

$$\mathbf{W} = \begin{bmatrix} -\sin\theta & 0 & 1 \\ \cos\theta\sin\psi & \cos\psi & 0 \\ \cos\theta\cos\psi & -\sin\psi & 0 \end{bmatrix}.$$

The only potential energy to be considered is the gravitational potential given by $U = mgz_E$.

The Lagrangian of the rotorcraft is

$$L(q,\dot{q}) = T_{\text{trans}} + T_{\text{rot}} - U, \qquad \dot{\xi}^T \dot{\xi} + \frac{1}{2}\dot{\eta}^T J \dot{\eta} - mgz_E = \frac{m}{2}.$$

The full rotorcraft dynamics model is derived from the Euler-Lagrange equations under external generalized forces: $\frac{d}{dt}\frac{\partial L}{\partial \dot{q}} - \frac{\partial L}{\partial q} = (F_\xi,\ \tau)$, where $F_\xi = R\hat{F}$ is the translational force applied to the quadrotor due to the throttle control input, $\tau \in \mathbb{R}^3$ represents the pitch, roll, and yaw moments and *R* denotes the rotational matrix $R(\psi,\theta,\phi) \in$ SO(3), which represents the orientation of the rotorcraft relative to a fixed inertial frame. Since the Lagrangian contains no cross-terms in the kinetic energy combining $\dot{\xi}$ and $\dot{\eta}$, the Euler-Lagrange equation partitions into two parts. One obtains

$$m\ddot{\xi} + \begin{pmatrix} 0 \\ 0 \\ mg \end{pmatrix} = F_\xi, \qquad J\ddot{\eta} + \dot{J}\dot{\eta} - \frac{1}{2}\frac{\partial}{\partial \eta}\left(\dot{\eta}^T J \dot{\eta}\right) = \tau.$$

And the last equation in general form as $J\ddot{\eta} + C(\eta,\dot{\eta})\dot{\eta} = \tau$, where $C(\eta,\dot{\eta})$ is referred to as the Coriolis terms and contains the gyroscopic and centrifugal terms.

3.2. Newton-Euler Formalism

Typically, it is necessary to define two frames of reference, each with its defined right-handed coordinate system, as shown in Fig. 11. *X*, *Y*, and *Z* are orthogonal axes of the body-fixed frame with its correspondent body linear velocity vector $\vec{V} = \begin{bmatrix} u & v & \omega \end{bmatrix}^T$ and angular rate vector $\vec{\Omega} = \begin{bmatrix} o = p & q & r \end{bmatrix}^T$. Another one is an Earth-fixed inertial (also known as navigation) coordinate system $E = \left(X_E, Y_E, Z_E \right)$ with which initially the body-fixed coincides. The attitude of the quadrotor, expressed in terms of the Euler angles ϕ (roll), θ (pitch), and ψ (yaw), is evaluated via sequent rotations around each one of the inertial axes. Herein, a reference frame by O_{NED} (North-East-Down) denotes an inertial reference frame and O_B a body-fixed reference frame.

Generally, a quadrotor is considered as a rigid body in a three-dimensional space. The motion equations of a quadrotor subject to external force $F \in \mathbb{R}^3$ and torque $\tau \in \mathbb{R}^3$ are given by the following Newton-Euler equations with respect to the body coordinate frame $B = \left(X_B, Y_B, Z_B \right)$:

$$\begin{bmatrix} mI_{3\times 3} & 0 \\ 0 & I \end{bmatrix} \begin{bmatrix} \dot{V} \\ \omega \end{bmatrix} + \begin{bmatrix} \omega \times mV \\ \omega \times I\omega \end{bmatrix} = \begin{bmatrix} F \\ \tau \end{bmatrix}.$$

The rotorcraft orientation in space is presented by a rotation *R* from *B* to *E*, where $R \in SO(3)$ is the rotation matrix:

$$R = \begin{bmatrix} \cos\psi\cos\theta & \left(\sin\phi\sin\theta\cos\psi - \cos\phi\sin\psi\right) & \left(\cos\phi\sin\theta\cos\psi + \sin\phi\sin\psi\right) \\ \sin\theta\sin\psi & \left(\sin\phi\sin\theta\sin\psi + \cos\theta\cos\psi\right) & \cos\phi\sin\theta\cos\psi \\ -\sin\theta & \sin\phi\cos\theta & \cos\phi\cos\theta \end{bmatrix}.$$

With the transformation *R*, the first equation assessing the translational dynamics can be written in *E*: $m\ddot{\xi} = RF - mgZ_E$. Recall the kinematic relationship between the generalized velocities $\dot{\eta} = \left(\dot{\phi}, \dot{\theta}, \dot{\psi} \right)$ and the angular velocity $\Omega = W\dot{\eta}, \ W \in \mathbb{R}^{3\times 3}$. Defining a pseudo-inertia matrix $I\left(\eta\right) = JW$ and a Coriolis vector $C\left(\eta, \dot{\eta}\right) = I\dot{\eta} + W\dot{\eta} \times I\dot{\eta}$; one can obtain

$$m\ddot{\xi} = RF - mgZ_E, \quad I\left(\eta\right)\ddot{\eta} + C\left(\eta, \dot{\eta}\right) = \tau.$$

This model has the same structure as the one obtained by the Euler-Lagrange approach, in which the main difference is the expressions of *I* and *C*, which are more complex and more difficult to implement and to compute in the case of the Euler-Lagrange method. It is important to note that this model is common for all aerial robots with six degrees of freedom.

4. Basic Dynamic Model of a Quadrotor

This section introduces the basic quadrotor dynamic modeling with rigid body dynamics and kinematics. This model, based on the first order approximation, has been successfully utilized in various quadrotor control designs so far.

In the first place, some assumptions are reasonable and essential shown as follows: (i) The structure is supposedly rigid. (ii) The structure is supposedly symmetrical. (iii) The CoG (center of gravity) and the body fixed frame origin are assumed to coincide.

4.1. Dynamic Model of a Quadrotor

As we know, Newton second law is applied to the translational motion in inertial frames. From the equation of Coriolis, one can obtain

$$m\frac{\mathrm{dv}}{\mathrm{d}t_i} = m\left(\frac{\mathrm{dv}}{\mathrm{d}t_b} + \omega_{b/i} \times \mathrm{v}\right) = \mathrm{f},$$

where m is the mass of the quadrotor, $\mathbf{f}^b \triangleq \left(f_x \; f_y \; f_z \right)^T$ is the total force applied to the quadrotor, and **v** is the translational velocity. $\omega_{b/i}$ is the angular velocity of the airframe with respect to the inertial frame. Since the control force is computed and applied in the body coordinate system, and since ω is measured in body coordinates, and abovementioned equation is expressed in body coordinates, where $\mathrm{v}^b = \left(u, v, \omega\right)^T$ and $\omega_{b/i} = \left(p, q, r\right)^T$. For rotational motion, Newton's second law state is $\frac{\mathrm{dh}}{\mathrm{d}t_i} = \frac{\mathrm{dh}}{\mathrm{d}t_b} + \omega_{b/i} \times \mathrm{h} = \mathrm{m}$, here **h** is the angular momentum and **m** is the applied torque. $\mathbf{h}^b = \mathbf{J}\mathbf{w}^b_{b/i}$; **J** is the constant inertia matrix. The quadrotor is essentially symmetric about all three axes, which implies that $\mathbf{J} = \mathrm{diag}(J_x, J_y, J_z)$. Given $\mathbf{m}^b \triangleq \left(\tau_\phi, \tau_\theta, \tau_\psi\right)^T$, which denote the rolling torque, the pitching torque, and the total yawing torque, are induced by the rotor thrust and rotor drag acting on the airframe.

The six-DoF - model for the quadrotor kinematics and dynamics can be summarized as follows:

$$\begin{pmatrix} \dot{x} \\ \dot{y} \\ \dot{z} \end{pmatrix} = \begin{pmatrix} \cos\theta\cos\psi & \left(\sin\phi\sin\theta\cos\psi - \cos\phi\sin\psi\right) & \left(\cos\phi\sin\theta\cos\psi + \sin\phi\sin\psi\right) \\ \cos\theta\sin\psi & \left(\sin\phi\sin\theta\sin\psi + \cos\phi\cos\psi\right) & \left(\cos\phi\sin\theta\sin\psi - \sin\phi\cos\psi\right) \\ \sin\theta & -\sin\phi\cos\theta & -\cos\phi\cos\theta \end{pmatrix} \begin{pmatrix} u \\ v \\ \omega \end{pmatrix},$$

$$\begin{pmatrix} \dot{u} \\ \dot{v} \\ \dot{\omega} \end{pmatrix} = \begin{pmatrix} rv - q\omega \\ p\omega - ru \\ qu - pv \end{pmatrix} + \frac{1}{m}\begin{pmatrix} f_x \\ f_y \\ f_z \end{pmatrix}, \quad \begin{pmatrix} \dot{\phi} \\ \dot{\theta} \\ \dot{\omega} \end{pmatrix} = \begin{pmatrix} 1 & \sin\phi\,\mathrm{tg}\,\theta & \cos\phi\,\mathrm{tg}\,\theta \\ 0 & \cos\phi & -\sin\phi \\ 0 & \sin\phi/\cos\theta & \cos\phi/\cos\theta \end{pmatrix} \begin{pmatrix} p \\ q \\ r \end{pmatrix},$$

$$\begin{pmatrix} \dot{p} \\ \dot{q} \\ \dot{r} \end{pmatrix} = \begin{pmatrix} \frac{J_y - J_z}{J_x} qr \\ \frac{J_z - J_x}{J_y} pr \\ \frac{J_x - J_y}{J_z} qr \end{pmatrix} + \begin{pmatrix} \frac{1}{J_x}\tau_\phi \\ \frac{1}{J_y}\tau_\theta \\ \frac{1}{J_z}\tau_\psi \end{pmatrix}.$$

Equation of the quadrotor kinematics and dynamics is a full nonlinear model for a quadrotor, in which the complex dynamics is shown obviously, such as strong nonlinearity like the multiplication between system states, intensive coupling among the variables, and the multivariable features intuitively, that imposes the difficulties on the controller design and, on the other hand, attracts great interest of research.

4.2. Forces and Moments

The forces and torques that act on the quadrotor are primarily due to gravity and the four propellers shown in Fig. 3. The steady-state thrust F_i generated by a hovering rotor (i.e., a rotor that is not translating horizontally or vertically) in free air coincides with $-\mathrm{Z_B}$ axis. The total force acting on the quadrotor is given by $F = F_f + F_r + F_b + F_l$. The rolling torque, the pitching torque, and the total yawing torque are given by

$$\tau_\phi = l\left(F_l - F_r\right), \quad \tau_\theta = l\left(F_f - F_b\right), \quad \tau_\psi = \tau_r + \tau_l + \tau_f + \tau_b.$$

The gravity force acting on the center of mass is given by

$$f_g^b = R^T \begin{pmatrix} 0 \\ 0 \\ mg \end{pmatrix} = \begin{pmatrix} -mg\sin\theta \\ mg\cos\theta\sin\phi \\ mg\cos\theta\cos\phi \end{pmatrix}.$$

Equation of the quadrotor kinematics and dynamics shows strong coupled dynamics: the speed change of one rotor gives rise to motion in at least 3 DoF. For instance, the speed decrease of the right rotor will roll the craft to the right under the imbalance between left and right lift forces, coupled with the rotorcraft's yaw

to the right due to the imbalance in torque between clockwise and counter-clockwise, so the translation changes direction toward the front. Nevertheless, in some cases that the rotating movement is slight, the Coriolis terms *qr*, *pr*, and *pq* are small and can be neglected. So, the dynamics of the quadrotor is simplified and given as

$$\ddot{x} = \frac{\left(-\cos\phi\sin\theta\cos\psi - \sin\phi\sin\psi\right)}{m}F, \quad \ddot{y} = \frac{\left(-\cos\phi\sin\theta\sin\psi + \sin\phi\cos\psi\right)}{m}F,$$

$$\ddot{z} = \frac{g - \cos\phi\cos\theta}{m}F, \qquad \ddot{\phi} = \frac{1}{J_x}\tau_\phi, \qquad \ddot{\theta} = \frac{1}{J_y}\tau_\theta, \qquad \ddot{\psi} = \frac{1}{J_z}\tau_\psi$$

This model is shown in Fig. 12.

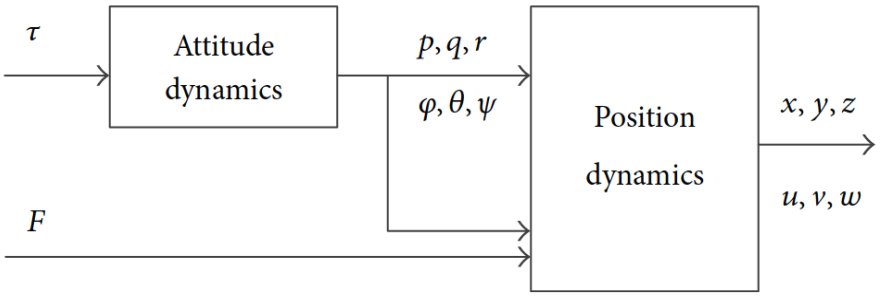

Fig. 12. Simplified block diagram of the quadrotor's dynamics.

Note that the attitude of quadrotor is changed, subject to the input τ (moment) produced by each rotor. However, the *position* / *altitude* dynamics block is affected by T_f and angle variables.

Remark. Intuitively, Fig. 11 gives the insight of the dynamic of the quadrotor that the angles and their time derivatives do not depend on translation components, whereas the translations depend on angle (and not on angular velocities). Based on the characteristics of the dynamics, a quadrotor control problem can be split into two distinct control problems, the inner attitude / altitude loop designed for stability and tracking of desired Euler angles and the outer *X*, *Y*, and *Z* position loops for regulating the vehicle position. State space equations are applied in the control design and system identification generally. Hence, the nonlinear system of a quadrotor is illustrated as the formulation, which is described in different manner as following: $\dot{x} = f(x) + g(x)U$, where $x = \left[x, y, z, \psi, \theta, \phi, u, v, \omega, p, q, r\right]^T$, $\mathrm{y} = \left[x, y, z, \psi\right]^T$, $U = \left[F, \tau_\phi, \tau_\theta, \tau_\psi\right]^T$. Herein the output *y* is composed of *x*, *y*, *z* and ψ is for the trajectory track, but if for the hovering control, $y = \left[\phi, \theta, \psi, Z\right]^T$ should be selected because in translation movement shown above, the three state variables, *x*, *y*, and *z*, are subordinated to the same control parameter *F*; hence only one state is controllable and the others are subjected to the controlled translation and angular motions.

4.3. Gyroscopic Torques

At the normal attitude, namely, Euler angles are zero and the axes of the rotors with higher speeds spinning are coincident with the z_B axis of the robot frame. However, while the quadrotor rolls or pitches, the direction of the angular momentum vectors of the four motors is forced to be changed. A gyroscopic torque will be imposed on the airframe that attempts to turn the spinning axis so that it aligns with the precession axis. It is noted that no gyroscopic torque occurs with rotation around the z_B axis (yaw) because the spin and precession axes are already parallel. The gyroscopic (inertial) moment is modeled as ${}^b_G\vec{M}_J = \sum_{i=1}^{4} J_r \left(\omega_{b/i} \times \begin{bmatrix} 0 \\ 0 \\ 1 \end{bmatrix} \right) \Omega_i$, where J_r is the gyroscopic inertia, namely, that of the rotating part of the rotor and $\boldsymbol{\Omega}_i$ is the angular rate of the rotor *i* (*i* =1, 2, 3, 4).

4.4. Quaternion Differential Equations

A problem, so called gimbal lock, will appear with the Euler angle θ close to $\theta = 90^0$, and then the Roll angle ϕ loses its meaning. To overcome this problem, the quaternion method, which offers a mathematical notation that allows the representation of three-dimensional rotations of objects in 4D space, is selected to be the alternative remedy. Above it gives a quaternion dynamics description and proposes a new quaternion-based feedback control scheme for the attitude stabilization of a quadrotor aircraft. In fact, every parameterization fails to fully represent rigid body pose in every case. That is to say, Euler angles cannot globally represent rigid body pose owing to the gimbal lock, whereas quaternions cannot define it uniquely. Although researchers proved the effectiveness of using quaternions to describe aircraft dynamics, Euler angles are still the most common way of representing rigid body pose.

5. Aerodynamic Effects

In most of research projects, quadrotor dynamics has often ignored known aerodynamic effects of rotorcraft vehicles because only the stability while hovering is the aim, as stated before. At slow velocities, such as while hovering, this is indeed a reasonable assumption. However, in case of demanding flight trajectories, such as fast forward and descent flight maneuvers, as well as in the presence of the In Ground Effect, these aerodynamic phenomena could significantly influence quadrotor's dynamics, and the performance of control will be diminished if aerodynamic effects are not considered, especially in situations where the aircraft is operating at its limits (i.e., carrying heavy load, single engine breakdown, etc.). Acting as a propulsion system, the aerodynamics of rotors plays the most important role on the movement of the quadrotor excepted with gravity and air drag with respect to the airframe. The kinematics and dynamics of the rotors are fairly complex, resulting from the combination of several types of motion, such as rotation, flapping, feathering, and lagging; normally the last two items are neglectable. The theoretical models based on the blade element theory (BET) combined with momentum theory (MT) show many advantages such as more flexible, simpler, and convenient in contrast with the empirical models based on empirical data typically obtained in the wind tunnel.

Note that the application of helicopter theory to a quadrotor is not straightforward for the reason of many important differences between conventional helicopter and quadrotor. In order to address the issues, the specific research, with the aim at a quadrotor vehicle, is necessary to establish full model with complex dynamics subject to aerodynamic forces and moments. Many works on rotor model have been done based on the results obtained for conventional helicopters. Blade flapping is of significant importance in understanding the natural stability of quadrotors. Since it induces forces in the x - y rotor plane of the quadrotor, the underactuated directions in the dynamics, high gain control cannot easily be implemented against the induced forces. On the other hand, the total thrust variation owing to the vertical maneuver also imposes nonignorable influence on the quadrotor behavior.

5.1. Total Thrust

In case of simplifications in aerodynamic effects, the assumption that a rotor's thrust is proportional to the square of its angular velocity is the most common consideration. However, it is proved that this assumption about rotor's thrust is especially far from reality in the cases of non-hovering regime. The helicopter literatures give analysis about many effects on the total thrust in more detail, in which translation lift and change of angle of attack act as the two related effects. As a rotorcraft flights across translation, the momentum of the airstream induces an increase in lift force, which is known as translational lift. The angle of attack (AOA) of the rotor with respect to the free-stream also influences the lift, with an increase in AOA increasing thrust, just like in aircraft wings.

Applying blade element theory to quadrotor construction, the expression for rotor thrust T is given:

5.2. Mathematical model of 4-rotor UAV and conventional control

When approaching the mathematical description (model) of a multi-rotor UAV in terms of control, it should be noted that the development of a dynamic UAV model, including its simulation, is necessary first of all in the aspect of testing in the field of navigation and control in a closed room. The model of dynamic equations, describing the character and position of the 4-rotor UAV, is a fundamentally immovable construc-

tion with six degrees of freedom and four entrances. The dynamic model of the 4-rotor UAV system has already been thoroughly examined, tested and compared to the actual flight test results, therefore, it is sufficiently reliable to be used as a basis for simulating the model, without taking into account the additional effects that have been investigated in other publications. The modeling process was started from defining the reference system, with two systems being distinguished in this respect. One of them is the gravitational system (associated with the Earth), described with axes 0_e, X_e, Y_e, Z_e, allowing to determine the motion of the aircraft (not taking into account the rotation of the Earth). In turn, the second system is the structural system (associated with aircraft), described in the axes 0_b, X_b, Y_b, Z_b, allowing to determine (in connection with the gravitational system) the spatial position of the aircraft. The above systems are presented in the figure below (Fig. 13).

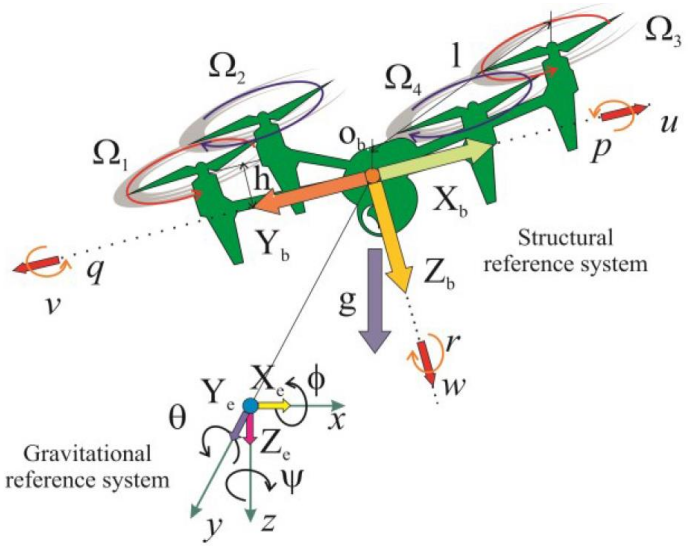

Fig. 13. Gravitational and structural reference system

The current position of the 4-rotor UAV is described by three axes (*x*, *y*, *z*) with the center of gravity, taking into account the gravitational system. In turn, the current height is shown in the form of three *Euler* angles (ψ,θ,ϕ). These three angles are respectively defined by a deviation($-\pi \le \psi < \pi$), inclination ($-\frac{\pi}{2} \le \theta < \frac{\pi}{2}$) and tilting ($-\frac{\pi}{2} \le \phi < \frac{\pi}{2}$).

In the next stage of the modeling process was the presentation of kinematic links (relationships) relating to motion and rotation in the inertial reference system, connected with the Earth to the structural system. Derivatives with respect to time for angles (ψ,θ,ϕ) can be expressed in the following form: $\left[\dot{\psi},\dot{\theta},\dot{\phi}\right]^T = N(\psi,\theta,\phi)\omega$, in which $\omega = \left[p,q,r\right]^T$ are angular velocities with reference to the reference construction system, and $N(\psi,\theta,\phi)$ is a matrix that can be represented in the following form: $N(\psi,\theta,\phi) = \begin{bmatrix} 0 & \sin\phi\sec\theta & \cos\phi\sec\theta \\ 0 & \cos\phi & -\sin\phi \\ 1 & \sin\phi\tan\theta & \cos\phi\tan\theta \end{bmatrix}$. It should be noted that this matrix depends only on (ψ,θ,ϕ) and is reversible in case if its limits on (ψ,θ,ϕ) are maintained. Analogously, a derivative with respect to the position time (*x*, *y*, *z*) can be represented as: $\left[u,v,w\right]^T = V_0\omega$, where $V_0 = \left[u_0,v_0,w_0\right]^T$ is the current speed of the 4-rotor UAV in relation to the reference system associated with the Earth. Determining by $V = \left[u,v,w\right]^T$ - the current UAV speed, expressed in the reference system associated with the aircraft, then *V* and V_0 are bound by: $V_0 = R(\psi,\theta,\phi)V$, where: $R(\psi,\theta,\phi)$ - describe the UAV rotation matrix:

$$R(\psi,\theta,\phi)=\begin{bmatrix}\cos\theta\cos\psi & (\sin\phi\sin\theta\cos\psi-\cos\phi\sin\psi) & (\cos\phi\sin\theta\cos\psi+\sin\phi\sin\psi)\\ \cos\theta\sin\psi & (\sin\phi\sin\theta\sin\psi+\cos\phi\cos\psi) & (\cos\phi\sin\theta\sin\psi-\sin\phi\cos\psi)\\ -\sin\psi & \sin\phi\cos\theta & \cos\phi\cos\theta\end{bmatrix}$$

For the purpose of creating a UAV model, fully compatible with reality, later in the article some simplifications have been made, among others: the UAV structure is rigid and symmetrical, the rotors are rigid, and the product of the inertia matrix and the Earth effect can be omitted.

5.3. Aerodynamic forces and moments acting on the rotor

Using the theory of the blade element, it is possible to calculate the forces acting in parallel and perpendicular to the rotor shaft and the moments acting on the shaft and the rotor hub. Assuming that the rotors are rigid, forces acting parallel to the rotor shaft are defined as a rotor series T, while forces acting perpendicular to the rotor shaft act on the rotor hub H. In addition, there are two moments acting on the rotor: moment of resistance M_Q and torque M_R. It can be assumed that the lifting force acting on the rotor blade is an order of magnitude higher than the resistance. Correspondingly, forces and moments will be defined for each rotor. In the Fig. 14, forces and moments are illustrated.

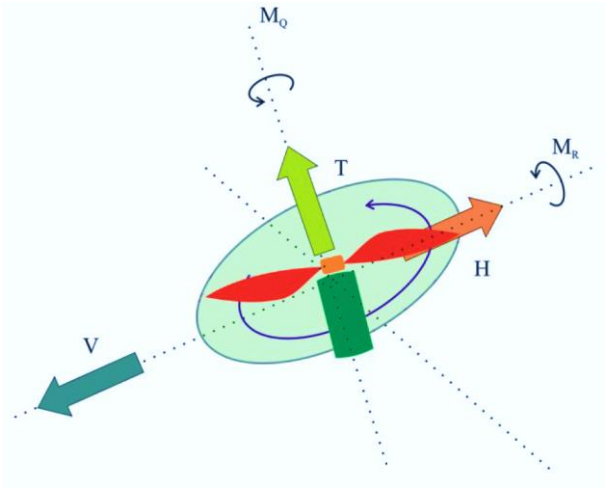

Fig. 14. Forces and moments affecting the equator

Thrust results from the forces acting on all components of the blade perpendicular to the rotor shaft, which can be written as abovementioned.

6. Propeller-type Wall-Climbing Robots

Many efforts have been exerted in the robot's field which have ability to climb vertical plane. The result was various types of climbing robots. These robots have a mixture of different principles of adhesion and locomotion in many applications. Propeller thrust is one of the approaches that has been developed to generate the required adhesion force to enable the robot to climb walls. Due to the promising merits of this principle, the current paper deals with propellers-type wall-climbing robots (PRWCRs) and introduces features, applications and challenges for these robots. PRWCRs are examined depending on a set of given requirements. This mechanism has connected between two wide fields: wall climbing robots (WCRs) and unmanned aerial vehicles (UAVs). For many reasons, each adhesion mechanism has more preference than others for a specific job; surface requirements are the main of them. Propeller-type WCRs are less affected by the nature of the surface, where it can climb many types of vertical planes: smooth, rough, and ferromagnetic or not. On the other hand, most of the introduced designs still have some problems and issues like transition operation, mission time and payload limitation [5-8].

The tendency of utilizing mobile robots is growing every day in different tasks such as construction, maintenance, wall- scrub of high-rise structures and screening of storage tanks, and damage observation of different structures like ships and planes. Therefore, many studies have been conducted along years to devel-

op wall-climbing mechanisms. In general, wall climbing techniques such as magnetic, suction module, adhesive material, mechanical claws, micro spine, pneumatic-adhesion, and tether-supported climbing methods are dependent on the material or the shape of the surface. In addition to the mentioned pneumatic mechanisms, the thrust force of propellers is used as another approach. Propellers-type wall-climbing robot (PRWCR) utilizes the propellers thrust in order to generate the required adhesion force.

As is well known, the climbing robot applications grow with its ability to handle different types of surfaces. Therefore, these robots will have a wide utilization in both military and civilian areas. This Item presents the current state-of-the-art in robots which used aerodynamic thrust generated from propellers, to climb vertical planes. Usually, research categorizes the WCRs according to the locomotion type as well as the adhesion mechanism. Since this work is restricted to a certain type of adhesion principle, the robots will be classified according to their flying ability. The locomotion types of climbing robots and the other adhesion principles was well explained above.

6.1. The general requirements in PRWCR design

Climbing robots must have the ability to mobilize on the interested vertical plane and ability to hold itself to the surface when it is necessary. To achieve that, the design of PRWCR should meet some conditions:

- *Drag torque*. As mentioned before, in PRWCRs, the required adhesion force is generated by high speed rotors and a drag torque is produced as a result of this mechanism. This torque tends to rotate the robot body around the spinning axis of rotors in opposite direction. This undesirable torque should be eliminated by a reversal torque of another rotor system spinning in counter direction. Therefore, the number of rotors, their speed and distribution on the robot body should be taken into account.

- *Transition*. Transition operation in PRWCT has two definitions depending on the flying ability of the robot. Where, in drone –type wall climbing robot (DRWCR) deals with "*transition between modes*": flying and climbing. For non-flying robot, it is concerned with "*transition between planes*": like ground, wall and ceil. The design of these robots (non-flying type) will determine whether the robot can achieve one or more of these transition modes. Also, the robots differ in their degree of dependence on propeller thrust during this process. It is assumed that transition happens gradually to minimize the collision intensity with the wall.

- *Weight*. Lightweight is an important condition in the flying world; therefore, steadily shrinking microprocessors, actuators and sensors cause an explosion in the popularity of MAV (micro air vehicles). Moreover, a robot that functions in two distinct locomotory modes must make compromises in weight and complexity to accommodate the different interaction mechanics, control approaches, and power requirements for the modes of interest. Therefore, a key research problem in the design of PRWCR robots is to maximize the ratio between thrust output and vehicle weight.

- *Safety.* To meet the requirement of increasing the robot payload capacity, the electric power needs to be maximized and the rotor size and motor power should be increased. This design with a high-power motor and a large rotor would be unsafe to serve in urban area, where serious injuries on the civilian can occur because of the rotor. Therefore, a rotor guard must be designed for protection and to prevent any unintentional contact with the structure. The guard is preferred to be made with a shock-absorbing material with elastic characteristic like EPP (Expanded Polypropylene). In addition, the robot must attach to the protection rope to protect the hardware of the robot in case of losing contact with the surface especially in the performance testing phase. To increase the mission life, the power can be supplied and sensor signal and the control signal can be uploaded through the safety rope if that does not conflict with the task.

- *Coefficient of friction*. The value of friction coefficient is a crucial issue in wall climbing as its value will specify the maximum allowable total weight of robot. As it is known, flying vehicles depend on the weight of the system only, while, in climbing, in addition to the weight, surface topography is also a significant parameter. The vehicle will have sticking capability on the wall, if the total weight is less than the product of the total thrust force and friction coefficient between the wall and the wheels of mobile robot. If the frictional force is higher than the critical value, the mobile robot will hold on the wall. To maximize friction between wheels and the surface and to minimize dependence on rotor thrust force, wheels themselves should have adhesive characteristics. The required level of thrusters

is different according to the change of friction coefficient. In the real world, it is hard to estimate precisely the friction coefficient at the contact point. Therefore, it could overuse energy or fail to climb the wall.

- Although too much thrust force produces high frictional force but it is inefficient in terms of energy consumption. To be efficient, the total thrust force should be controlled according to the robot pose, disturbance, and frictional coefficient and then the robot can operate longer. The accelerometer signal can be processed and thrust force is controlled to prevent slip, where detecting a drop in vertical acceleration means change in friction value mostly.
- *Power source*. In PRWCR, the required thrust force is generated by brushless DC motors. These motors consume a high-level current. Therefore, it is necessary to secure a sufficient current to power these motors and to provide a stable power source to feed the motors driving wheels.
- *Center of mass location*. In addition to flying requirements, the robot center of mass (COM) should be close as possible to the centroid of the body. Also, in climbing mode, it is more favorable to keep COM at the nearest point to the wall.

6.2. Drone-type wall-climbing robot (DRWCR)

In the past years, multi-propeller aerial robots have attracted a great interest in civilian and military applications because of their versatile usability and wide possibility. At a recent time, many researchers have examined the potential of drone to be a wall climber. The flying - climbing mechanism depends on the ground vehicle system and the multi-rotor system. Quadrotor is the most common in DRWCR. It is a well-known VTOL (Vertical Take-Off and Landing). The fundamental idea of DRWCR depends on utilizing propeller thrust to provide the essential force to adhere on the wall in addition to flying. Based on the combination of the wheel drive force and thrust force, the friction between the wheel and the wall can be maximized.

Encouragement. Many reasons have encouraged the development of DRWCRs; these are:

1. Other adhesion principles cannot be applied to various material walls. Meanwhile, these robots are independent of nature of target wall and do not need any extra infrastructures.

2. Both functions, flying and climbing, are mutually supportive. Thus\, unique environmental conditions like powerful wind gusts often make it difficult for traditional drones to hover to complete the task. Therefore, landing on wall is necessary until the situation be suitable. On the other hand, if the robot lose contact with wall during climbing for any unexpected accidents, the robot can simply fly safely to the ground. Also, some types of infrastructure inspections require stable contact with structures, and drones are undesirable for these missions.

3. DRWCR can reach the remote target directly without the need for crawling along the surface, which makes these robots have high maneuverability. Furthermore, flying enables the robot to overcome the obstacles that exist on walls such as window frames.

4. A single multi-purpose robot is cost-effective than multiple dedicated robots. Finally, as a result of the close correlation, all works in UAV like innovative designs and researches can be employed to improve DRWCRs design, also saving cost, time and increase the effectiveness.

Aspects demand attention. Below some aspects should be taken into consideration:

1. The average mission time of the conventional MAVs is about few minutes. But actually, many tasks in urban area demand more than that.

2. Multi-function robots may have complexity in both structure and control. But for applications, where falling to death at any moment is a serious concern, it is probably worth all the hassle.

3. Although flying, perching and crawling operations confer advantages and provides synergies. It also can double the weight of the vehicle, so it is not easy to be installed with heavy or complicated equipment, in addition to a corresponding deterioration in flying performance. Therefore, efficient design with light weight and high strength is essential.

6.3. PRWCRs model analysis with flying ability

Most PRWCRs have ability to fly. This section presents and discusses these robots. Contact-based interaction on the side of a UAV was formerly introduced by Albers [1] where a quadrotor is endowed with an additional propeller oriented horizontally to generate a normal force to a vertical wall for cleaning purposes. No specific design for a manipulator is proposed but rather the addition of a cleaning tool/brush to use such force output for cleaning purposes, as illustrated in Fig. 15.

Fig. 15. An unmanned aerial vehicle with a fixed brush tool on the side deployed for window cleaning

The collaboration between Disney Research Zurich and ETH produced VertiGo, as shown in Fig. 16, a.

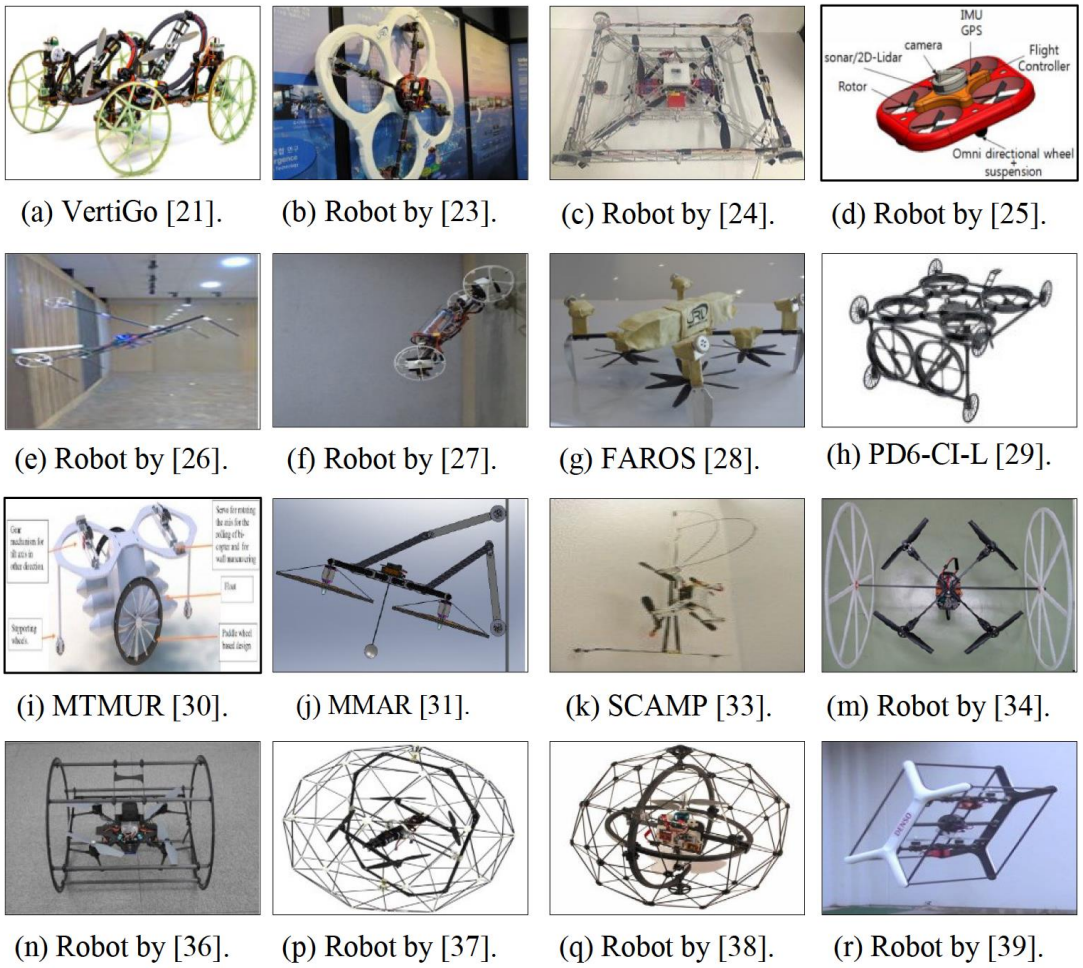

(a) VertiGo [21]. (b) Robot by [23]. (c) Robot by [24]. (d) Robot by [25].

(e) Robot by [26]. (f) Robot by [27]. (g) FAROS [28]. (h) PD6-CI-L [29].

(i) MTMUR [30]. (j) MMAR [31]. (k) SCAMP [33]. (m) Robot by [34].

(n) Robot by [36]. (p) Robot by [37]. (q) Robot by [38]. (r) Robot by [39].

Fig. 16. Propeller-type wall climbing robots with flying ability

VertiGo has the ability to achieve smooth transitioning between the ground and the wall. The robot chassis contains two adjustable tilting rotors of two degrees of freedom and has four passive wheels supplied with a suspension system. The front pair of wheels is steerable. The two rotors generate the force required to drive and attach the robot on floor and wall. Based on the information of a 6-axis IMU as well as two infrared distance sensors mounted in front of the robot, the onboard controller then devises the best positions for all actuators to achieve the orders of human operator with RC (remote control).

For this design, it can be concluded:

- The reaction torque of the two propellers is hard to eliminate by each other. Because the rotational speed and tilt angle of each rotor are not necessarily identical. These two parameters are directly related with robot pose requirements.
- Including braking system was essential, especially on robots which use passive wheels and adopting aerodynamic force for navigation. Without this system, it is difficult to track a desired path accurately by these robots.
- In general, robots with passive wheels are less affected by surface friction coefficient.
- To drive this robot, it is need to control eight actuators. Therefore, this system is relatively complicated.

Related works and comments. Peculiarities of models presented in Fig. 16 are following:

- KAIST (Korea Advanced Institute of Science and Technology) has much support in the field of wall-climbing robot with a drone platform, called CAROS (Climbing Aerial Robot System). Figure 16,b shows a prototype of drone equipped with four wheels which work as a differential drive framework. According to robot design, the transition operation must happen very quickly without depending on any external structure, where the pose change is impossible to be achieved slowly, as it is easy to expect that the robot will fail. Therefore, a harsh impact on the wall surface is an inevitable consequence of this operation. To overcome this problem, a suspension system was adopted to reduce the collision intensity. For structural health monitoring (SHM) application, a wireless vision sensor is fixed to take the pictures of the structural wall surface.
- Shin et al. presented the micro-aerial vehicle type wall-climbing robot mechanism for the same application, as shown in Fig. 16,c. Feasibility has been seen with simulations and indoor experiments. This robot still has some problems that the system was unsuited for outdoor environment due to the vibration effect. The vibration effect makes the sensor data of IMU unstable. As a result, it makes control very hard. Also, the robot was prepared for planar walls and climbing the flat only.
- To address the difficulty and risk of wind blades inspection, a new design was proposed, as shown in Fig. 16,d which is a quadcopter with four wheels. It can fly, stick, and move on a vertical and non-flat surface. However, the proposed design was verified only throughout simulations where the manufacturing and the outdoor experiments were proposed as a future work.
- Previous KAIST climbing drones regard only the friction force generated by thruster's normal force. To mitigate this problem, W. Myeong et.al. proposed a drone equipped with a rotary arm for climbing, as shown in Fig. 16,e. The arm has two free rotating wheels at both sides, while driving wheels are installed at the front part of the robot body. The main concept of the proposed system is to control the thruster direction to the wall. In addition, the arm allows soft attaching and detaching to the wall. Another purpose of the rotary arm mechanism is to moderate the pose change speed. According to the angle of the arm, the robot can change its pose against the wall and divide the thrust force into two components; one is the force that compensates gravity and another is the force that generates friction. Comparing with a previous version of CAROS, the climbing speed is 8 times higher with a lower level of thrust force. However, the additional weight of a rotation arm and its high moment of inertia are unfavorable factors in flying vehicles. This technique pushes COM of the robot away from the wall, which makes robot highly affected by the disturbances of the surroundings such as winds. Also, the work of some sensors requires keeping a constant distance to a target object which cannot be secured with this mechanism.
- W. MYEONG and H. MYUNG developed another approach to address the problem of fast landing speed in previous version of KAIST climbing robots. The proposed design-based X-configuration

quadcopter and a tilt-rotor mechanism is combined into the two axes such that the front thrusters and the rear thrusters are paired respectively, as shown in Fig. 16,f. This mechanism showed a soft landing on wall, and reduced the thrust force for climbing. However, the rotors configuration caused an air obstruction which led to losing about 25% - 75% of front rotors thrust.

- Also, KAIST developed FAROS (Fire-proof Aerial Robot System), as shown in Fig. 16,g. The robot can help in firefight work by detecting fire or people, as the robot platform is covered with aramid fiber. The robot design is based on CAROS to navigate through narrow space in case of fire disaster. When meeting narrow space, the robot is expected to pass through by climbing the wall.
- To keep constant distance with wall surface which is an essential condition for inspection tools and considering a low level of frictional coefficient in the real world, Prodrone Co., Ltd. has developed PD6-CI-L. It is a self-propelling surface-clinging drone that is able to inspect both ceilings and vertical surfaces for the civil infrastructure inspection market. It has an L-shape with six rotors: two rotors in horizontal plane and four rotors in vertical plane. Three pairs of wheels are distributed to the corner and both ends of the body to move on the surface during inspection, as shown in Fig. 16,h. PD6-CI-L does not inspect while hovering, but instead uses negative pressure to cling directly to the target surface. PD6-CI-L design has advantage in providing safe, smooth and quick transition from flying to climbing mode and between wall and ceiling. Yet, the L – shape keeps the COM away from target surface. This system contains high numbers of actuators, which requires a high degree of coordination between these motors to keep continuous contact with the surface.
- MTMUR was introduced to address the problems of inability of the robot to adapt to different terrains and reduce the cost of multiple dedicated robots. MTMUR is a bi-copter, multipurpose robot capable of flying, and moving on ground and water with wall climbing ability, as shown in Fig. 16,i. During climbing, the thrust of the propeller is directed in the opposite direction by changing the axis of rotation. Once the robot sticks against the wall, with the help of differential driven wheels, it moves over the surface of the wall. As the robot is supposed to deal with different terrains, MTMUR needs to satisfy many requirements, which may affect the general performance of the system such as mission time. However, MTMUR is only a suggested design and has not been implemented yet.
- Figure 16, j shows an aerial manipulation, MMAR, a robot designed by X. Ding et.al. The structure of MMAR includes two identical manipulators and four fixed-pitch propellers. Each manipulator has two joints. The two joints rotate in a plane, which is normal to the main body of MMAR. The two manipulators of MMAR can be utilized as undercarriage when it touches down on land, and can be used as arms for operating when it is in flight mode. When MMAR is in wall-climbing mode, the robot will be in contact with the surface by two wheels at the end of manipulators and the manipulators can be used as legs to support it on the wall. The manipulators succeeded to provide safe and gradual transition to climbing mode, and control the thrust force applied to wall. But it has disadvantages of complexity of the control system, increasing the total weight and inertia of the robot, and coupling interference with the robot body. Also, during climbing, the arms joints must be powered enough to withstand the applied torque by the propellers thrust force.
- The limitation in battery life can be compensated by perching mechanism, where the rotors are turned off to extend the life of the battery. From this viewpoint, Pope et al. introduced SCAMP, as shown in Fig. 16,k. A small robot is SCAMP that combines a commercial quadrotor (Crazyflie2) with perching and climbing ability inspired by various animals like insects and birds. It can fly outdoors and land on unprepared walls made from stucco or concrete. However, the perching and climbing gears reduce the UAV's flight time by 30%. SCAMP has two more different things than other DRWCR, the positive one: it is quiet during climbing, while the negative is that SCAMP still has restriction to the surfaces because of the use of spine for moving. Also, it has long tendons and the propellers are installed at the robot side which is close to the surface. Therefore, there is possibility that those propellers or the tendons hit the surface with unexpected protrusion.
- To protect the blades from touching the structures and keep a fixed distance with the target that will be inspected, a novel UAV with two wheels is introduced. This robot was designed for bridge inspections, and was tested on real bridges, as shown in Fig. 16,m. The robot consists of two passive wheels that are installed on both sides of the quadcopter. While testing the robot, two problems in the structure appeared: (1) the wheels and wheel shaft strength were low because these parts are built to be light as possible, (2) due to the design of wheels, the air resistance increases.

- The treatment of these issues were proposed, as shown in Fig. 16,n. Where a quadcopter is installed inside a cage of cylindrical shape. Two spoke less ring-shaped wheels were attached to the protector. Those wheels could rotate freely with respect to the quadcopter. This design reduces the air resistance and improves durability of the UAV.
- There are some related designs introduced by Mizutani et al. and Briod et al. who developed a UAV inside a spherical shell rotating passively, as shown in Figs 16,p,q). Their studies demonstrate that the spherical cage is efficient for flying through complex structures or in limited areas, where touching the surrounding environments is possible. However, according to these designs, it is difficult to constrain the locomotion on the plane surface because of protector shape. That means, operating the UAV manually is still hard.
- Also, the cage interferes with camera, which is installed on the UAV to capture images, due to passive rotating of protector around the robot. Kawasaki et al. improved a dual connected bi-Copter. This UAV can effectively climb walls and run on the ground, but it requires a special flight controller and additional actuators to work because of its very specific structure, as shown in Fig. 16,r.

6.4. Unable to fly PRWCRs

This category of robots represents the oldest WCR introduced. Hence, Nishi in 1991 developed a climbing robot adopting the thrust force of two rotors. The tilt angle of these rotors can be manually adjusted, as shown in Fig. 17,a. The robot was also equipped with two pairs of passive and non-steerable wheels. Therefore, the robot cannot make turn.

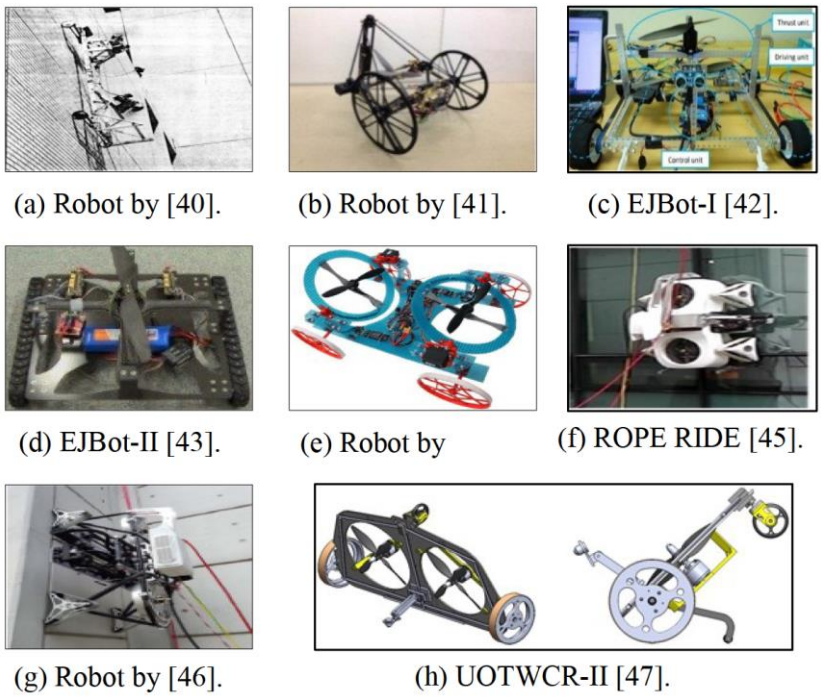

Fig. 17. Unable to fly propeller-type wall climbing robots

Related works and comments. Peculiarities of models presented in Fig. 17 are following:

- Kinki University developed climber robot which has two driving wheels and adjustable tilt rotor with a pair of AC brushless motors. These motors were attached to the set of coaxial propellers to provide the adhesion force. Also, two rollers with dampers and springs were connected to the rear caster wheels at the end of the robot, as shown in Fig. 17(b). By changing the tilt angle of the thruster, the robot has the ability to reversibly vary its configuration top and bottom. This merit is helpful for quick and small turn in narrow environments with floors or walls. Because the thrust force was insufficient, the climbing test on a vertical wall is not carried out for this model. But it is experimented that the robot will not slip down on an inclined wall with an angle of 60 degrees. On the other hand, the caster wheel which has been used in the robot may hinder the robot movement, since it is difficult to steer this type of wheel on wall and its direction will be submitted to gravity effect.

- For visual inspection, EJBot-I and EJBot-II were introduced, as shown in Figs 17,c,d respectively. The experimental tests showed that robots are able to overcome obstacles up to 40mm. EJBot-II used a flat track to increase the friction. Nevertheless, tracks are not efficient during transition between ground and wall, as the flat tracks configuration would not pass inner corners without a high torque.
- Kasetsart university produced climbing robot which is broadly similar to VertiGo with less capabilities, as shown in Fig. 17,e. Where, this robot design does not include steering and suspension system. Also, each rotor has one degree of freedom. The advantage of this design is simple to control than VertiGo but with sacrifice the maneuverability and other operations like transition, turning and flying.
- Many studies have been conducted to develop infrastructure-based wall-climbing robots because of their features. ROPE RIDE is one of these robots with cable-driven and triangular tracks to climb obstacles. Two propeller thrusters are adopted, in order to efficiently keep the contact with the wall during climbing, as shown in Fig. 17,f. But ROPE RIDE has relatively heavy weight, huge size and trouble in detachment/ attachment of the cleaning unit. To improve these shortcomings, a new platform has been introduced, as shown in Fig. 17, g. Where, the overall weight and size of the new platform are decreased approximately by 50% and 17% respectively.
- University of Technology (Baghdad/Iraq) presented UOTWCR-II. It is a novel design of PRWCR which can climb different surfaces. UOTWCR-II design supported two ground navigation modes.
- Also, these modes provided two various transitioning scenarios between ground and wall, as shown in Fig. 17,h. To extend the robot mission life, the limitation on power source was overcome by proposing mechanism of perching.

Finally, Table 3 presents a complete list of climbing robots according to the above-mentioned classes with application tasks.

Table 3. A complete list of climbing robots PRWCRs

ROBOT	Country	Application	Locomotion	Flying ability
VertiGo	US/ Switzerland	Filming as well as a fun product	Passive wheel	yes
-	South Korea	SHM	Driven wheel	yes
-	South Korea	SHM	Driven wheel	yes
-	South Korea	Inspection of wind blades	Driven wheel	yes
-	South Korea	SHM, maintenance and visual inspection	Driven wheel	yes
-	South Korea	-	Passive wheel	yes
FAROS	South Korea	Firefight	Driven wheel	yes
PD6-CI-L	Japan	Civil infrastructure inspection\ shipment	Driven wheel	yes
MTMUR	India	Search and rescue, mapping, surveillance military purposes	Driven wheel	yes
MMAR	China	-	Legged wheel	yes
SCAMP	US	Rescue, Surveillance	Feet with small spines	yes
-	Japan	-	Passive wheel	yes
-	Japan	SHM	Spokeless wheel	yes
-	Japan	SHM	Spherical Shell	yes
-	Switzerland	search and rescue	Spherical Shell	yes
-	Japan	Multiple fields	Passive wheel	yes
-	Japan	Wall inspection	Passive wheel	no
-	Japan	-	Driven wheel	no
EJBot-I/II	Egypt	Inspection of petrochemical vessels	Wheel /track	no
-	Thailand	-	Passive wheel	no
ROPE RIDE	South Korea	Cleaning/painting/ inspection	Rope	no
-	South Korea	Cleaning/painting/ inspection	Rope	no
UOTWCR-II	Iraq	Multiple fields	Driven wheels	no

According to their flying ability, which represents the most distinguishing feature for this type of climbing robots, propeller -type climbing robots applied in different applications and have been classified. Also, a comprehensive table of the studied robots has been presented along with their applications, locomotion mechanism, and flying ability.

From this study [9-14], it can be stated that:

- Propeller-type WCR has no surface constraints and can trade with various kinds of surfaces: smooth, rough, and magnetic and non-magnetic. Yet, it has restriction in life assignment.
- PRWCRs have large-scale applications and can be found with most types of locomotion principles.
- DRWCRs are multimodal robots and have intrinsic ability to maneuver, but this was at the expense of significantly increasing in the vehicle weigh, besides the adverse impact in flying mode performance.
- Despite the success of adjusting the thrust direction in variable-tilt rotor mechanism, it has drawbacks in complexity, and serious coupling interference with motion of the main body.
- The drones inside cages have non continuous contact to the wall surface and it can be said that they hover near the wall more than climbing.
- The main disadvantage of dispensing with the driving wheels and entirely dependent on aerodynamic system for moving is that it is hard to have a precise gait.
- Generally, propeller-type WCRs face challenges in transition operation, and the proposed solutions often lead to increasing the total weight, inertia, the height of robot center of mass and system complexity.

7. Wall-Climbing Robot Using Propulsive Force of Propeller – Example

According to the adsorption method, described above, the robot can be divided into vacuum negative pressure, magnetic adsorption, bionic, and reverse thrust. According to the movement mode, it can be divided into wheel, crawler, foot, and wheel-foot compound movement. Vacuum negative pressure robots are mostly used on walls with relatively smooth walls and are widely used for cleaning glass walls, but the adsorption surface is prone to gas leakage, and the wall surface has high requirements for flatness and almost no obstacle crossing ability. Magnetic adsorption wall mobile robots are mostly used for the inspection of the inner and outer surfaces of large metal utensils. They are only suitable for the walls of magnetically conductive materials, which have poor wall adaptability. Bionic wall mobile robots are based on the use of bionics to make adhesive materials and attach them to the wall contact structure to adhere to the robot; biomimetic nature animal foot characteristics for paste or hook. This adhesive material is not self-cleaning, the driving control is complicated with fuzzy hook. In recent years, many scholars and research institutions have carried out a lot of research on anti-thrust wall adsorption robots. Alkalla Mohamed G and others have successively developed EJBot I and EJBot II, which can be applied to a variety of vertical wall robots. Shin, Jae-Uk and others used a multi-axis rotorcraft to turn around 90_ and attach it to the wall after taking off from the ground. During the attaching movement, the robot body control is more complicated.

This item uses dual propellers as the reverse thrust power unit, and the front wheel differential steering power unit. Design and plan the robot movement from the ground to the wall, analyze the stable adsorption conditions of the robot wall, and carry out the robot's motion performance and adaptability test under different ground/wall environments. According to the reverse thrust of the propeller, the robot makes the robot move forward, backward, and cling to the ground/wall surface stably. The robot is not affected by the contact medium, the shape of the contact surface, whether the contact surface is smooth, and the unevenness of convexity and concave. The robot has a simple structure and control, easy operation, and excellent motion stability.

7.1. Robot design

The robot is composed of a front and rear platform frame, a front wheel drive system, a rear wheel driven system, two rotor power drive unit, a hinge connection unit, a control module, and a communication module. The overall model of the robot is shown in Fig.18.

The rotor power is driven by the paddles installed on the brushless motor, and the brushless motor is installed on the connected fixed frame. The angle of the rotor is adjusted by the steering gear, and the rotor is fixed on the front and back moving platform, respectively. They are what provide the necessary thrust to hold and maneuver ascension while it's on the wall and while it's on the ground. This project uses two 10-inch

propellers because they are smaller and lighter while still providing sufficient thrust. This size propeller also allows for smaller rotating mounts, which ultimately results in a small chassis. n order to control the overall weight of the robot, the body of the robot mostly uses 3D printed parts, and the platform frame is made of a composite of carbon fiber and honeycomb material.

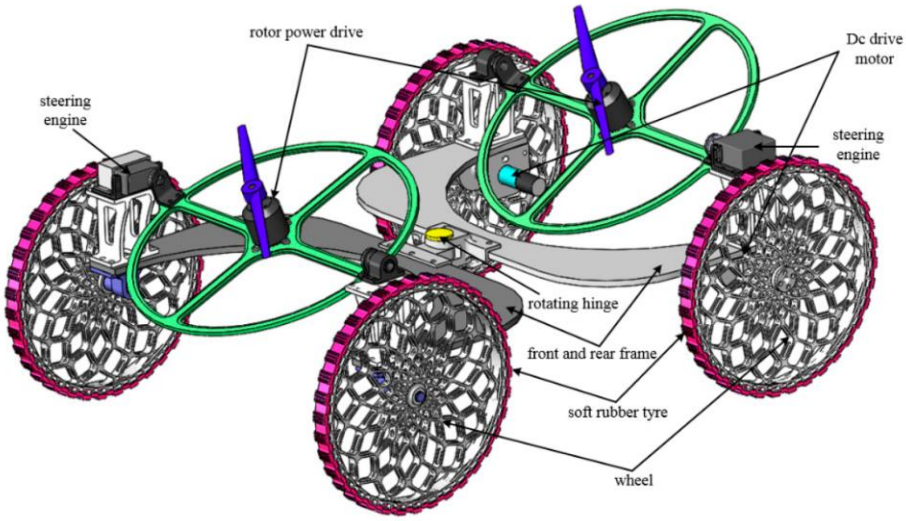

Fig. 18. Overall diagram of multi-mode wall mobile robot

The propeller reverse thrust robot uses the brushless motor to generate the reverse thrust to make the robot obtain the force of adsorption on the wall. By adjusting the change of the tilt angle of the front and rear rotors, the robot produces different motion effects. The robot movement process mainly includes ground/wall moving and turning, ground climbing to the wall, wall-to-wall, and wall-to-ground motion modes. During the movement of the ground/wall, the front drive system of the robot mobile platform drives the mobile platform and the driven system to move forward, backward, and turn. The robot motion plan is shown in Fig. 19.

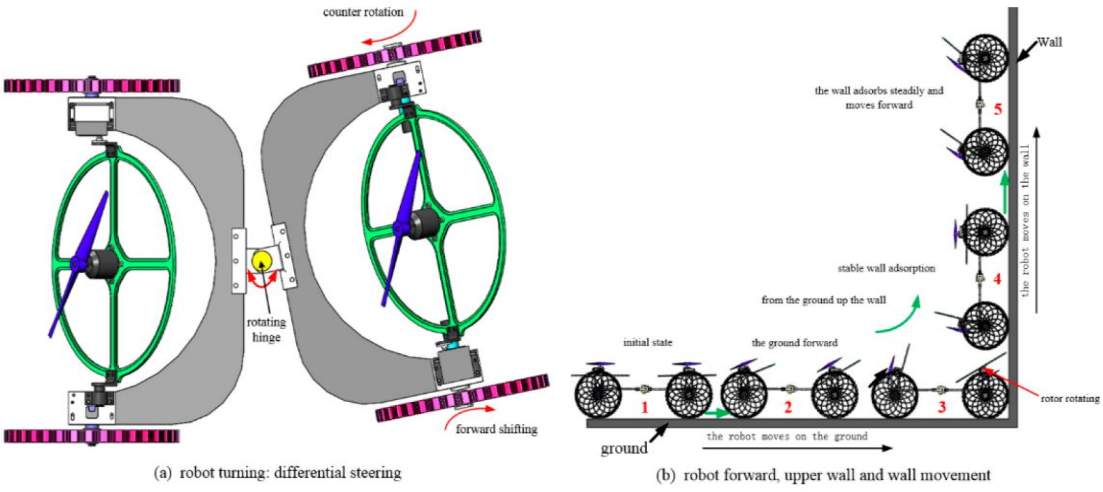

Fig. 19. Example of transfer sequence between walls

Figure 18,a is a schematic diagram of the robot's turning, which is turned by the front wheel drive motor differential speed. Figure 19,b is an example of the robot moving from the ground to the vertical wall. In general, change the tilt angle of the front and rear rotors to adjust the robot's movement posture, and then the moving process of the mobile robot. When the robot approaches the wall from the ground, the front rotor power mechanism rotates 180^0 to generate an upward pulling force perpendicular to the robot's forward direction. The front wheel mechanism can be raised, and under the action of the forward thrust of the rear rotor, the robot transitions from the ground to the wall. When the rear wheel is attached to the wall, the front

propeller changes its angle, and the lift is transformed into the thrust of the suction wall. Under the combined action of the front and rear propellers, the robot sticks and moves on the wall. In order to plan the robot motion process, it is usually necessary to obtain the robot motion state, which must be sensed and planned by some sensors attached to the robot itself.

It is estimated that the propeller output reverse thrust is also proportional to the controller output current. Rotor reverse thrust test experimental device, including battery, digital display tensile tester, brushless motor, paddle, electronic governor, receiver, remote control, etc., as shown in Fig. 19.

Fig. 19. Experimental device for reverse thrust test of pro thrust test of propeller motor

7.2. Robot Electrical System Design

STM32 6-way Arduino is selected as the underlying embedded controller, and the internal measurement unit is IMU (Inertial Measurement Unit). It uses a combination of angular velocity meter and gyroscope sensor to construct a system detection unit to determine the angle and angular velocity of the robot. An Intertia Measurement Unit, which is a combination of accelerometer and gyro sensor, is used to construct the observer system in order to determine the robot angle and angular velocity. Two 60A BLDC ESC is used as a brushless motor driver, which can drive each brushless motor up to 60 A continuous driving current. Two servo motors are used to control the change of the inclination angle of the rotor, two quadcopter motors are used, they need more power to operate. This means a bigger battery is needed. For testing times and run times of around five minutes operating the motors at full speed as well as powering the processor, IMU, and servos, a 4 cell 4000 mAh battery is used. The transmitter/receiver pair is used for long range control of the vehicle. It operates using a 2.4 GHz frequency, which can allow for ranges up to 20 m of control. The receiver outputs a PWM signal to the on-board processor, which then determines the user's desired direction of travel. The electronics system is shown in Fig. 20.

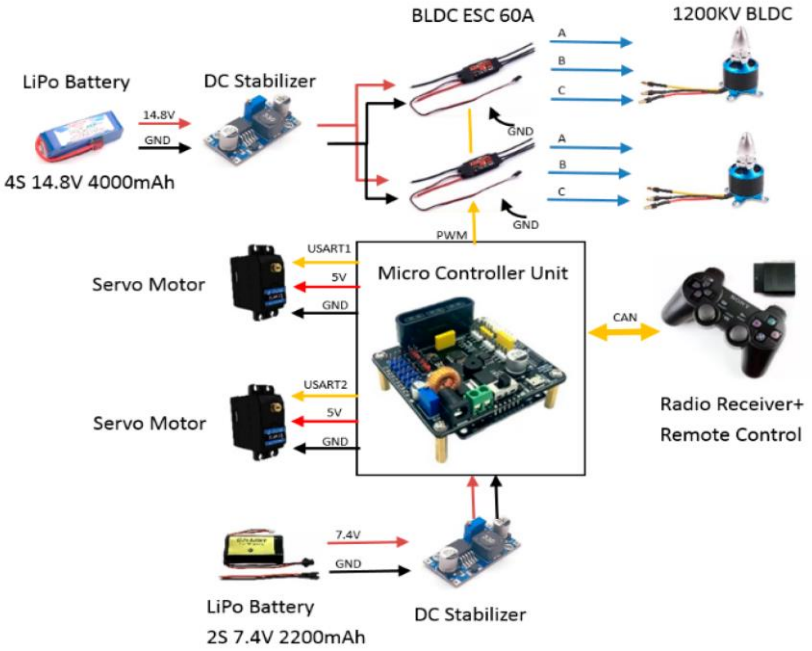

Fig. 20. Electronics system

In order to obtain the maximum traction force of the robot under different tilt angles of the rotor, the horizontal tension value of the mobile platform of the robot in different gears and different rotor tilt angles is measured with a spring tension meter (considering safety and laboratory site restrictions, the maximum gear of the robot is only open during actual measurement to 6 gears, 10 gears are designed), as shown in Fig. 21, the robot traction force measurement under different rotor tilt angles.

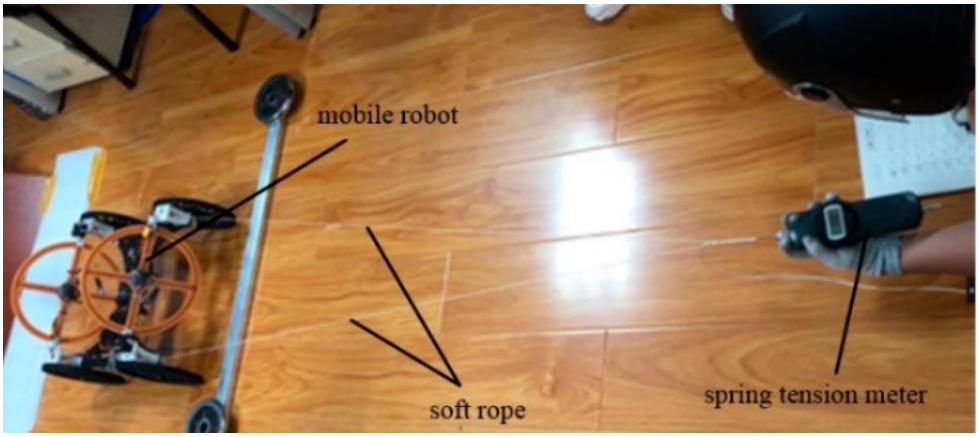

Fig. 21. Robot traction measurement under different rotor tilt angles

As the robot moves from the ground to the wall at a small angle, the robot moves directly to the inclined surface at the initial speed of the ground. When the inclination angle of the bottom plate increases to a certain extent, the robot touches the bottom plate from the ground.

The impact force can easily cause damage to the robot structure, so the small-angle slope ground-to-wall motion test is designed to 45°. As shown in Fig. 22, describe the robot's movement from the ground to 20°, 25°and 45°.

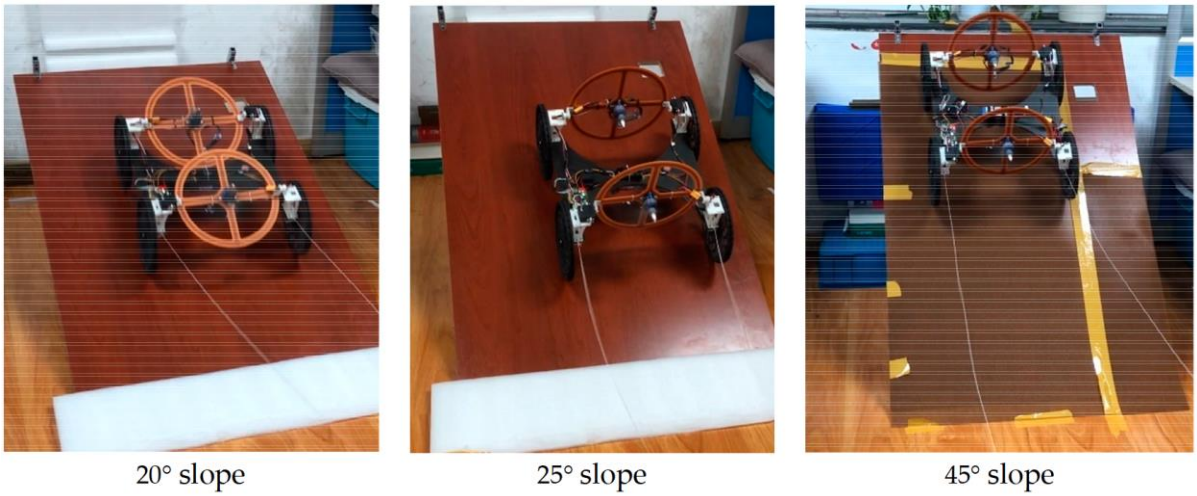

Fig. 22. Robot stable motion test under different slopes

As the angle of the inclined plane increases, a larger rotor inclination angle and blade rotation speed are required.

In order to measure that the robot can be stably attached to the vertical wall, the robot is hoisted on the vertical wall. To prevent the robot from rushing out of the wall, a certain length of soft rope is installed under the robot so that the robot can move within a certain range of the wall. The robot wall surface stable adsorption movement process is shown in Figs 23,a–h. (a) Initial state; (b) Movement start; (c) Rotor tilt angle adjustment; (d) Rotor tilt angle adjusted to 60_, the upper end rope starts to relax; (e) The upper end rope is completely loose; (f) The robot starts to move upwards; (g) The bottom limit rope is straightened, and the robot can be completely adsorbed on the wall; (h) The speed of the blade is reduced, and the robot falls.

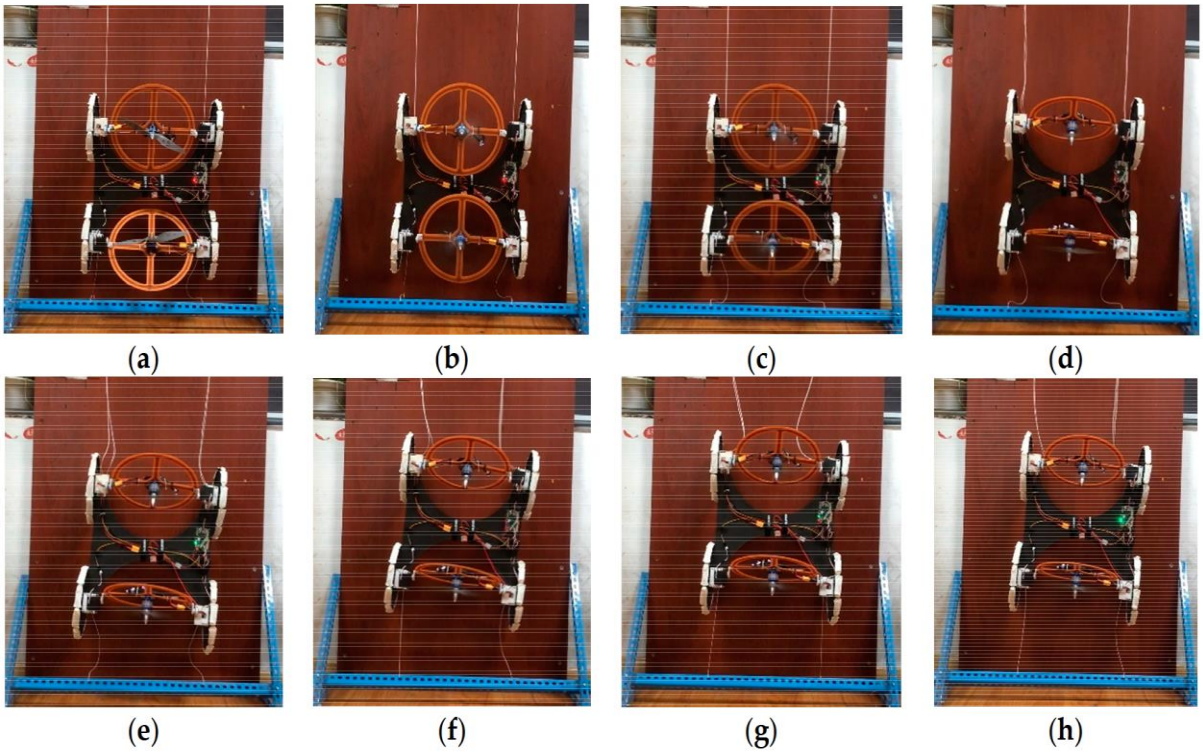

Fig. 23. Stable adsorption movement process of the robot wall [2]

During the test movement, the upper and lower traction ropes in Fig. 23, d–f are in an unstressed state, the maximum rotor speed of the robot is 7 gears, and the robot can stably adsorb on the vertical wall. The smooth progress of the experiment lays a good foundation for carrying out ground to wall compliant control of the robot in the later stage.

A dual-propeller wall-climbing robot that can stably adsorb on a variety of different walls is designed. By analyzing the robot's movement from the ground to the wall and the robot's stable adsorption conditions on the wall, a dual-propeller-type wall mobile robot is produced. The robot climbing experiment under a small slope and the 90^0 slope stable adsorption experiment verified the feasibility of the robot moving stably on the vertical wall.

With regard to the future work, it is significant to build WCRs with more capabilities such as high speed of operation, high energy efficiency, and sufficient payload.

8. Wall-Climbing Drone Capable of Vertical Soft Landing Using a Tilt-Rotor Mechanism - Example

Wall-climbing drones have many applications, including structural health monitoring of civil structures, such as bridges and high-rise buildings, cleaning of solar panels to improve power generation effciency, and airplane visual inspections. For these applications, the drone requires a high-payload capacity, and consequently the size and weight of the drone increase. The drone also should not damage the target structures considering the purpose of its mission. The previous versions of a wall-climbing drone could have high-impact force on the surface where the drone perches and on the platform itself because of the impact caused by a fast pose change and landing speed. In order to overcome this potential risk, a mechanism and a control algorithm for perching on a vertical surface through low-speed pose change are proposed [3].

8.1. Configuration of drone platform

The drone platform is based on an X-configuration quadcopter, and a tilt-rotor mechanism is incorporated into the two axes, such that the front thrusters and the rear thrusters are paired. The vertical soft-landing mechanism using the tilt-rotors is validated by the experimental tests of the prototype. The basic mechanisms and strategies for vertical soft landing and wall-climbing with neccesary symbols description in Fig. 24 introduced.

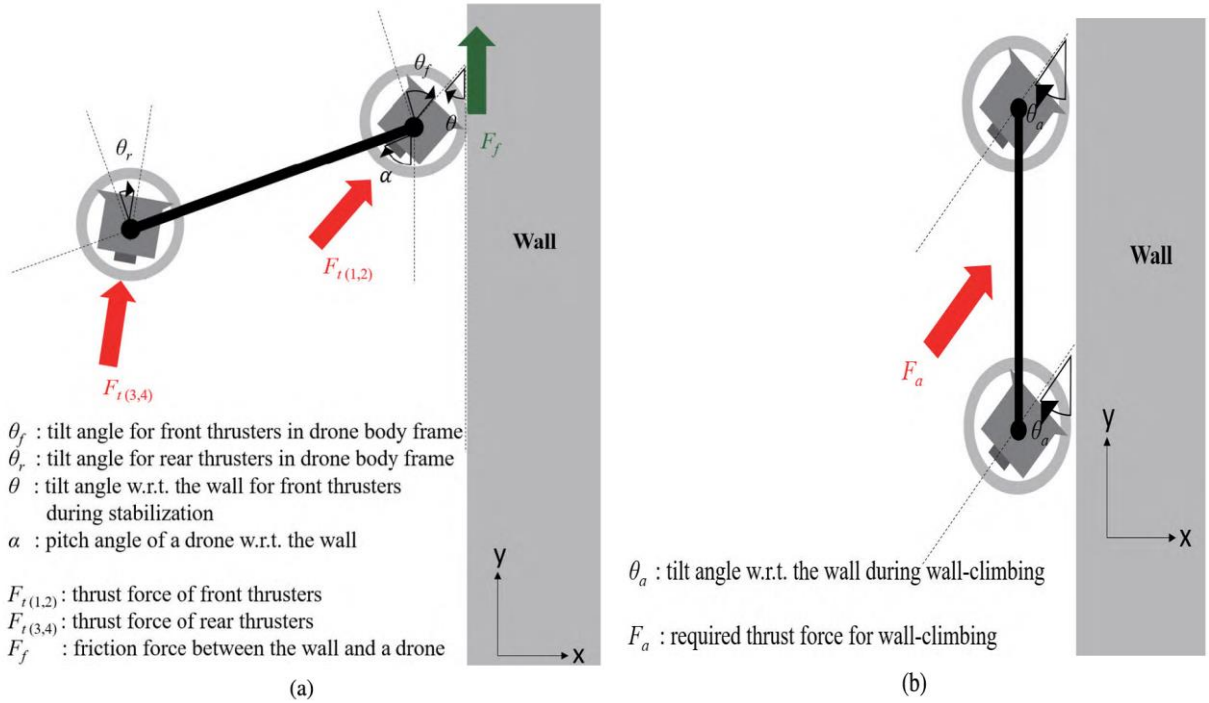

Fig. 24. A free body diagram and used symbols during (a) stabilization process and pose change (b) wall-climbing

The soft-landing procedure is aimed at low-impact perching on vertical walls such as façades of high-rise buildings, and it consists of three steps: stabilization process, pose change, and being ready for wall-climbing (sticking) mode. For perching, the drone changes its pose along the pitch angle direction using only two actuators for the tilt-rotor mechanism. The angular range of the tilt mechanism is 180^0 in order to make

the direction of the thruster normal to the wall when the drone sticks to the wall. Before changing its pose, in order that the first contact point is fixed to the wall and acts as a hinge point, various perching mechanisms such as suction cups and an adhesive gripper were developed. The stabilization method of our proposed system is conceptually similar to the wall-sticking principle of CAROS. Once the drone contacts its head to the wall, it starts to change the tilting angle of thrusters adjacent to the wall, generating frictional force between the drone and the wall. This state is similar to the state of wall-sticking of CAROS except that the remaining thrusters still try to maintain the hovering state of the drone. Without loss of generality, we assume that the wall is perfectly vertical. When the tilting angle, θ, is 90^0 that is, the direction of thrust force is normal to the wall, all the thrust force is used for making frictional force, as in CAROS. This is not a favorable condition with a low friction coefficient because a large normal force is required (see, Remark below). Therefore, assuming that the drone only uses the same level of thrust force as in the hovering state, the drone can maintain the force equilibrium against gravity by changing the tilting angle for stabilization.

Remark. The wall-sticking mechanism is based on the friction force at contact points, which is caused by the normal force to the wall generated by the thrust force for flight, the friction coefficient is a very important factor and the energy efficiency is greatly affected by the unknown friction coefficient. Due to the uncertainty of the surface condition, for example, the irregular shape or various contaminants, ideal condition with a high friction coefficient cannot be assured. For the same reason, when CAROS perches on the wall, assuming a low friction coefficient, the pose of the drone should be swiftly changed with large thrust force to maximize the normal force to the wall. From the viewpoint of protecting the wall and the drone, impact from high speed for perching is not favorable.

Although the tilt mechanism for drones has high potential to broaden the application area, only a few commercial racing drones use tilt mechanism to increase the speed. Because the payload of drones is very limited, an additional mechanism could decrease the operation time and the energy efficiency. Considering these limitations, we aim to develop a tilt-rotor-based wall-climbing drone using a minimum number of actuators. Using only two actuators, the drone is designed to perch on the wall with gentle motion and climb the wall with higher energy efficiency.

Assuming that the drone only uses the same level of thrust force as in the hovering state, the drone can maintain the force equilibrium against gravity by changing the tilting angle for stabilization. The FBD (Free Body Diagram) can be formulated as follows in Fig. 25.

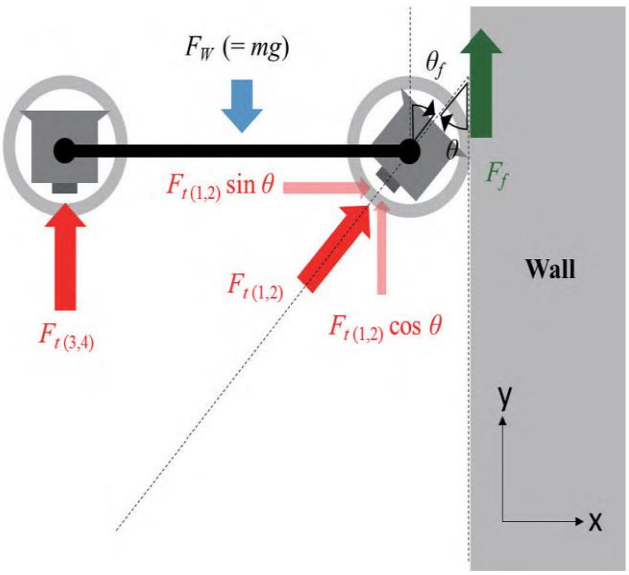

Fig. 25. A free body diagram in the stabilization process

The relationship between the friction coefficient and the required tilting angle is described as following: $\mu = \frac{1-\cos\theta}{\sin\theta}$, where θ is the tilt angle for stabilization.

While the tilting process is performed, a PID (Proportional Integral Derivative)-based flight controller still operates in the same manner as normal flight status. Therefore, if slip-page is detected by measuring the angular acceleration from an IMU (Inertia Measurement Unit), the thrust level at the front side naturally increases. When the ratio of the front thrust to rear thrust is over a specific threshold, the drone stops tilting and proceeds to the next step. The friction coefficient μ is approximately estimated by the maximum tilting angle θ.

Theoretically, if the friction coefficient is 1, the tilting angle can be 90 degrees. However, since this aerial drone plat-form is based on an X-configuration quadrotor (see Fig. 26(a)), the airflow from front thrusters is obstructed by the rear structure of the drone with 90 degrees tilting angle, as shown in Fig. 26(b).

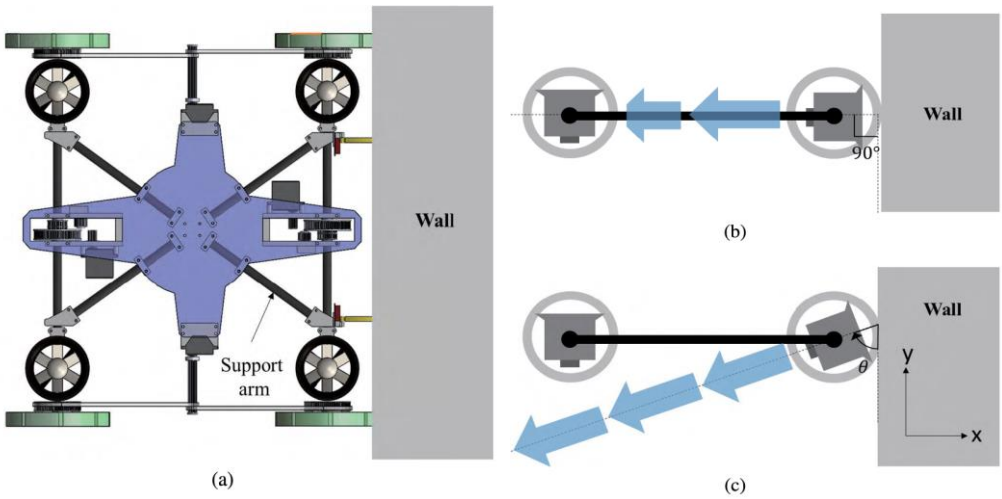

Fig. 26. Obstruction of airflow in an X-configuration quadrotor layout design (a) Top view (b) Side view when tilting angle is 90^0 (c) Side view with different tilting angle

Then it is difficult to deal with accidental slippage with limited angular speed of the tilt-rotor mechanism. Therefore, as in Fig. 26(c), the tilting angle should not be 90 degrees, but rather about 35 to 45 degrees practically, which is also related to the pose change process.

Though stabilization process is not affected by the obstruction of airflow, obstruction is inevitable during pose change process because of the X-configuration design. If the air obstruction occurs at a specific pose of the drone, it defines it as an intersection zone. The range of the intersection zone is determined by θ as shown in Fig. 26(c).

As shown in Fig. 27, to control the tilting angle to the wall, θ, we have to determine the range of intersection zone and other phases as well.

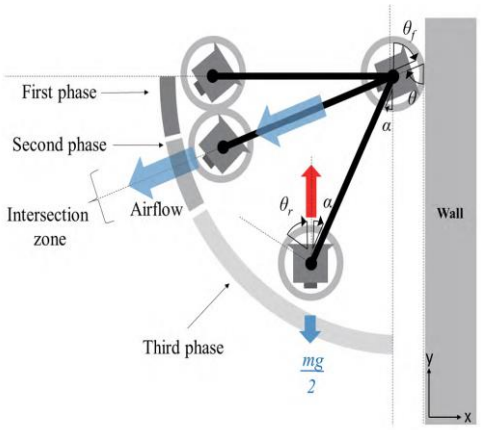

Fig. 27. The pose change process (tail-down) and FBD for the torque. Angle symbols are expressed for the third phase except θ_f for the first phase

Before the second phase of entering the intersection zone, the drone starts to change its pose while maintaining the direction of the forward thrusters against the wall. At the same time, the tilting angle of the tail-side thrusters, θ_r, becomes $(90-\alpha)^0$ as the direction of thrusters becomes vertical where α is the pitch angle of the drone to the wall that can be acquired from the IMU. This posture is advantageous to prevent falling accidents by aligning rear thrusters to the direction of gravity force. With this condition, the angle of the rear thrusters increases as the pitch angle to the wall, α, decreases as follows: $\theta_r = (90-\alpha)^0$. Regarding the range of the intersection zone, θ_r should be close to 90 degrees as the rear thruster direction aligns with the direction of the airflow of thrusters at the front side and prevents the sidewall of the rear thruster from directly blocking the airflow. Under this condition, smaller tilting angle of forward thrusters, θ_f, is better as long as the sticking force to the wall is sufficient. Otherwise, large tilt angle leads to obstruction of the airflow, which can lead to falling by slippage. Another strategy to overcome air obstruction in the inter-section zone is to decrease the duration in the intersection zone by rapidly increasing the angle of the forward thrusters to the wall at the moment of entering the intersection zone, as described in Fig. 27.

After passing the intersection zone, assuming the first contact point is a hinge support, the thrust force $F_{t(3;4)}$ causes a torque and the drone's body leans toward the wall. The torque at the first contact point *A*, T_A, is expressed (se, Fig. 28(a)) as follows: $T_A = l \cdot \left(\frac{mg}{2} \sin\alpha - F_{t(3,4)} \sin\alpha \right)$, where *l* is the body length of the drone.

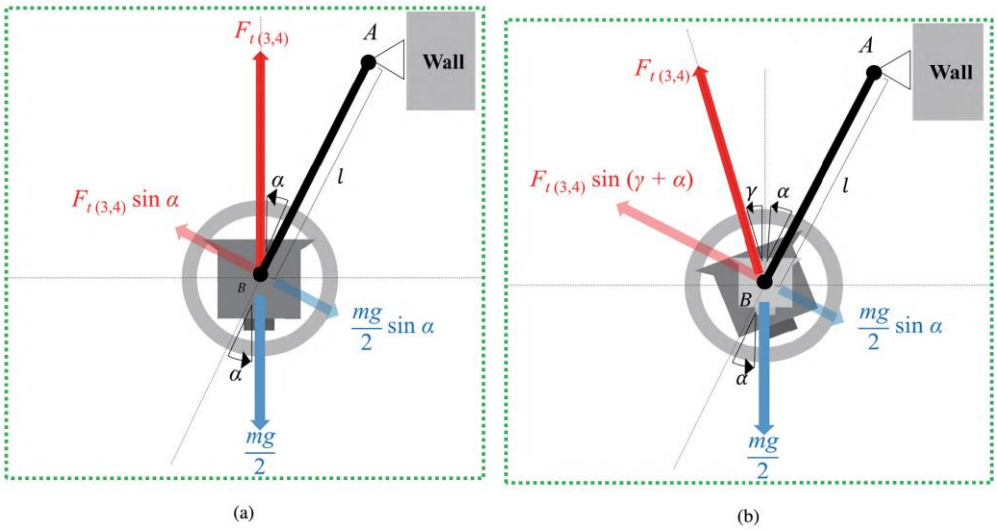

Fig. 28. (a) FBD without pitch offset a

However, as the pitch angle of the body α decreases, the thrust force may not generate the torque for pose change, since T_A approaches to 0 when α approaches to 0. We define pitch offset angle

γ as the additional tilt angle for rear thrusters to generate the torque for pose change, as described in Fig. 28(b). We determine γ in the attitude control mechanism for the third phase. Depending on the angle γ, the torque can be generated as follows: $T_A = l \cdot \left(\frac{mg}{2} \sin(\alpha+\gamma) - F_{t(3,4)} \sin\alpha \right)$.

PID control mode. For the attitude control, two PID controllers are used for controlling $F_{t(3,4)}$ and γ, respectively. The pose error $\tilde{\theta}$ is calculated as follows: $\tilde{\theta} = \theta_d - \hat{\theta}$, where θ_d is the target pitch angle of the drone and $\hat{\theta}$ is the drone's current pitch angle estimated from the IMU. Then, the control values of the rear thrust level $\delta_{t(3,4)}$ and pitch offset angle δ_γ are calculated based on the pose error ($\tilde{\theta}$) as follows:

$\delta_{t(3,4)} = K_{P_t}\tilde{\theta} + K_{I_t}\int_0^t \tilde{\theta}dt + K_{D_t}\dot{\tilde{\theta}}$, where $K_{P_t}, K_{I_t}, K_{D_t}$ are coefficients for the proportional, integral, and derivative terms for thruster control, respectively, and $\delta_\gamma = K_{P_\gamma}\tilde{\theta} + K_{I_\gamma}\int_0^t \tilde{\theta}dt + K_{D_\gamma}\dot{\tilde{\theta}}$, where $K_{P_\gamma}, K_{I_\gamma}, K_{D_\gamma}$ are coefficients for the proportional, integral, and derivative terms for pitch offset angle control, respectively.

8.2. Wall-climbing mode

After a pose change, in order for the airframe to stay on the wall with minimum thrust force, the drone enters the wall-climbing mode. Under the thrust level same to the hovering state, it adjusts the direction of all thrusters with the estimated friction coefficient from the stabilization process. According to the relationship between the friction coefficient and the required tilting angle, the direction of thrusters is calculated. Another purpose of the tilt mechanism is to climb the vertical wall efficiently. The tilt mechanism helps the drone stick to the wall with a low friction coefficient by mitigating the dependency on the friction force generated by the normal force to the wall surface. The relationship between the required thrust force and the friction coefficient can be represented as follows:

$$F_\alpha = \frac{mg}{F_f + \cos\theta_\alpha} = \frac{mg}{\mu\sin\theta_\alpha + \cos\theta_\alpha},$$

where F_a is the required thrust force for wall-climbing, θ_α is the tilt angle with respect to the wall, and F_f is the friction force caused by the normal force to the wall. F_f is directly proportional to the friction coefficient μ .(see, Fig. 29)

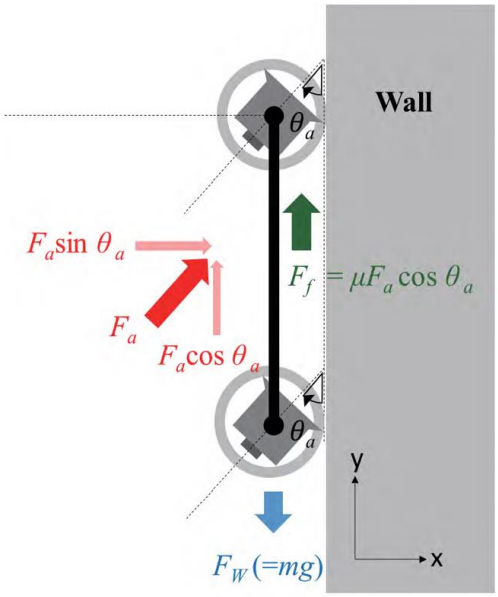

Fig. 29. FBD for wall-climbing with tilting angle

The required thrust force drastically decreases as the tilt angle θ_α decreases in the low friction coefficient environment. Depending on the friction coefficient, there is a range of tilt angle that requires small thrust force and a specific optimal angle with minimum required thrust force. Due to the reduced required thrust force, the energy efficiency can increase.

For flight stability, a general MAV (Micro Aerial Vehicle) has design principles and constraints.

- *First*, most drones consist of a main body at the center, support arms connecting thrusters with the main body, and landing gears. To maximize flight stability, the main body is located at the center of the drone to ensure that the center of mass is located at the center of the drone and to minimize the moment of inertia.

- *Second*, from the main body, support arms are arranged radially or symmetrically. The connecting material should be rigid and should not transfer vibration. If it is not rigid, the thrust force will not be fully delivered to the main body, and as a result a feedback controller such as the PID controller will not work well because of incorrect feedback information.
- *Third*, the parts containing heavy components such as the battery, electric devices, and landing gears should be placed near the center of gravity as long as they do not hinder pitch or roll motion. This condition increases flight stability and helps pose change with small thruster force.

Under these design constraints of the typical MAV structure, there are practical difficulties in applying the tilt-rotor mechanism. In particular, the propeller's large diameter makes applying a tilt mechanism harder in that the propeller size increases in proportion to the payload according to the momentum theory or actuator disk theory. In order to carry 2,500 to 3,000 g of payload with a moderate flight time, the required propeller diameter is about 10 to 12 inches.

Like this, as a normal propeller requires large diameter and volume for tilting, a duct fan unit can be considered as an alternative. Most importantly, it can save space because of its smaller outside diameter of about 70 mm. The overall layout of the main body frame is based on a general X-configuration quadrotor. Two thrusters are connected with a tilt arm and rotate together along the tilt axis as shown in Fig. 30 (a).

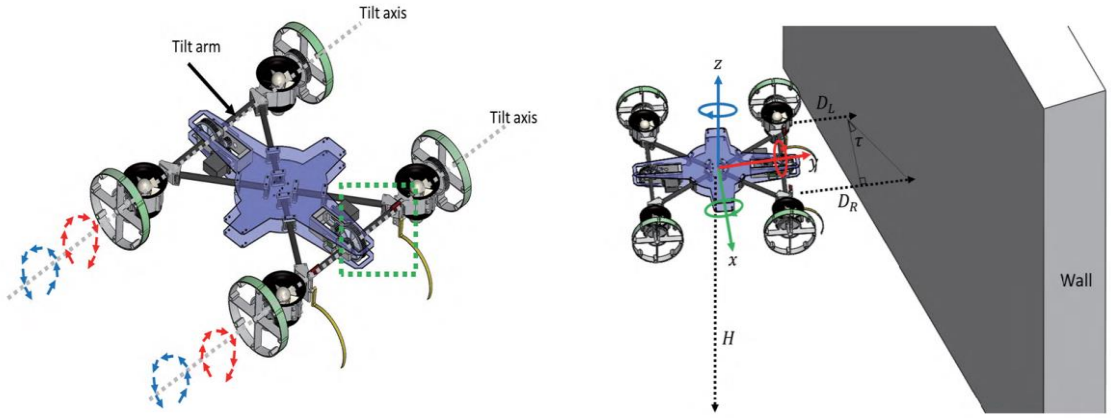

(a) (b)

Fig. 30. (a) Mechanical design for the drone's transformation; (b) The drone approaching the wall with an approach angle

Considering that the pitch and yaw angle in the body frame is very small in a moderate flight state, the drone has two sonar sensors measuring the distance to the wall, D_L, D_R, and calculating the approaching angle to the wall, τ, as shown in Fig. 30(b). When the drone detects a specific distance of about 10 to 150 *cm* from the wall, the landing assistant system is activated to make the drone's heading normal to the wall by decreasing the approaching angle and maintaining the altitude from the ground. This self-alignment system is working in the high-level flight controller for yaw motion control and thrust level control by using *z*-axis acceleration and altitude information *H*, as illustrated in Fig.30(b).

In step 1 of the control algorithm, the drone reads sensor data $D_{(L,R)}$, $C_{(L,R)}$, and $Acc_{(x,y,z)}$. Using $D_{(L,R)}$, the drone computes approach angle, τ, as in Fig. 8(b) and adjusts the heading angle of the drone to be aligned with the wall. At the same time, the drone checks whether the front part of the drone contacts to the wall for the stabilization process.

In step 2, the drone starts the stabilization process and measures tilt angle of front thrusters to determine whether the stabilization process is finished.

In step 3, after the stabilization process, the drone proceeds to the second phase of pose change before the intersection zone. As mentioned before, the obstruction area is determined by tilting angle to the wall θ. The drone can determine whether the drone is before or after the intersection zone by comparing θ with the pitch angle of the drone.

Finally, in step 4, the drone starts the third phase of pose change right after the intersection zone.

In this process, the drone decreases the pose change speed to the target speed and finally enters the final landing process.

When the pitch angle of the drone reaches 90^0, the landing process is finished.

As mentioned before, during pose change, there is an inter-section zone where the airflow of the thrusters at the front side could be obstructed by the structures of the thrusters. The effect of decreasing thrust force caused by air passage obstruction is verified by an experimental test as shown in Fig. 31. In the experiment, a drone is installed on a linear guide, on which the drone moves freely along the guide rail.

The thrust force of right thrusters in Fig. 31(a) is set to 16 N equal to the hovering or stabilization level, and the tilt angle of the other thrusters, θ_r, confronting airflow of right thrusters is varied from zero to 90 degrees. We used a force gauge to measure tensile force caused by thrust force of right thrusters to verify the effect of the air passage obstruction. Fig. 31(b) shows the result of experimental tests. The result shows that as the tilt angle becomes close to 90 degrees, the tensile force is decreased. On the contrary, the closer _*r* gets to zero, the less air obstruction is caused and consequently the net thrust force increases. To overcome this platform limitation, we separated the pose change process into three phases depending on the intersection zone as in Fig. 32.

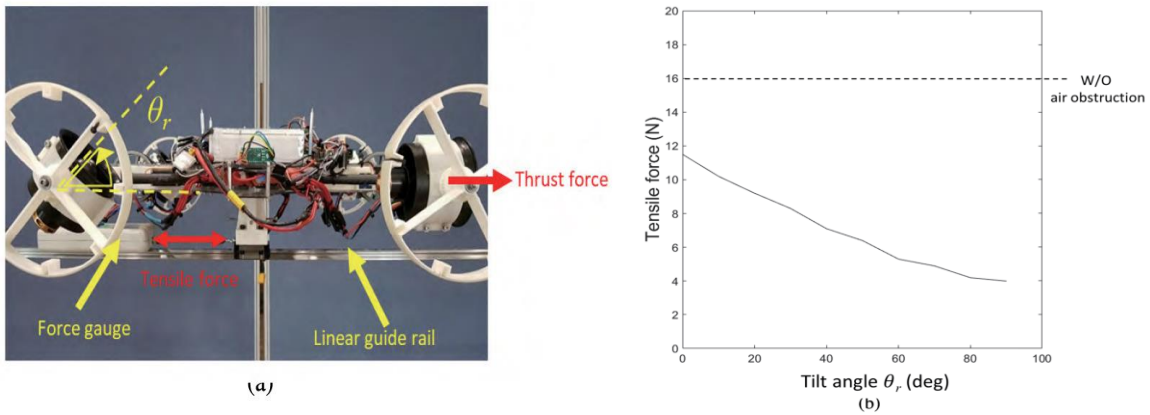

Fig. 32. Experimental test for the effect of the obstruction of airflow. (a) Test setup. (b) Test results

The main contribution is to mitigate the impact of perching by controlling the pose change speed with a tilt-rotor-based airframe. Since the non-tilt approach only changes its pose as fast as possible to prevent falling by slippage, the impact could be high enough to damage the wall or the drone itself. Therefore, experimental tests are conducted to verify the performance of the mechanism and control algorithm by measuring the angular speed of the pose change and comparing it with that of a non-tilt approach. In the experiment, the target angular speed set to 1.0, 3.0, and 5.0 deg/s for the proposed approach, and measure the angular speed with an IMU installed for flight control.

The non-tilt approach changes its pose within 1.5 seconds and the average angular speed is about 84.72 deg/s, which is significantly higher than the soft-landing approach. Consequently, the experimental tests show that the proposed system allows the drone to perch on a vertical wall with a desired angular velocity and guarantees a soft landing. In order to verify the effect of reduced perching impact, we installed an accelerometer on the drone and target wall, compared acceleration data, and calculated the impact for both approaches. Regarding the non-tilt approach, when the front part of the drone firstly contacts the wall, low level of impact force occurs. Within 1.2 seconds, a drone completes perching process by changing its pitch angle and the rest of its body bumps into the wall. On the contrary, in proposed approach with the pose change speed of 5 deg/s, the impulse level of the first contact is the same with the non-tilt approach; however, the impulse from the second contact was significantly decreased to 0.05 kg m/s.

Figure 33 shows an exemplary tail-down perching process using a tilt-rotor mechanism.

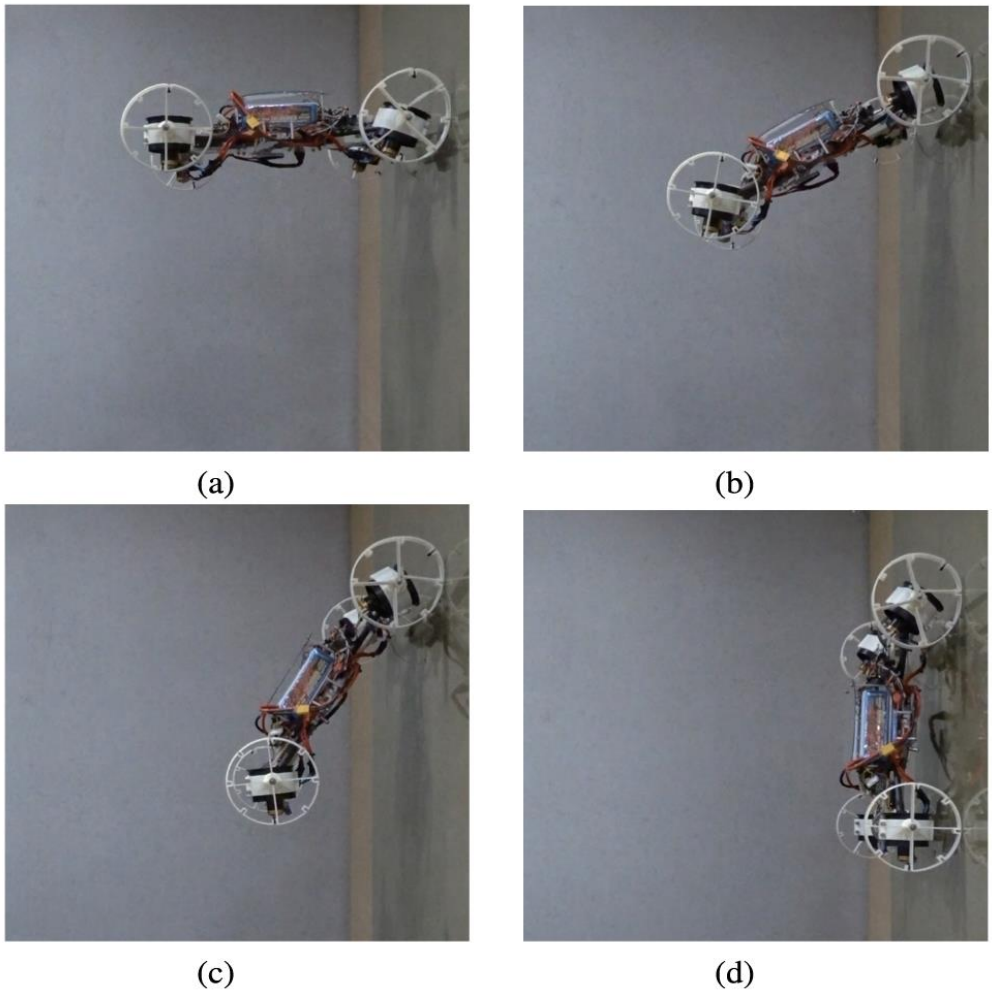

Fig. 33. Experimental test for the proposed perching (a) the first contact and starting stabilization (b, c) pose change (d) the second contact and completing perching process

Wall-climbing tests are conducted to verify energy efficiency of tilt-rotor mechanism. The surface material of the wall is tempered glass and the material of the wheel surface is 1 mm-thick silicone sheet. By using a force gauge, the average friction coefficient between them is measured to be 0.53. From 40 to 80^0 of tilt angle, the drone can climb the vertical wall with lower energy consumption than that of the hovering state. When tilting angle is 65^0, the drone consumes the lowest energy. These results are consistent with the result of wall-climbing simulation when friction coefficient is 0.5.

The proposed tilt mechanism-based landing system shows [3] the ability to perch on a wall with low angular speed of pose change and consequently it can reduce the landing impact significantly. In addition to that, in terms of thrust-assisted wall-climbing mechanism, the tilt mechanism can help a drone to stick to the wall with small thrust force by adaptively changing the direction of thrusters.

8.3. Unconventional aerial WCR models

A large number of professions engaged with high-risk factor are dismissed and replaced by the development of robots. However, due to the technological limitation, human resources are still required to execute some dangerous work, e.g. cleaning up high-rise buildings and performing Structural Health Monitoring (SHM) for large bridges or disaster sites. Thus, in this case, their exposure to danger is indeed unavoidable. For bridges extending over the oceans, frequent inspections are necessary since the components have a high probability of being damaged by salt and wind. Moreover, since such bridges are generally large and long, it is not easy for persons to inspect and maintain by themselves. To solve this problem, it suggested the two-step inspection process: macro inspection for an approximate diagnosis using a non-contact-type unmanned aerial vehicle and micro inspection for the detailed inspection using a wall-climbing robot that is able to check the condition of the bridge in particular in this paper as shown in Fig. 34.

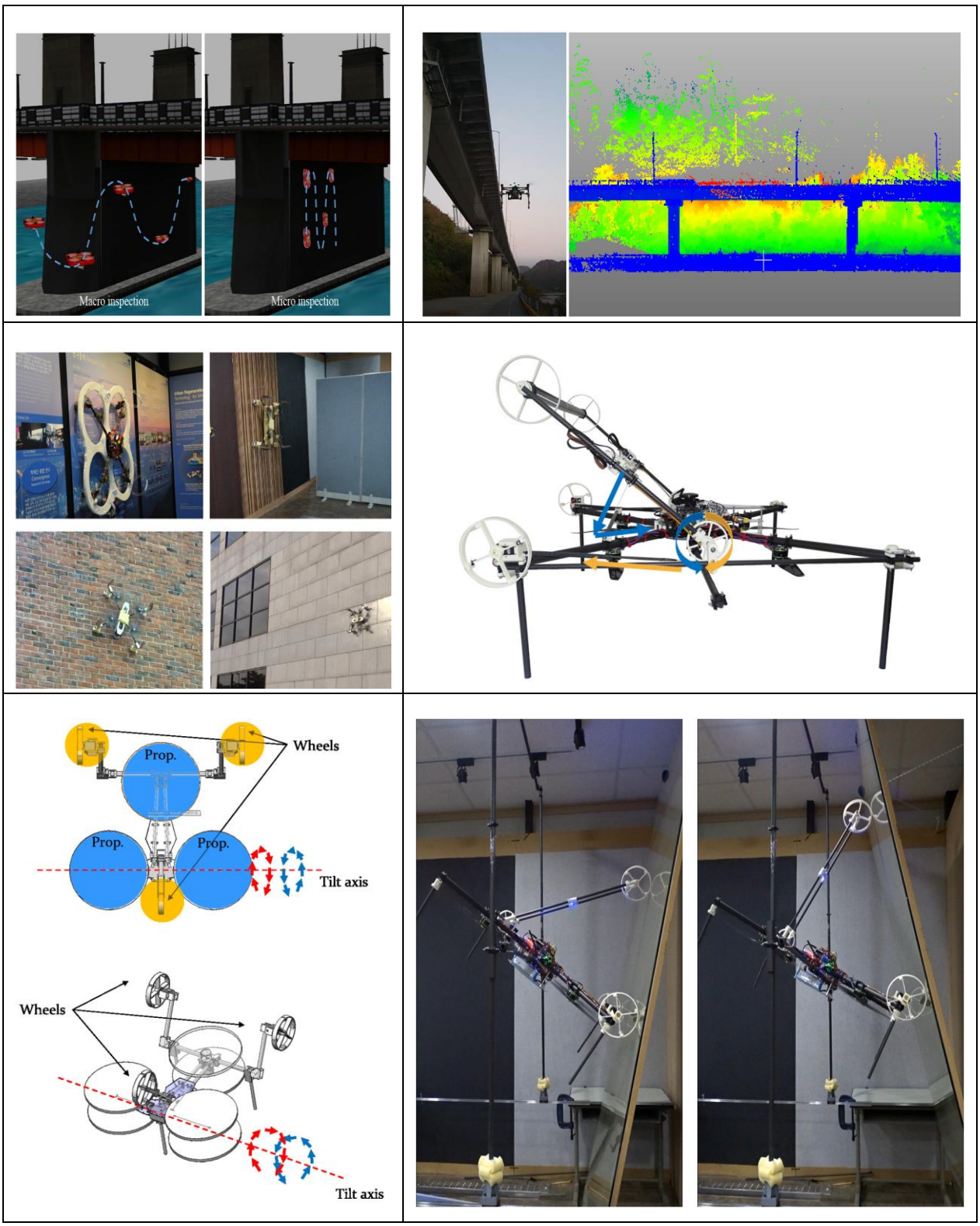

Fig. 34. Inspection WCR drone examples

A non-contact-type drone that checks the condition of the bridge, in brief, the non-contact type drone can be used to quantify surface cracks or damaged parts such as bolts (Fig. 35).

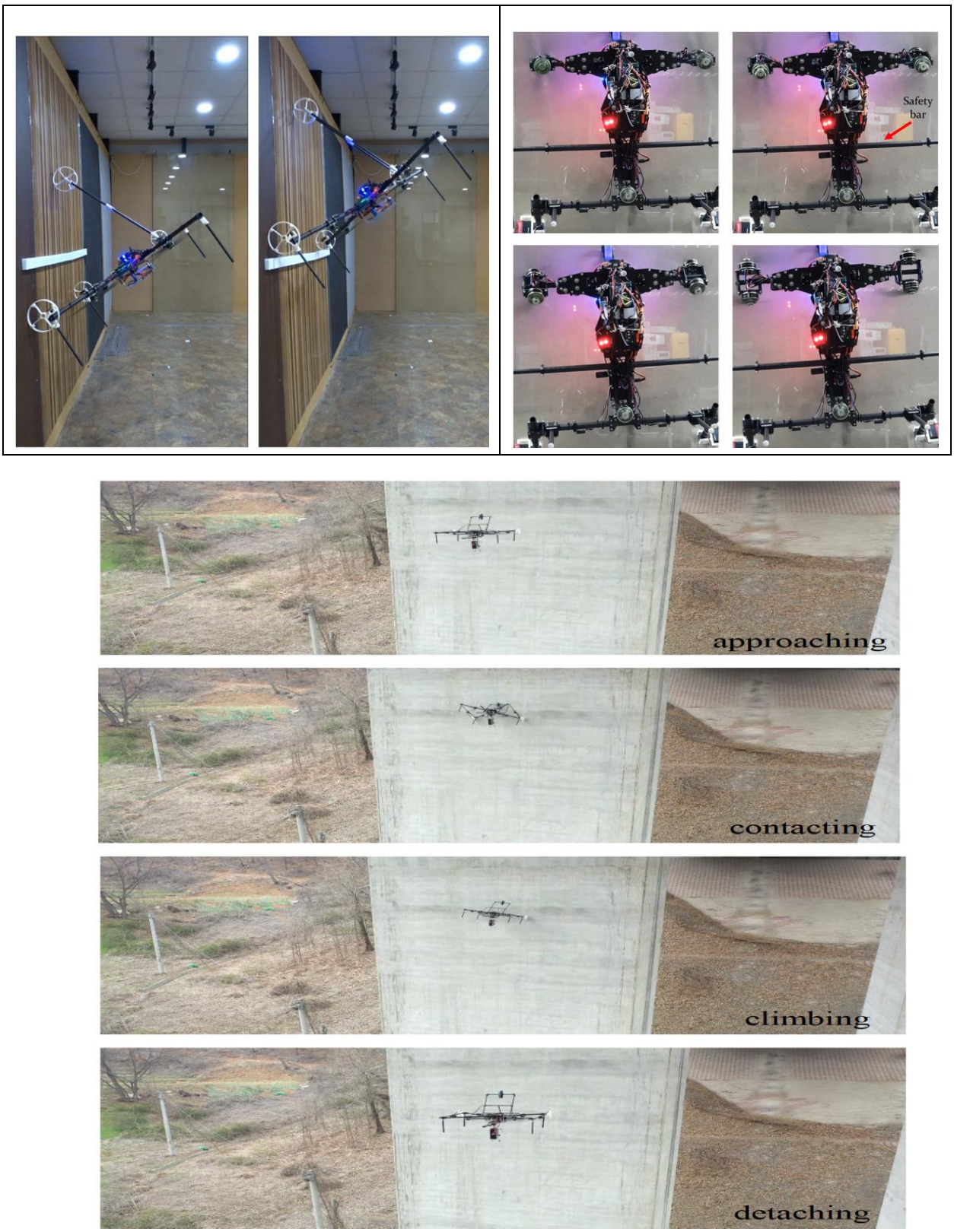

Fig. 35. Inspection non-contact WCR drone examples

Researchers have developed systems that inspect the sur-face civil structures using of non-contacting UAV systems by flying around there. However, given the environment in which general civil structures are exposed to strong winds and considering the flight performance of UAVs, such methods can cause safety problems and make the mission itself impossible. The wall attachment method of our proposed wall-climbing UAV system is a propulsion-based method. In this UAV platform, the propulsion system used for the flight can act as pushing force against the wall and convert that force into friction with the wall to attach or to move on the wall surface. As shown in Fig. 35, an early version of our wall-climbing UAV has applied

force only in a direction perpendicular to the wall. This was designed assuming that the coefficient of friction between the wall and the UAV contact surface was high. However, when applied to the actual environment, it was found that the initially assumed friction coefficient was not maintained due to dust and other contaminants. This also led to the discovery that a high-level propulsion is needed to generate enough friction to attach to the wall.

Two mechanisms have been applied to implement the concept of wall attachment and movement. The first instrument is to control the direction of propulsion by adjusting the angle of the airframe to the wall using an auxiliary arm. As mentioned previously, UAVs have limited propulsion and payloads. Thus, installing additional manipulator and equipment is not desirable in terms of flight stability and energy efficiency. Therefore, the primary consideration in designing the auxiliary arm is the weight reduction problem. In order to adjust the direction and size of the force received by the auxiliary arm to control the angle of the airframe, the wires responsible for the attenuation structure (relief structure) and tensile force were utilized as shown in Fig. 36.

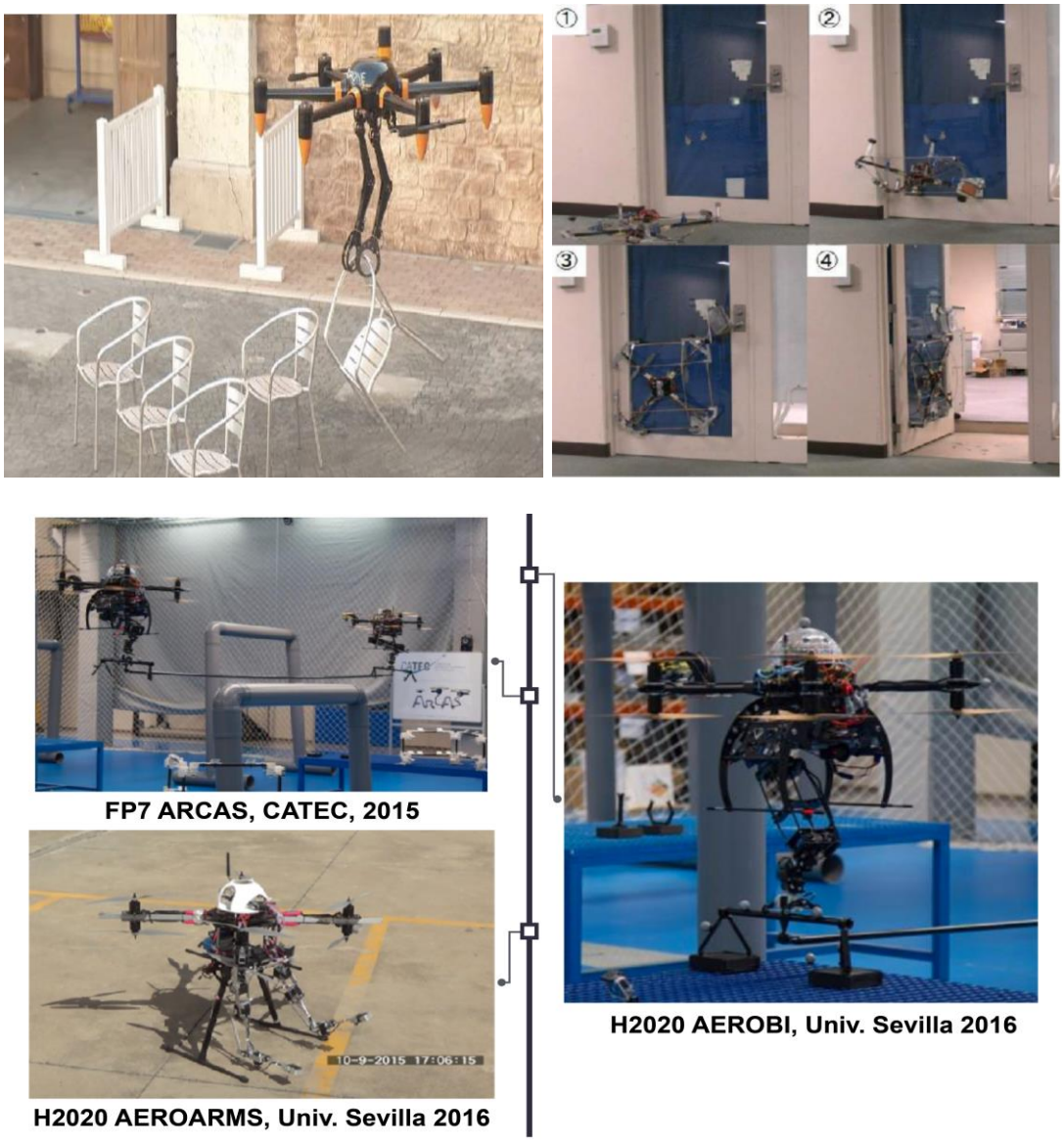

Fig. 36. Control the direction of propulsion by adjusting the angle of the airframe

Through this same mechanism, UAVs are able to respond to wall surfaces with different angle slopes and have faster moving speeds with lower levels of propulsion compared to the early developed wall-climbing UAVs. Another strategy for adjusting the angle of thrust is by applying the tiltrotor mechanism. In this structure, since rotation occurs only on the axis which is connected to the propeller and motor, not the whole body, the ability to achieve design simplicity becomes one of the prominent advantages. However, due to the large radius of rotation of propeller and its high cross-sectional ratio, it is highly challenging to

secure space for tilting without any interference with other major components. As mentioned previously, it is also important to achieve the maximum result by employing minimum manipulators considering the limited payload of UAVs. For this purpose, the design is based on the UAV platform of Hexa-Y type.

As shown in Fig. 36, four of the six propellers located at the front of the platform are connected on one axis and designed to be able to change the direction of 66.6% of the thrust with a single manipulator.

This design strategy has enabled to achieve a similar level of propulsion accomplished by a quadrotor-based platform while reducing the size of the airframe by 30%.It is well known that the platform is likely to perform its mission in an environment where GPS signals are unreachable, such as under the bridge, or in a situation where the GPS signals become weaker as approaching a large structure.

Therefore, the method of accessing the structure's walls by relying on GPS signals is unreliable. In order to overcome this obstacle, the platform is equipped with distance sensors (IR sensor) and a location estimation algorithm that can estimate the approach angle to the wall when flying close to ward it.

Two mechanisms are proposed to redirect the propulsion for efficient wall movement and the prototypes are also produced. The performance is verified by indoor experiments in limited environments. Through the lightweight design of the arm mechanism with reel/wire structure and the PID-based controller, it is confirmed that the angle control of the arm is correctly accomplished. As shown in Fig. 36, the drone can control the direction of thrust and its the attitude by adjusting the angle of the auxiliary arm according to the slope of the wall which then enables the movement on the wall. In addition, as shown in Fig. 36, the fusion of the driving friction force of the wheels moving on the wall and the upward force of the propellers show the ability to move over obstacles (height 30 mm, width 50 mm) which is difficult to be overcome by the conventional platforms.

Based on the efficient design using minimal manipulators, the drone has a smaller size and smaller weight than the previous platform. Additionally, by adjusting the thrust angle, the drone can perform a faster movement speed when it moves along the wall, even though it has low thrust (Fig. 36).

Moreover, for the actual feasibility test, we have verified the outdoor experiments as well. Fig. 36 shows the rotary arm mechanism UAV can actually attach and move on the concrete surface of the bridge column.

In order to overcome the limitations of propulsion and friction-based wall-climbing methods in real-life environments where high friction coefficients are not secured, two mechanisms that can change the direction of propulsion have been proposed and their performances were verified through experiments. Further studies require comparison of flight stability and wall-climbing performance between typical approach flight type UAV and wall-climbing UAV under the condition of strong winds environments, and verification of quantitative performance improvements for structural inspection through comparison of the quality level of acquired inspection results.

The system used for tethering the UAV can be observed in Fig. 37.

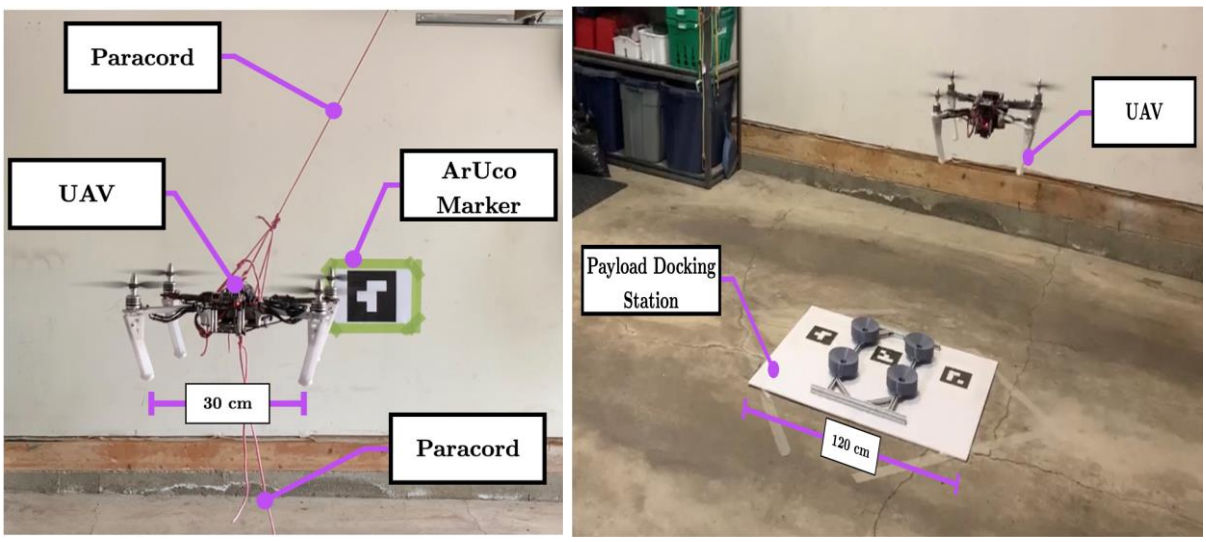

(a) (b)

Fig. 37. (a) Tethered UAV During Flight; (b) UAV Payload Docking Station with Approaching UAV

The system works by constraining the UAV with two lines of paracord. To prevent the UAV from striking the ground, paracord was tied to the UAV's top and fed through two pulleys and then fixed to the ground. A small mass was fixed on the paracord to compensate for the tether's mass and prevent it from being caught in the propellers. To prevent the UAV from flying into the roof, an additional length of paracord was tied to the bottom of the UAV and fixed to the ground.

Both directions of tethers worked in tandem to prevent the UAV from flying away in the lateral direction. The paracord's elastic properties and the amount of given slack in the system allowed for an operating volume of approximately 1.5 m x 1.5 m x 1.5 m.

The UAV cannot reliably position itself with millimetre accuracy. However, should the UAV achieve centimetre accuracy, a passive system can align the UAV to achieve millimetre accuracy and allow for the retrieval of a payload using the quick connect system. The passive payload docking station features a broad white background measuring 120 cm x 90 cm to allow for clear detection of ArUco markers. An aluminum extrusion structure holds four 3D printed funnels that allow for inaccuracies of up to 7 cm in the north and east direction and 13^0 of yaw. The entire system is fastened to the ground using clear packing tape to limit the effects on the vision system and prevent the system from shifting from rotor wash. A photo of the docking station can be observed in Fig. 37. With the UAV system's layout and quick connect development complete, a novel payload is designed in the following chapter to interface and demonstrate the capabilities of the UAV and its universal payload system.

Similar to the payload swapping experiment, the developed navigation system could not reliably perform the positioning requirements demanded to remove a cap; therefore, the experiment was manually performed. Four circular caps measuring 3.9, 5.4, 6.6, and 9.1 cm in diameter were selected for removal to show the cap manipulator's spanning capabilities. As with the lack of standardization of the sump cavity, no standard cap torque specification was found; thus, each cap was tightened to its reservoir so that fluid would not escape if inverted. The UAV was then placed on the cap, the manipulator was closed, and the UAV was manually yawed, yielding four successfully removed caps. Photos of the UAV removing the four caps are observable in Fig. 38.

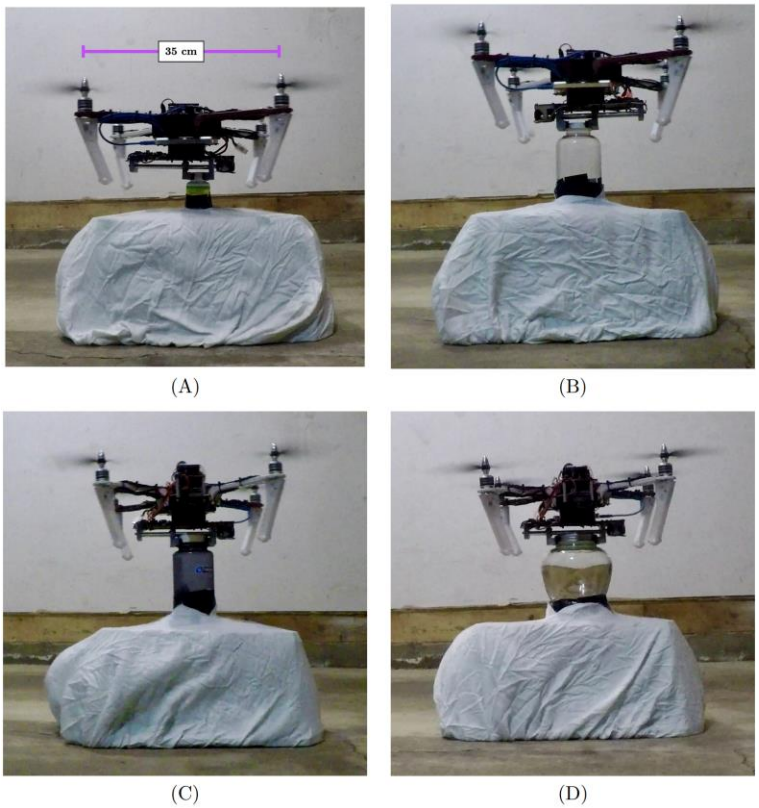

Fig. 38. Cap Removal: (A) Small Diameter 3.9 cm, (B) Medium Diameter 5.4 cm, (C) Large Diameter 6.6 cm, and (D) Extra Large Diameter 9.1 cm [4]

During testing, three observations were made about the developed cap manipulator payload system. Firstly, the threshold for the gripping strength was found to be cap-dependent; what worked for one cap, elastically deformed another. If the gripper squeezed too tight, the UAV had to fight an increased release torque, as the normal contact force had also increased. After iterating through the selected caps, a single threshold value was determined for all four; however, a more extensive study of the caps should be considered. Otherwise, the manipulator was functional and was confirmed not to be back driven when the servo was placed in an idle state. While interfaced with the quick connect, the cap manipulator had sufficient gripping strength to hold the UAV upright on the cap. The gripping provided the UAV with the maximum torque scenario where only two adjacent propellers operate, as the remaining propellers do not need to generate lift.

Using a UAV to physically interact with an environment is termed "aerial manipulation". Among nearly 8500 published papers relating to UAVs between 2008 and September 2017, only 1.7% of them related to aerial manipulation. However, using the same search terms and database, interest in aerial manipulation was found to have more than doubled (to 4.6%) as of November 2020, and research relating to UAVs is increasing exponentially. Researchers have demonstrated multirotor UAV capabilities such as the ability to open drawers, open doors, unscrew light bulbs, interface and rotate valves as in Fig. 39, acquire water samples, have two UAVs work together to overcome payload restrictions, and acquire volcanic rock samples, which shows that aerial robotics is indeed in its golden period, or perhaps just entering it.

Fig. 39. Quadrotor UAV Autonomous Valve Interfacing Task [5]

One of the many challenges with aerial manipulation is controlling the UAV due to interactions with its environment. UAVs interacting with the environment can be simplified into three main categories: Momentary coupling (interacting with objects of finite mass in the air that are not fixed to the surrounding environment); loose coupling (interacting with objects attached to the environment without securing to the environment, in tasks such as assembling, inserting, pushing, or pulling); and strong coupling (securing or perching onto fixed objects in the environment and becoming part of it). The challenge of executing any of the three coupling types is compensating for the reaction dynamics. When a UAV has coupled itself with the surrounding environment, the forces the UAV experiences interfere with the aerodynamics and associated model of free flight, creating a risk of the UAV becoming unstable and failing its assigned task. An analogy is to imagine a scuba diver turning an underwater valve. The diver contorts his body and aggressively kicks his legs in order to throw his body weight into turning the valve with his arms. Likewise, a UAV must 'swim' through air and may have to vector its body in order for the arms to dexterously manipulate an object.

9. Aerial manipulators platform

To address the issue of reaction dynamics and maintain a stable system, different approaches can be taken. Firstly, a well-designed mechanical system can significantly reduce the influence of reaction dynamics. Approaches such as soft contact dynamics and smooth actuation of a manipulator can significantly improve the system's capability. The planning and modelling of the system is critical; there are two main approaches, a centralized approach and independent approach. A centralized approach considers both the UAV and payload to be one system, and the controller treats everything as such. In an independent approach, the UAV

and payload are treated separately, and the effects of the payload on the UAV (and vice versa) are treated as disturbances. A centralized approach is simpler to implement than an independent approach; however, an independent approach tends to yield a more accurate and responsive system.

Other challenges exist with aerial manipulation systems, such as localization and control, which were previously discussed. The single greatest challenge of aerial manipulation is that most designs are complex mechatronic systems in a relatively new field. Aerial manipulation requires developing many different sub-systems that must all work together for reliable and robust performance. Entire teams often work together for years to develop an end product such as the AEROARMS Project, which aims to develop aerial robots with advanced manipulation capabilities for various inspections and maintenance. Examples of four different AEROARMS platforms can be viewed in Fig. 40.

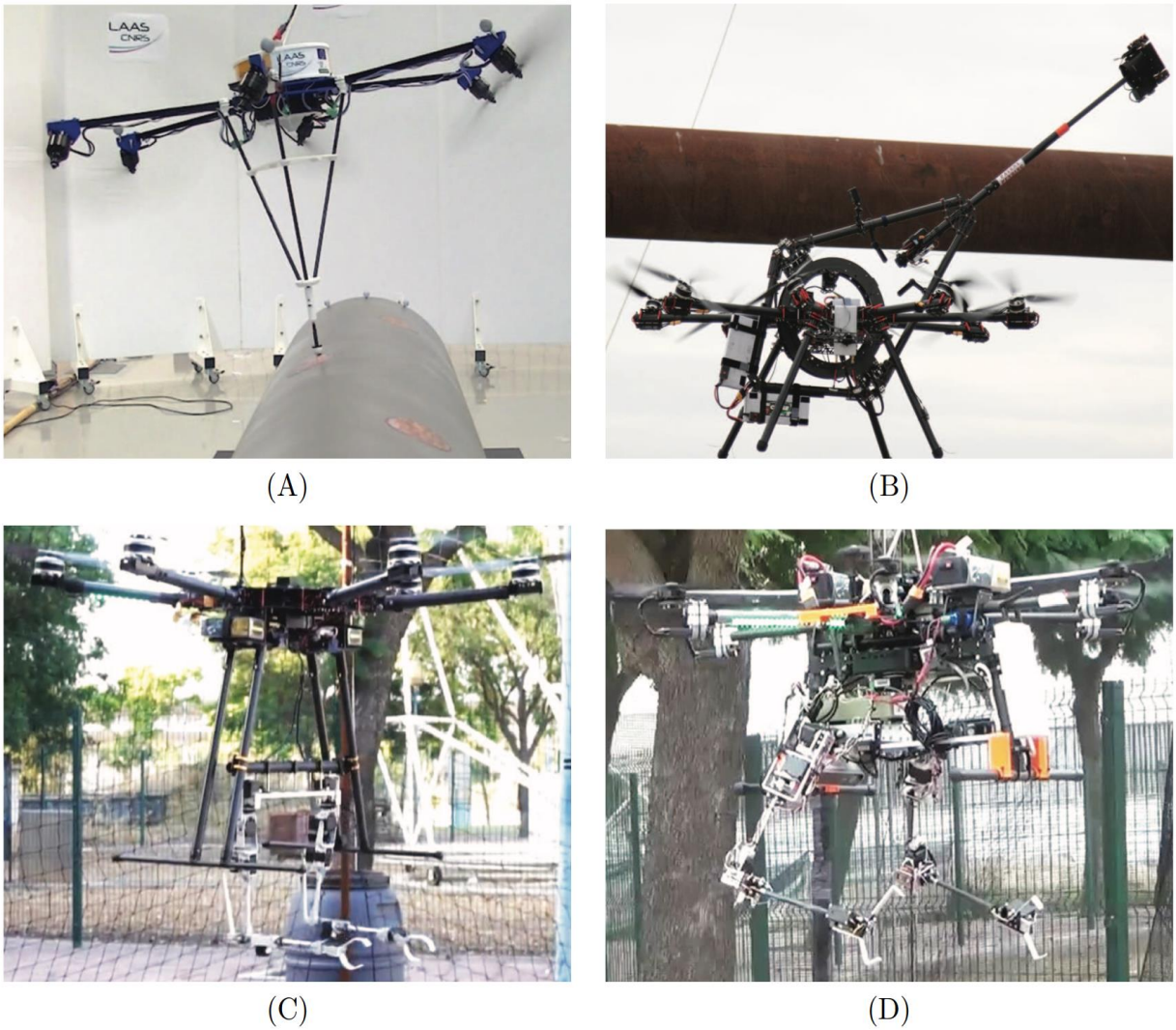

Fig. 40. Four AEROARMS platforms: (A) multidirectional-thrust hexarotor with a rigidly attached end effector, (B) multidirectional-thrust octorotor with inspection arm, (C) aerial dual-arm manipulator with stiff joints, and (D) aerial dual-arm manipulator with compliant joints [6]

Aerial Physical Interaction (APhI) is a generic term to design all physical interactions between one AV and its environment. A very early example can be the in-flight refueling maneuver, demonstrated as early as June 1923. As of today, this procedure is still not fully automated and requires the dexterity of an aircraft pilot or a boom operator in the case of rigid boom, while the probe-and-drogue system is close to be automated. The following developments are going to focus on to APhI for unmanned aircraft, whether it be for probing the environment, react to collision or manipulate objects. In order to perform APhI with MAV a few require-ments are set and will be developed at length. The first two simple tasks of APhI, that come to mind, are

pocking the environment, i.e., exerting force trajectories on surfaces and perching, i.e., allowing the MAV to perch on the environment in order to recharge battery or acquire data, see Fig. 41.

Fig. 41. Examples of Aerial Physical Interactions: (a) pocking a surface and (b) perching on a wall

Another conceptually simple APhI tasks consists in linking a MAV to the ground by mean of a tether. These tasks will be described more in depth below.

9.1. Aerial Manipulation

A subfield of APhI can be recognized for Aerial Manipulation (AM), being the use MAV to complete complex manipulation tasks. In the literature there is a confusion between transportation and manipulation, the latter being a special case of transportation including a dexterity component inherent to manipulation. In the following, transportation might be used as an illustration of basic manipulation capabilities. As such, AM regroups all the tasks where an object has to be trans-ported or manipulated by one or a group of MAV, see Fig. 42.

(a) [Nguyen–2015] (b) [Mellinger–2010]

Fig. 42. Examples of Aerial Manipulation: (a) drawer opening/closing and (b) collaborative load transportation

Typical off-the-shelf MAV are not mechanically fit for APhI tasks, often the propellers volume is open to collision and they don't have specific termination for contact with the environment. Therefor to pave the way to APhI and AM the first modification of standard MAV concerns mechanical design to enable APhI capacities. For sake of completeness some mechanical designs only fit for APhI that does not involve manipulation are presented here, with a selection depicted in Fig. 43.

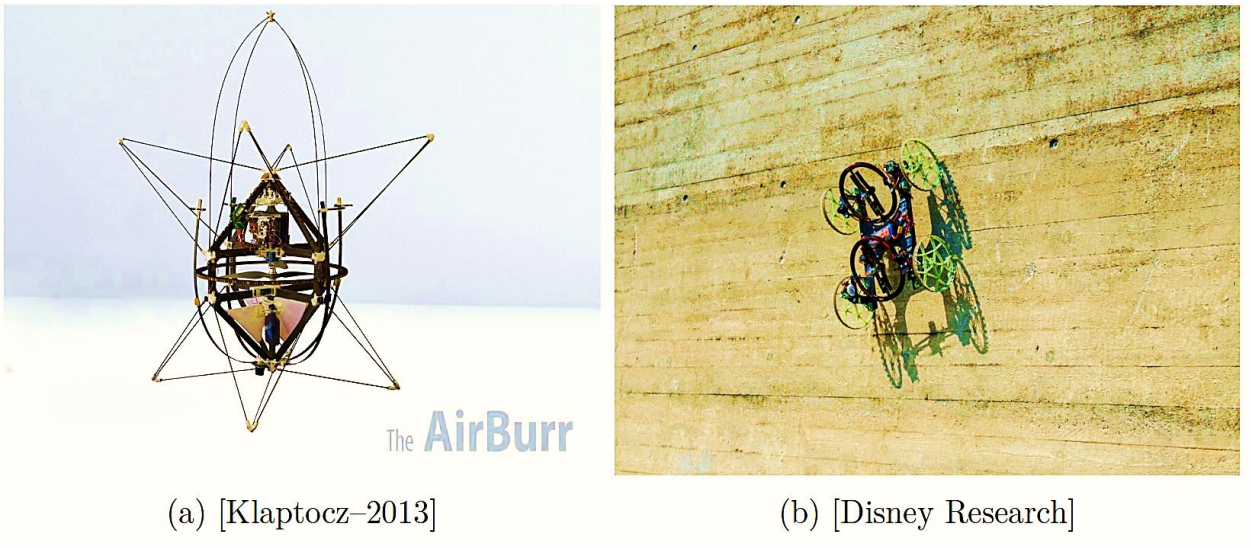

Fig. 43. Two Original Designs: (a) the AIrBurr capable of falling to the ground without breaking and upright itself to take-off again, and (b) the Vertigo capable of climbing walls

A primary target of APhI mechanical design is to protect the propeller volume from intrusions and alleviate collision contact disturbances *w.r.t.* the flying behavior. One approach is to mount to passive rotating spherical shell around the main frame of a classical Vertical Landing and Take-Off Vehicle (VTOL), this mechanism enables the UAV to collide with obstacles without compromising its flight stability.

In order to pass from APhI to AM, a manipulator or at least a prehension mechanism needs to be embedded on AV. With this extension AV can be properly called Aerial Robot (AR). In the literature, several different design approaches for manipulator were identified, see Fig. 44.

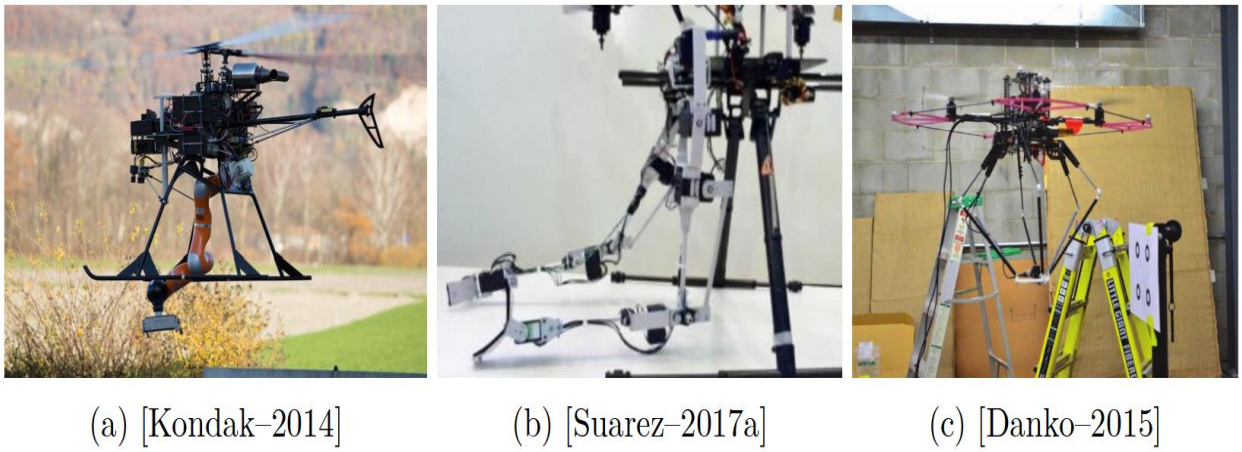

Fig. 44. Different kind of aerial manipulators: (a) industrial 7-DoFs, (b) dual arm manipulator and (c) parallel manipulator mounted below a MAV

The main idea remaining that a manipulator increases the dexterity of the AR for manipulation tasks, eventually compensating for under-actuated AV.

9.2. Collaborative Aerial Physical Interaction

From a semantic stand point, collaboration (working jointly with other toward a common goal) and cooperation (operating together to realize a task) are considered equivalent. A collaboration denotes a joint work, it does not necessary involve physical interaction, with the environment or with the other collaborators, that is to say heterogeneous robots, ground and AV, mapping/monitoring an area is a collaboration task but not relevant in the scope of APhI. A few works considering swarm, or team of AR, performing APhI with the environ-ment or inside the swarm have been presented, see Fig. 45.

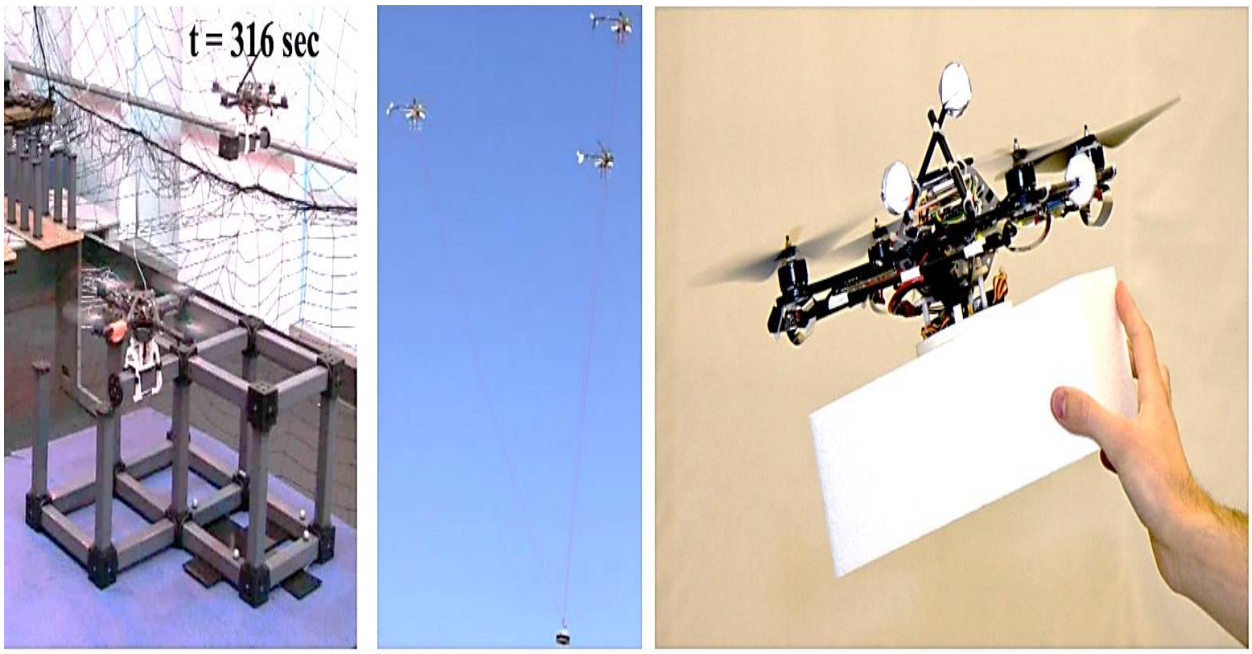

Fig. 45. Aerial Robot collaborations, (a) collaborative structure assembly by a team of ARs, (b) collaborative load transportation via tether and (c) human-AR collaboration for assembly tasks

Most notably, swarm of AR are used for collaborative construction to build a tower structure out of bricks or to build tensile structures, *e.g.*, bridge or to assemble cubic structure or more complex structure with a dedicated construction planning. In this case the physical interaction is not affected by the other members of the swarm. Or in the well-developed case of cooperative load transportation, by team of AR. This results in a group of AR tasked to transport a load in a coordinated fashion.

10. Problem-oriented unmanned aerial vehicles: applications of the aerial manipulation

Unmanned Arial Vehicles (UAV) are being developed to perform a set of tasks, such as: parcel delivery in logistic business, implementation of search and rescue operations, the assistance in emergency situations, industrial inspection1 and maintenance. The UAV additionally equipped with one or several robotic arms can perform significantly a greater number of tasks for third and fourth applications. For example, such flying robots are able to carry out a detailed inspection of the pipelines and bridges, holding a heavy object with the swarm of drones, ecological sampling or land in point of interest and perform a detailed environmental exploration. The first studies in the area of aerial manipulation were carried out in 2010-2011. It was the experiments on moving objects using a swarm of UAVs, grabbing an object using a UAV equipped with a grip, and applying an unmanned helicopter with a gripper. In 2013 the control system, research on dynamics and stabilization, and flight experiments of the first multirotor with manipulators were presented in three studies. The aerial manipulation has evolved from the laboratory tests to the validation experiments in conditions close to actual exploitation (e.g., pipeline inspection). Nevertheless, the question of controlling similar flying robots remains open, whether it is necessary to control manually, automatically, or in semi-autonomous mode.

A large number of the works [14-39] propose the autonomous performance of individual specific tasks, such as the insertion tasks, valve turning, grabbing objects in flight, surface inspection, object grasping by two aerial manipulators, maintenance of the power lines, and others (Fig. 46, b).

The industrial maintenance and assistance in rescue operations are the two areas that require the most versatile robots. The usage of robots for these purposes often implies the ability to perform non-standard actions that arise already during task execution. In this case, the flying robots capable of performing aerial manipulation are of particular interest. For instance, at the present time industrial tasks are carried out by personnel. Some of these tasks must be performed using high-altitude equipment. Even partial implementation of these activities by the robot can help to reduce human risk and cost, as evidenced by the focus of European projects ARCAS and AEROARMS. For this purpose, the robot should carry out different specific

tasks with high accuracy that could not be performed only in autonomous mode. The robot control can be achieved by teleoperation methods. In this case, the robot and the operator can be located in remote places, that is especially important for hazardous conditions.

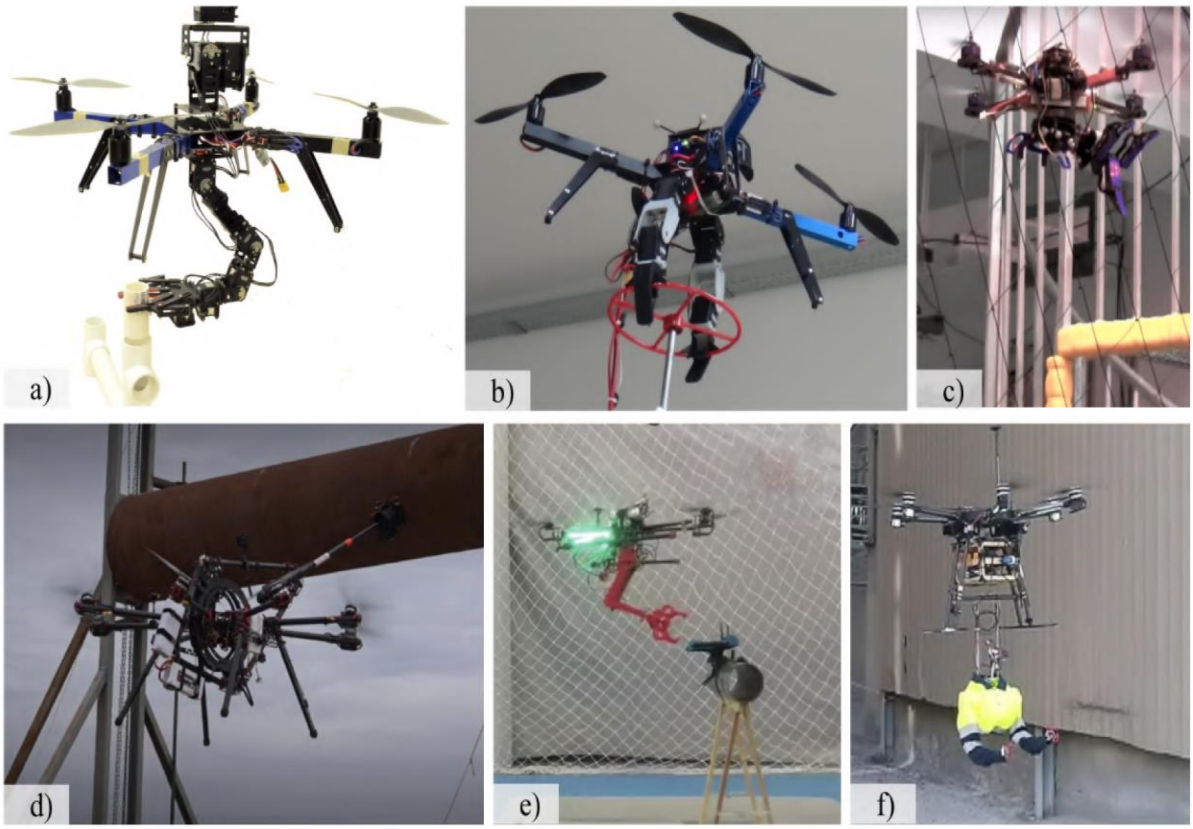

Fig. 46. Applications of the aerial manipulation: (a) the insertion task, (b) valve turning, (c) grabbing objects in flight, (d) surface inspection, (e) object grasping by two aerial manipulators, (f) flying robot for maintenance of the power lines

UAV with one or several robotic limbs can significantly extend the application of robots in rescue operations by accompanying such activities in the conditions of destroyed urban infrastructure and natural landscape, when it may be necessary to deliver medicine, drinking water or ancillary equipment (for instance, spare batteries for power tools or repair kits). The equipment of the flying robots with several manipulators can be useful not only for performing operations with objects, but also for landing on uneven surfaces. With such functionality, the robots can spend their power sources more efficiently due to the rational use of flight and ground modes.

However, it can notice that in recent times, research in the field of using a group of robots for search and rescue operations is carried out using highly specialized robots with a bias in the mapping and indoor localization. At the same time, significantly less research is devoted to the development of a multifunctional robots. The application of the robotic arms designed for aerial manipulation not only for performing operations with objects, but also for landing on uneven surfaces, is of considerable interest for research. It is worth considering another combination of functions for the robotic limbs of flying robots, this is the usage of landing gear to move on the ground. This necessity arises when there are cavities in the ground or it is required to pass through a narrow passage and move in a dilapidated room with a low ceiling.

It is expected that UAVs will be launched and land on a moving car (e.g., in Walmart's concept).

After the landing, the UAV needs to move to the charging station. Another example of the application of the multifunctional robots can be found in exploring under-ground caves. Delivering or extracting things, that are located in hardly accessible places are potential tasks in this mission. Examples of this would be ecological sampling or installation of the observation sensors deep inside the caves, that can be reached only through narrow tunnels. Based on state of the art, it was defined the main problem as developing a multi-

functional flying robotic system and methods for effective remote control of such a system. In order to better characterize this problem, two clarifying subtasks were formulated. It is necessary to design a comfortable control interface to perform the various aerial manipulation tasks with a cognitive perception of the robot state.

And the second subtask is the development of a locomotion algorithm for the landing platform.

There is a tendency of active development of both multifunctional robots and the execution of operations by groups of robots in order to more efficient implementation of critical tasks for shorter periods of time. The main potential fields of application for such robots are search and rescue operations on the reserves, underground tunnels, mines, in areas following natural disasters. Although such robots can also be used for industrial maintenance. In order to promote these developments in the world, competitions are held on the usage of robots for search. and rescue operations in forests6 and underground environments. The first competition is aimed to develop devices or technologies capable of detecting the exact coordinates of the location of a missing person without means of communication in the natural environment. Despite the competition focus in the field of image processing, it is worth noting that the list of necessary tasks in these conditions can be expand by delivering essential items, as well as methods to inform the found person about subsequent actions using the robot. The DARPA challenge is addressed to development of novel approaches to rapidly map, navigate, and search underground environments during disaster response scenarios. Tunnel, urban underground and cave are used as a test zones in this competition. Examples of some types of the cluttered environments are shown in Fig. 47.

Fig. 47. Types of the cluttered environments: (a) the interior of the building after earthquake, (b) mine after collapse, underground tunnel (c) and cave (d)

At this time, mine robots were used to manipulate fan doors, push aside obstacles, and transmit video and atmospheric monitoring information (mine gas and temperature readings).

In the field of aerial manipulation, several types of interaction with payload can identify. It can be simple load carrying, grabbing objects using 1-DoF gripper, manipulation by one or two multi-DoF robotic arms, or aerial interaction with objects using cable-Suspended manipulator (Fig. 48).

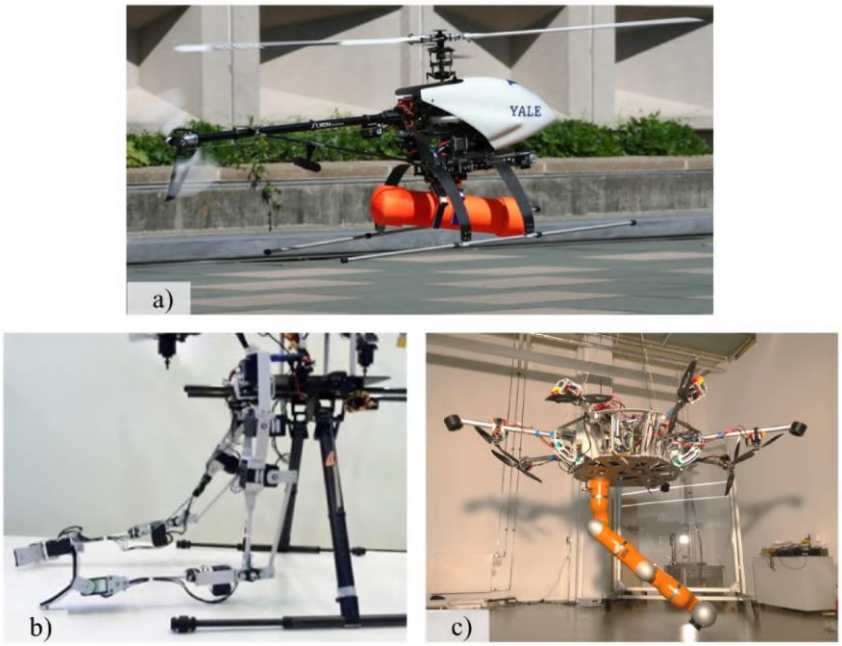

Fig. 48. Types of aerial manipulators: (a) 1-DoFgripper, (b) two multi-DoF robotic arms, (c) cable-suspended manipulator

These technologies are intended for different applications and, accordingly, distinguished by the hardware design, maximum payload, dynamic loads, and type of control methods. The diversity of structures for manipulating objects in the midair reflects the trend of the scientific search for a minimalistic design of the manipulator, which would have a lightweight and high strength characteristic. At the same time, the rigidity of the structure should ensure the damping of vibrations that can arise both during the flight of the robot and due to dynamic loads during the manipulation process. The manipulator actuators must ensure stable interaction with objects of a certain weight, which is determined by the carrying capacity of the carrier UAV.

In addition to technical requirements, the choice of the manipulator configuration is carried out based on the functionality which the flying robot should perform.

As noted above, to perform simple operations for the delivery of various goods, only a grabbing device is generally sufficient, while it makes sense to perform the inspection or maintenance of industrial facilities using multi-DoF manipulators. The installation of the sensors may require the usage of multiple robotic arms, as was done when installing the sensors on the power line.

For example, 4-DoF manipulator consists of three motors in articulated joints (Dynamixel servomotors MX-106T, MX-64T and AX-12 in the shoulder, elbow and wrist joints respectively), two links, one servomotor for the grip rotation (Dynamixel AX-12) and the grip with 1-DoF (Futuba S9156). 3D model of flying robot is developed in CATIA and shown in Fig. 49.

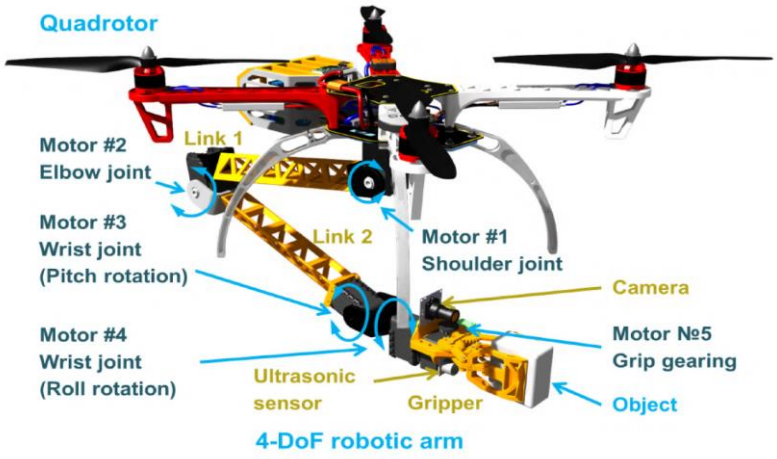

Fig. 49. Layout of the manipulator servo motors

The manipulator servomotors are chosen based on the necessary values of the maximum torque in the manipulator joints.

To implement a ground emergency operation in unstructured terrain conditions, a flying robot should perform a safe landing. Conventional aerial vehicles without a landing platform are not able to land on uneven surfaces. Since 2012, the scientific community began the development of the adaptive landing gears for small unmanned aerial vehicles (aircraft, helicopters, and multi-rotors). A number of early articles were devoted to the design and calculation of a chassis designed like a bird legs. In 2013, the helicopter landing gear was demonstrated for landing on uneven surfaces in or-der to prevent from helicopter rollover, as happened during the crash of a Boeing Vertol CH-46 Sea Knight helicopter1. Currently, several UAVs are equipped with a special landing platform, for instance, this is a passive landing gear using coupled mechanical design, a robotic legged landing gear developed in Georgia Institute of Technology with funding from DARPA, and the landing platform with four legs designed to reduce the load during the landing. The first one can land only vertically, though it has some limitations in its operation. The second one has a landing gear that is equipped with force sensors in robotic leg feet used to sense ground contact and the CoM location. Third landing gear uses force-controlled algorithm. This chassis has an innovative actuation, composed of a parallel arrangement of motor and brake, which relieves the motor from large impact loads during hard landings. Besides the legs are equipped by a spring-damper system acting in series to the actuation. Among the robots that combine both considered abilities motion in the air and on the ground, can be noted: HyTAQ, HERALD, robot HexaWalker 2 and project Hexapod-Quadcopter Robot (Fig. 50).

HyTAQ is a micro UAV equipped with a rolling cage, which allows carrying out terrestrial locomotion. HERALD is a combination of two snake robots with a quadrotor using a magnetic docking system. HexaWalker is a robot assembled from hexacopter and hexapod without additional sensors. The last of the above-mentioned hybrid robots is the prototype of a robot with frame rays, which can be transformed into legs; however, this robot does not have an adaptive landing algorithm.

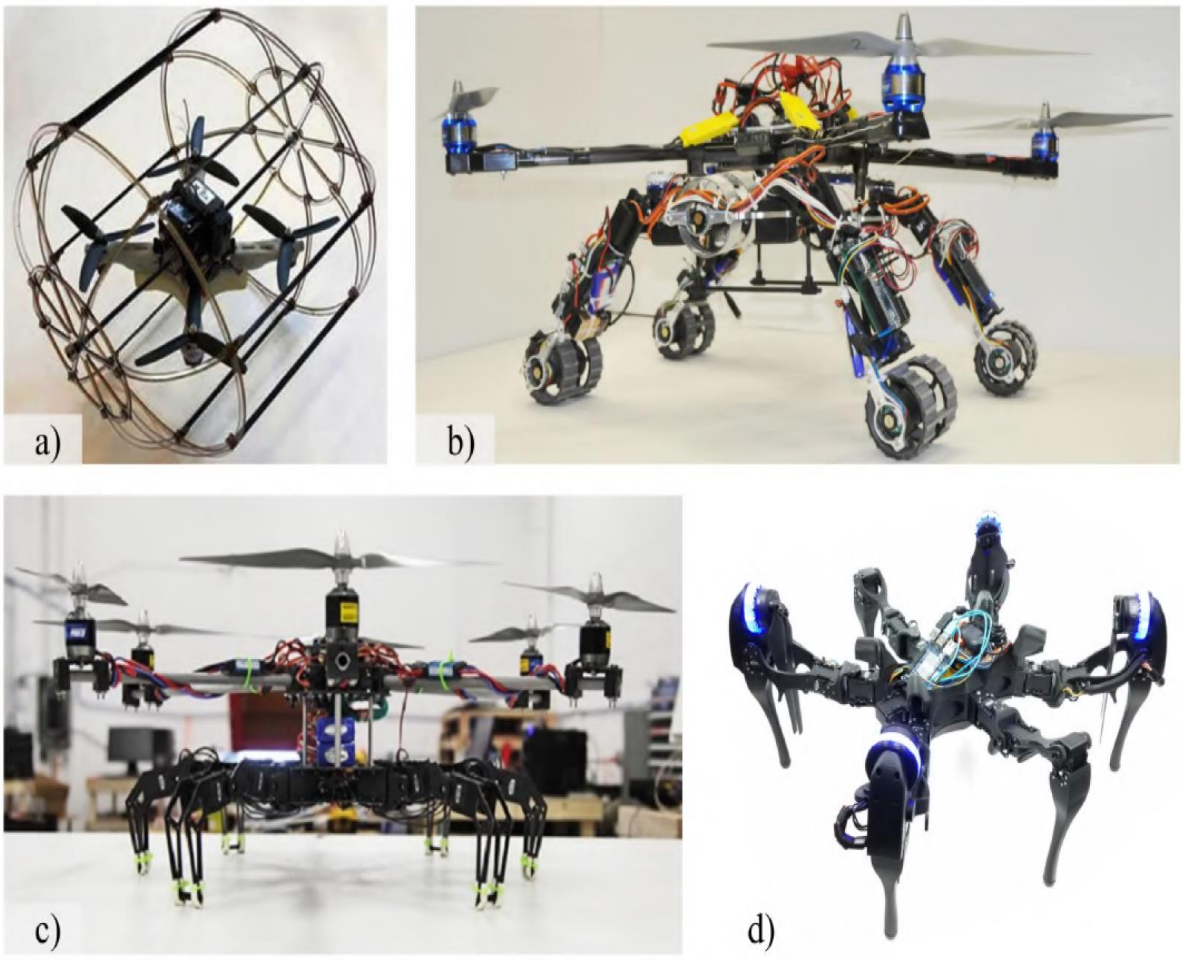

Fig. 50. The robots capable to fly and move on the ground: (a) HyTAQ, (b) HERALD, (c) HexaWalker, and (d) Hexapod-Quadcopter Robot

The robot is a hexacopter with landing gear attached to its bottom (Fig. 51 a)).

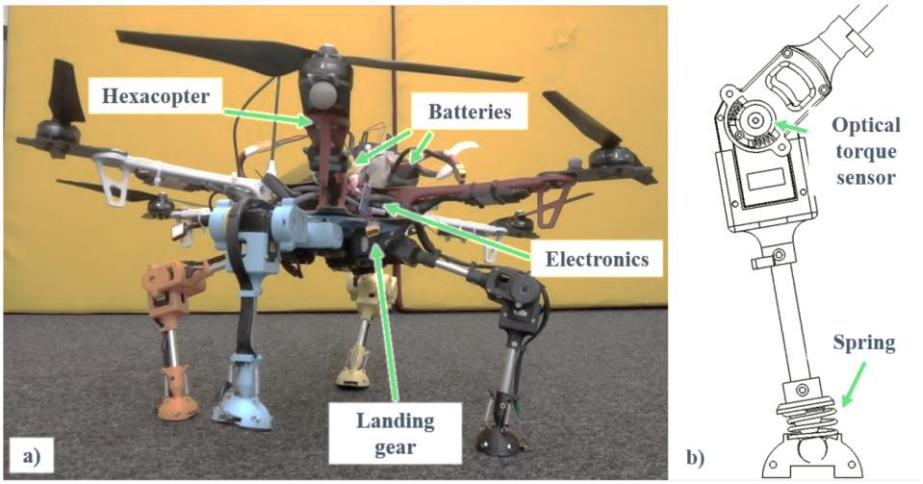

Fig. 51. The landing platform for the multicopters (a) and the leg structure (b)

The hexacopter is assembled from DJI Flame Wheel ARF KIT F550 frame with DJI E600 propulsion system and NAZA M flight controller. The landing platform consists of four 2-DoF legs, which are located in increments of 90 degrees relative to the central axis of the robot.

Photos of each phase of the Motion cycle are shown in Fig. 52.

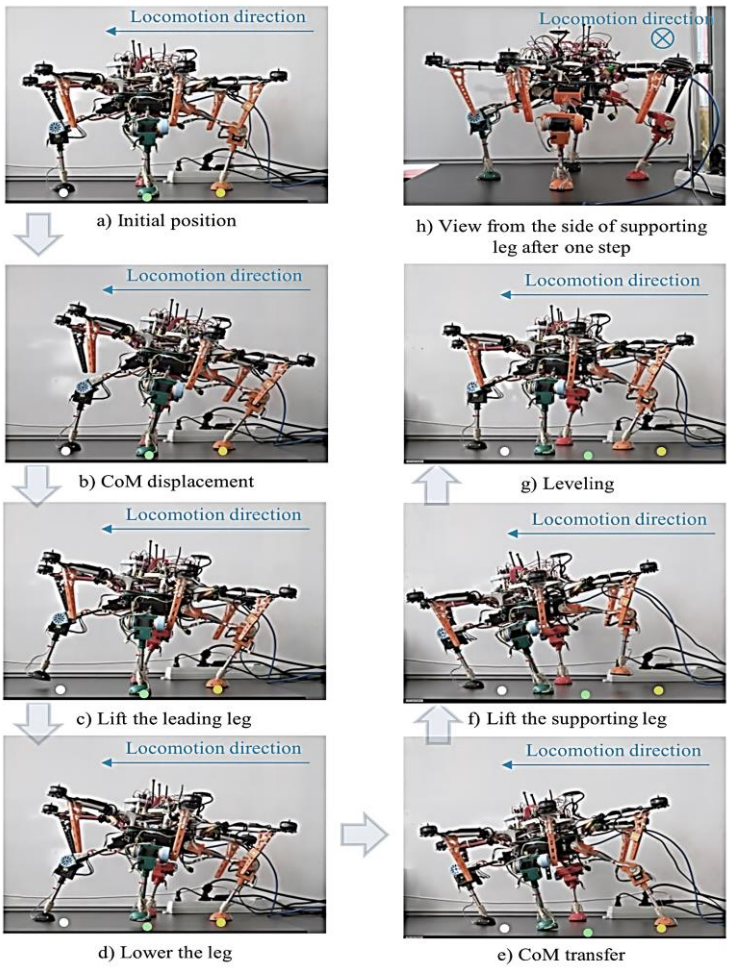

Fig. 52. The phases of the Motion cycle (the white and yellow points are the initial positions of the leading and left leg respectively)

The motion of the legs is executed by Dynamixel MX106 servomotors in the hip joints and Dynamixel MX28 servomotors in the knee joints. Also, the knee joints contain embedded optical torque sensors, which

are made from compression springs and an encoder, located in a plastic body (Fig.51, b). These sensors provide passive compliance of the legs. Each leg has a passive footpad, which is connected via a spherical joint to the tip of the second link.

The most challenging phase of the Motion cycle is the moving of the robot CoM from the supporting leg to the leading leg. The robot moves to a new position immediately during this step, thus, the previous phases are the preparation to the motion. At this phase, the robot should lift the side legs up and quickly move the CoM to a new position, so as not to incline to the side until the end of the movement. Thus, at this moment, the motors of the supporting and leading legs undergo maximum load. If the trajectory is incorrectly selected, the robot tries to lift up and remains in place, which is possible with an excessively large distance.

Also, the robot can tip over if the distance between the ground and the side legs is too small. This is due to the fact that the robot has time to slightly tilt to the side and one of the legs remains in the same place, while the leading leg will pull the robot behind it.

Fig. 52(e) demonstrates a slight side movement during this step. Fig. 52(h) also shows a slight inclination of the robot to the right. At other phases, the robot motion is performed stably. In all experiments, we visually detected the deviation from the desired position. After that, we check data about real angles from encoders of torque sensors in knee joints.

Conclusions

- The exertion of force and physical interaction are challenging tasks when performed on an aerial vehicle. The research community in aerial robotics started to approach such challenges in the past decade, with the use of interaction controllers tailored at aerial manipulators [15-39].
- Force exchange by an aerial vehicle was only tackled in more recent years however, as the state of the art progressed and reached higher maturity. The work hereby presented addresses some of the challenges of contact-based aerial interaction and proposes a novel approach to force generation by exploiting the aerial system as a whole, combining the action from the manipulator together with motion of the aircraft.
- A bespoke manipulation system featuring compliance is created to tackle force-driven tasks where the ability to adjust the force output, shape the load curve and tune the time in contact according to the task specifications is demonstrated throughout multiple experiments.
- Optimisation is carried out at both the design and control level, to further expand on the range of applications that can be accomplished with the compact, lightweight and compliant design. This, together with novel control strategies for aerial interaction allow to perform new aerial tasks, such as pushing against and tapping on a surface, install and retrieve sensors on vertical and cylindrical surfaces, and aerial contour following.
- Overall, the proposed approach demonstrates accuracy, robustness and reliability to tackle contact-based aerial operations in multiple scenarios.

References

1. Hamaza S. et al. Design, modeling, and control of an aerial manipulator for placement and retrieval of sensors in the environment. J Field Robotics. 2020. Vol. 37. Pp. 1224–1245. DOI: 10.1002/rob.21963.
2. Hassan M. A. H. Design and real time control of a versatile scansorial robot. A thesis submitted to The University of Sheffield for the fulfilment of the degree of Doctor of Philosophy. The University of Sheffield, 2016.
3. Sherstan M. J. Localization and Control of a Quadcopter Universal Payload System. A thesis submitted in partial fulfillment of the requirements for the degree of Master of Science, Department of Mechanical Engineering University of Alberta. 2020.

4. Bartelds T. et al. Compliant Aerial Manipulators: Toward a New Generation of Aerial Robotic Workers. IEEE Robotics and Automation Letters. 2016. Vol. 1, No. 1. Pp. 477-483. DOI: 10.1109/LRA.2016.2519948.

5. Mahmood S. K. et. al. Propeller-type Wall-Climbing Robots: A Review. IOP Conf. Ser.: Mater. Sci. Eng. 2021. Vol. 1094. Pp. 1-12. DOI:10.1088/1757-899X/1094/1/012106

6. Liang P et al. Design and Stability Analysis of a Wall-Climbing Robot Using Propulsive Force of Propeller. Symmetry 2021, 13, 37. DOI: 10.3390/sym13010037.

7. Myeong W., Myung H. Development of a Wall-Climbing Drone Capable of Vertical Soft Landing Using a Tilt-Rotor Mechanism. IEEE Access. 2019. Vol. 7. Pp. 4868 - 4879.

8. Sherstan M. J. Localization and Control of a Quadcopter Universal Payload System. A thesis submitted in partial fulfillment of the requirements for the degree of Master of Science, Department of Mechanical Engineering University of Alberta. 2020.

9. Myeong M. et al. Development of Wall-climbing Unmanned Aerial Vehicle System for Micro-Inspection of Bridges. ICRA. 23 May 2019.

10. Staub N., et al. The Tele-MAGMaS: An Aerial-Ground Comanipulator System . IEEE Robotics and Automation Magazine. 2018. Vol. 25, No 4. Pp.66-75.

11. Trujillo M. A. et al. Novel Aerial Manipulator for Accurate and Robust Industrial NDT Contact Inspection: A New Tool for the Oil and Gas Inspection Industry. Sensors. 2019. Vol. 19. Pp. 1305. DOI:10.3390/s19061305.

12. Morton K. An Extensible Framework for Nonlinear Aerial Manipulation. School of Electrical Engineering and Robotics Science and Engineering Faculty Queensland University of Technology. 2020. A dissertation submitted in fulfilment of the requirements for the degree of Doctor of Philosophy.

13. Ollero A. et al. Past, Present and Future of Aerial Robotic Manipulators. IEEE Trans. on Robotics. 2022. Vol. 38, No 1. Pp.626 - 645. DOI:10.1109/TRO.2021.3084395.

14. Yashin G. Development of Group of Flying Robots with Multifunctional Robotic Limbs aimed at Operations in Cluttered Environments. Doctoral Program in Engineering Systems. Skoltech, Mocow. 2020.

15. Tyatyushkina O.Yu. et al. Intelligent cognitive robotics.Vol. I: Soft computational intelligence and information — thermodynamic law of intelligent cognitive control. M.: Kurs. 2022.

16. Agha A. et. al. NeBula: Quest for Robotic Autonomy in Challenging Environments; TEAM CoSTAR at the DARPA Subterranean Challenge (preprint version). arXiv:2103.11470v1 [cs.RO]. 2021.

17. Hudson N. et al. Heterogeneous Ground and Air Platforms, Homogeneous Sensing: Team CSIRO Data61's Approach to the DARPA Subterranean Challenge. arXiv:2104.09053v1 [cs.RO]. 2021.

18. Yang G.-Z. The grand challenges of *Science Robotics* . Sci. Robotics. 2018. Vol. 3. Pp. 7650.

19. Chang Y. Development of a Wall Climbing Inspection Robot with High Mobility on Complex Shaped Walls. A thesis submitted in partial fulfilment of the requirements for the Degree of Master of Engineering in Mechanical Engineering in the University of Canterbury. 2015.

20. Ge D. et al. A Pressing Attachment Approach for a Wall-Climbing Robot Utilizing Passive Suction Cups. Robotics. 2020. Vol. 9, No 26. DOI:10.3390/robotics9020026

21. Faal S.G. Design and Analysis of a Robotic Duct Cleaning System. Thesis presented to Sharif University of Technology in partial fulfillment of the requirements for the degree of Master of Science in Mechanical Engineering (Mechatronics). Kish Island, Iran, 2011.

22. Silva M.F., Machado J.A.T. A Survey of Technologies and Applications for Climbing Robots Locomotion and Adhesion // Climbing and Walking Robots, Behnam Miripour (Ed.) InTech, 2010. [Available from: http://www.intechopen.com/books/climbing-and-walking-robots/a-survey-oftechnologies-and-applications-for-climbing-robots-locomotion-and-adhesion].

23. Horák M. et al. Service Robots for Motion and Special Applications on the Vertical Oriented Walls. In Service Robots (Chapter 5). INTECH. 2017. http://dx.doi.org/10.5772/intechopen.70. [Downloaded from: http://www.intechopen.com/books/service-robots].

24. Bian S. et al. A Novel Type of Wall-Climbing Robot with a Gear Transmission System Arm and Adhere Mechanism Inspired by Cicada and Geckom Appl. Sci. 2021, 11, 4137. https://doi.org/10.3390/ app11094137.

25. Yanagida T. et al. Design and Implementation of a Shape Shifting Rolling–Crawling–Wall-Climbing Robot. Appl. Sci. 2017. Vol. 7, No 342. DOI:10.3390/app7040342.

26. Wang, B.; Xiong, X.; Duan, J.; Wang, Z.; Dai, Z. Compliant Detachment of Wall-Climbing Robot Unaffected by Adhesion State. Appl. Sci. 2021. Vol. 11, No 13. P. 5860. https://doi.org/ 10.3390/app11135860.

27. Spenko M. J. et al. Biologically Inspired Climbing with a Hexapedal Robot. J. of Field Robotics. 2008. Vol. 25, No 4-5. Pp. 223-242. [URL: http://dx.doi.org/10.1002/rob.20238].

28. Nansai S. et al. Design and Implementation of a Lizard-Inspired Robot // Appl. Sci. 2021. Vol. 11, No 7898. https://doi.org/10.3390/app11177898.

29. Zhang J. et al. Transition Motion Planning for Multi-Limbed Vertical Climbing Robots Using Complementarity Constraints. arXiv:2106.07127v1 [cs.RO] 14 Jun 2021.

30. Han I.H. et al. A miniaturized wall-climbing segment robot inspired by caterpillar locomotion // Bioinspir. Biomim. 2017. Vol. 12. No. 4. Pp. 046003. https://doi.org/10.1088/1748-3190/aa728c.

31. Du Q. et al. Design of a micro pole-climbing robot , Intern. J. of Advanced Robotic Systems. 2019. No 3. Pp. 1-11. DOI: 10.1177/1729881419852813.

32. Du Q. et al. The obstacle-surmounting analysis of a pole-climbing robot. Intern. J. of Advanced Robotic Systems. 2020. No 6. Pp. 1-20. DOI: 10.1177/1729881420979146.

33. Gao R., Li M., Xu Y., Zhu W. Design and Stability Analysis of a Wall-Climbing Robot Using Propulsive Force of Propeller. Symmetry. 2021. Vol. 13. Pp. 37. https:// doi.org/10.3390/sym1301003.

34. Wang Y., Du Q., Zhang T., Xue C. The WL_PCR: A Planning for Ground-to-Pole Transition of Wheeled-Legged Pole-Climbing Robots. Robotics. 2021. Vol. 10. Pp. 96. https:// doi.org/10.3390/robotics10030096.

35. Schmidt D. Safe Navigation of a Wall-Climbing Robot – Risk Assessment and Control Methods. Doktor-Ingenieur (Dr.-Ing.) genehmigte Dissertation. Technischen Universität Kaiserslautern, 2013.

36. Stockton A. J. design, build, and control of a climbing robot for irregular surface geometry. Partial fulfillment of the requirements for the degree of MASTER OF SCIENCE. Texas A&M University. 2015.

37. Muthugala M. A. V. et al. Design and Control of a Wall Cleaning Robot with Adhesion-Awareness. Symmetry. 2020. Vol.12, No 122. DOI:10.3390/sym12010122.

38. Agha A. et. al. NeBula: Quest for Robotic Autonomy in Challenging Environments; TEAM CoSTAR at the DARPA Subterranean Challenge (preprint version). 2021.arXiv:2103.11470v1 [cs.RO].

39. Hudson N. et al. Heterogeneous Ground and Air Platforms, Homogeneous Sensing: Team CSIRO Data61's Approach to the DARPA Subterranean Challenge. 2021. arXiv:2104.09053v1 [cs.RO].